SHEAR CRACKING AND STIRRUP EFFECTIVENESS OF LIGHTLY REINFORCED CONCRETE BEAMS

by

Emmanuel K. Attiogbe

Michael N. Palaskas

David Darwin

A Report on a Research Project Sponsored by

ARMCO INC.

University of Kansas

Lawrence, Kansas

July 1980

ACKNOWLEDGEMENTS

This report is based on a thesis submitted by Emmanuel K. Attiogbe in partial fulfillment of the requirements for the MSCE degree. The support of Mr. Attiogbe's graduate study by the government of Ghana, the African-American Institute, and the Department of Civil Engineering at the University of Kansas is gratefully acknowledged.

The work described in this report represents a portion of the Ph.D. research of the second author, Michael N. Palaskas. The support of Mr. Palaskas' graduate study by the University of Kansas General Research allocation #3215-X038 and the Department of Civil Engineering is gratefully acknowledged.

Support was provided for this investigation by the Department of Civil Engineering.

ARMCO INC. donated the reinforcing steel and funded the reproduction of this report.

TABLE OF CONTENTS

LIST OF TABLES

LIST OF FIGURES

CHAPTER 1

INTRODUCTION

1.1 General

The failure of reinforced concrete beams in shear is associated with diagonal cracking. The load at which diagonal cracks form is thus of interest in determining the shear strength of beams. The shear-span to depth ratio has a significant influence on the cracking of reinforced concrete beams (3,5). For normal and long beams having shear-span to depth ratios greater than 4, without web reinforcement, the initial diagonal tension crack usually grows rapidly in length and width immediately after it forms, causing failure. In the case of beams with web reinforcement, the diagonal cracks stabilize and substantially more shear force may be applied before the member fails (3,14). It is generally agreed, as indicated in the report by ACI-ASCE Committee 326, Shear and Diagonal Tension (2), that expressing the shear carried by the concrete as equal to the diagonal tension cracking strength, results in a good correlation with test data. Thus, for a beam without web reinforcement, the diagonal cracking load is considered in design as the usable ultimate shear capacity, and, for a beam with web reinforcement, it is a good measure of the shear stress carried by the concrete at failure.

Various investigators (8,11,16,17,20,26) have conducted shear tests on reinforced concrete beams with low ratios of longitudinal reinforcement, ρ_w. Mathey and Watstein (20) have shown that even though the use of high strength reinforcing steel can result in a considerable savings in flexural steel, it can lead to a progressive loss of shear strength with the decreasing reinforcing ratio, ρ_w. MacGregor and Gergely, in a

paper (16) prepared in conjunction with the work of the ACI-ASCE Committee on Shear and Diagonal Tension, have suggested that a beam with a longitudinal reinforcement ratio less than one percent and having minimum web reinforcement can be understrength in shear, especially in regions away from points of maximum moment, where some of the longitudinal reinforcement has been terminated. Tests by Krefeld and Thurston (17), Rajagopalan and Ferguson (26), and Kani (16) have shown that the ACI Code provisions for shear strength appear unduly optimistic for beams without stirrups having a longitudinal reinforcement ratio less than one percent.

A better understanding of the shear behavior of beams with low ratios of longitudinal reinforcement is important in terms of safety, since beams of this type are presently allowed by the ACI Building Code (6). In many parts of the world, flexural reinforcing ratios less than one percent offer the most economical reinforced concrete sections. A better knowledge of the shear behavior of these beams will enable the considerable savings in steel to be used to best advantage. Since the shear strength of beams seems to be closely tied to the load at which diagonal cracking occurs, reliable methods of determining the cracking load are needed.

1.2 Previous Work

Researchers working on the shear strength of reinforced concrete beams have employed different laboratory techniques for testing and monitoring the behavior of the beams under load. One of the most important differences in these techniques is the method used to identify the cracking load, V_c. Depending on the technique used, V_c may be the load at which the diagonal crack crosses the estimated neutral axis (8,9,14,20), or the load at which a break in slope occurs in a compressive concrete strain (19,20,31) (or

tensile reinforcement strain (19,20) or vertical displacement (10,20)) vs. load curve. Most tests to determine cracking load have been conducted on beams without web reinforcement, because the action of shear can be studied more easily due to the fact that the initial "diagonal tension crack" usually grows rapidly in length and width immediately after it forms (14,28).

The overwhelming majority of investigators (1,5,7,8,9,10,11,12,13,14, 15,16,17,19,20,22,23,26,27,28,29,30,31) have determined the cracking load by identifying a "diagonal tension crack" as an inclined crack making an angle of about 45 degrees with the axis of a beam. Based on this definition of a diagonal tension crack, the load corresponding to shear cracking has been defined by various methods. Some researchers (8,9,20) tested rectangular beams and defined the cracking load as that obtained when a diagonal crack in the shear span extended from the tensile reinforcement toward the nearer concentrated load and intersected the level of tensile reinforcement at an angle of approximately 45 degrees. The diagonal tension cracking load was taken as the load at which this diagonal tension crack first crossed the neutral axis of the beam. Haddadin, Hong and Mattock (14) tested T-beams, and they defined the cracking load as load at which a diagonal tension crack made an angle of 45 degrees with the neutral axis of the beam. The load corresponding to a diagonal tension crack, the formation of which was immediately followed by a sudden increase in deflection of the beam, was chosen by Van Den Berg (31) as the diagonal tension cracking load. Morrow and Viest (23) and Acharya (1) defined the diagonal cracking load as the load at which a diagonal tension crack was first clearly observed. The lack of agreement on the definition of the diagonal cracking load makes it difficult to compare data from past and present tests on a precise basis.

Some investigators (19,20,31) have used strain gages on the compressive face of test beams to verify the accuracy of the cracking load, as defined from visual studies of the cracks. In their study of rectangular beams without web reinforcement, Mathey and Watstein (19, 20), applied strain gages to both the compressive face of the concrete and the tensile reinforcement in the shear span. For beams having shear-span to depth ratios of 1.51, they noted that there was an abrupt increase in the steel stress near the support and a marked reduction in the rate of development of strain in the compressive face of the beams near the concentrated loads, following the formation of a well defined diagonal crack.

Mathey and Watstein (20) and Bresler and Scordelis (10) used specially designed yoke extensometers to which dial gages were attached. Vertical displacements of the bottom of the beam with respect to the top surface at selected sections were recorded. Bresler and Scordelis tested rectangular beams with and without web reinforcement and took measurements at sections corresponding to stirrup locations. The diagonal cracking load was taken to be the point at which the curve of load vs vertical yoke displacement just deviated from the vertical.

Based on the cracking loads obtained from the different procedures indicated above, a number of equations have been proposed for the shear stress carried by concrete, v_c.

ACI-ASCE Committee 326 (2) used cracking loads determined by various investigators to obtain the equation which forms the basis for shear design of reinforced concrete members in the ACI Code (6):

$$v_c = V_c/b_w d = 1.9\sqrt{f'_c} + 2500\ \rho_w\ V_u d/M_u \leq 3.5\sqrt{f'_c} \qquad (1.1)$$

where V_c = shear force carried by concrete

b_w = width of web of T-beam

d = effective depth

f'_c = compressive strength of 6 x 12 inch cylinders

ρ_w = ratio of tensile reinforcement with respect to the web width and effective depth of the beam

V_u = factored shear force at section

M_u = factored bending moment at section.

They, also, proposed the simpler equation, $v_c = 2\sqrt{f'_c}$, to be used in place of Eq. (1.1). These equations are known to be unconservative for beams without stirrups having ratios of longitudinal reinforcement, ρ_w, less than one percent (8,11,16,18,20,26) and overconservative for beams with higher values of ρ_w (11,16).

Zsutty (32) combined test results from several different laboratory sources. He carried out a combination of dimensional and statistical regression analyses to reflect the different cracking load identification procedures used. He derived the equation:

$$v_c = 59(f'_c \rho_w d/a)^{1/3} \tag{1.2}$$

where a = length of the shear span.

Placas and Regan (25) derived the equation:

$$v_c = 8(f'_c\ 100\rho_w)^{1/3} \tag{1.3}$$

Eq. (1.3) and Zsutty's equation give the same prediction for v_c when a/d is about 4.

Rajagopalan and Ferguson (26) studied beams with no web reinforcement having ρ_w less than one percent. From their results and those of other investigators (12,16,17,19,20), they derived the equation,

$$v_c = (0.8 + 100\rho_w)\sqrt{f'_c} \leq 2\sqrt{f'_c} \qquad (1.4)$$

to represent the lower bound of the test results. ACI-ASCE Committee 426 (4) has proposed an equation which is similar to Eq. (1.4):

$$\sqrt{f'_c} \leq v_b = (0.8 + 120\rho_w)\sqrt{f'_c} \leq 2.3\sqrt{f'_c} \qquad (1.5)$$

for normal weight concrete, where v_b is known as basic shear stress (shear stress carried by concrete). This equation is currently under consideration for adoption in the ACI Building Code.

Batchelor and Kwun (8), from a study aimed at assessing the feasibility of using Eq. (1.5), have proposed an alternative equation:

$$\sqrt{f'_c} \leq v_b = (0.60 + 110\rho_w)\sqrt{f'_c} \leq 2.25\sqrt{f'_c} \qquad (1.6)$$

for normal weight concrete.

1.3 Object and Scope

The purpose of this investigation is to determine the shear cracking load and stirrup effectiveness for lightly reinforced concrete T-beams. The shear behavior of beams of this type is not fully understood, and reliable methods for determining their cracking loads are therefore desirable. Work of this type can help in the formulation of a rational theory for shear failure for reinforced concrete beams.

The primary variables in the investigation are the longitudinal reinforcement ratio, ρ_w, which varies from 0.0049 to 0.0095, and the amount of web reinforcement, $\rho_v f_{vy}$, which varies from 0 to 103. The thirteen beams tested are divided into three groups, A, B and C, representing the three different longitudinal reinforcement ratios used. Within each group, the amount of web reinforcement is varied. The beams have constant shape.

They are 20 feet long with a 13 foot simple span and 3½ feet cantilever overhangs.

Four methods are used to determine the shear cracking load: visual studies of the crack patterns; strain gages applied to the compressive face of the concrete; frames fixed to the top of the beams with dial gages to measure specimen depth; and strain gages applied to the web reinforcement, in the case of beams with stirrups.

The results obtained using these methods are compared with each other and with predictive equations developed by others (2,4,6,8,25,26,32).

A linear regression analysis is used to determine the effectiveness of web reinforcement, as measured by the increase in strength over the cracking load.

Design recommendations are made for beams with and without stirrups.

CHAPTER 2
EXPERIMENTAL STUDY

2.1 General

The experimental program reported here was designed to study the shear behavior of lightly reinforced concrete T-beams. The major emphasis of this work is to determine the shear cracking load and stirrup effectiveness of the beams. Four techniques are used to identify the formation of shear cracks. The results obtained using these techniques are compared with each other and with values predicted by other investigators.

Because of the low tensile reinforcement ratios used, all of the beams exhibited extensive flexural cracking. In all cases, however, failure coincided with the formation of a diagonal tension crack, which propagated through the flange toward the point of load application. The beams failed on a single side, but in general, the crack patterns were symmetrical.

The primary variables in the study were the longitudinal reinforcement ratio and the amount of web reinforcement.

2.2 Test Specimens

Thirteen T-beams, each having a flange width of 24 inches and a total depth of 18 inches, were tested in this investigation. The flange thickness and the web width were 4 inches and 7½ inches, respectively. The beams were 20 feet long and simply supported on a 13 foot span with 3½ foot cantilever overhangs. The shear-span to depth ratio for the beams was about 4. The dimensions of the beams and details of their reinforcement are shown in Figs. 2.1 and 2.2.

The beams were divided into three groups, A, B, and C. The six beams in group A had a longitudinal reinforcement ratio, ρ_w, of about 0.0066. The

three in group B had a ρ_w of about 0.005, while the four beams in group C had a ρ_w of about 0.0095. Within each group, the amount of web reinforcement was varied. Four values of web reinforcement were used ranging in nominal value from 0 to 100 psi. Beams in the "00" series had no web reinforcement. The value of nominal stress resisted by the stirrups, $\rho_v f_{vy}$, for beams in the "25" series was about 32 psi, (ρ_v is ratio of web reinforcement = $A_v/b_w s$, where A_v is the area of web reinforcement, b_w is the web width of the beam, and s is the spacing of web reinforcement; f_{vy} is the yield strength of web reinforcement). Beams of the "50" series had $\rho_v f_{vy}$ of about 75 psi, while the "75" series beams had a value of about 100 psi. The series designations were originally selected to represent the value of $\rho_v f_{vy}$ for the series. The actual stirrup strengths exceeded those originally specified, but the original designations were retained. The stirrup spacing was 7 inches.

The longitudinal reinforcement, consisting of non-prestressed Grade 270 stress-relieved strand, was placed in two layers. Three strands were placed in the bottom layer and two in the top layer. The flanges were reinforced transversely with number 3 deformed bars spaced at 7 inches and longitudinally with two number 4 bars. A schedule of the beams, indicating the flexural and shear reinforcement, is presented in Table 2.1.

2.3 Materials and Fabrication

The concrete was obtained from a ready-mix plant and hauled to the laboratory in transit mix trucks. The mix proportions by weight for cement, sand, and crushed limestone of 3/4 inch nominal maximum size (locally referred to as 1/2 inch) were 1.0:3.19:3.21 for seven beams, 1.0:2.86:2.88 for five beams, and 1.0:2.37:2.37 for one beam. Type I Portland Cement was used

for all beams. Air content and slump tests were conducted on the concrete. The mix design required an air content of five percent and a slump of two inches, but these values were not uniformly attained. Twelve 6 x 12 inch cylinders and two 6 x 6 x 21 inch flexural specimens were cast and cured alongside each test beam. Some cylinders were tested to insure that the concrete strength was about 4000 psi before testing each beam. The balance of the cyclinders were tested immediately after the beam failed. The flexural specimens were also tested to give a measure of the tensile strength of the concrete. The concrete properties are presented in Table 2.2.

Grade 270 stress-relieved strands with diameters of 7/16 inch, 1/2 inch, and 0.6 inch were used as flexural reinforcement. Wire stirrups with diameters of 0.132 inch, 0.186 inch, and 0.229 inch were used for web reinforcement. The wire stirrups arrived in coils of about 4½ feet external diameter and 1½ feet thickness. The wires were cut into lengths of about 40 inches, straightened, and then prestretched to eliminate residual stresses. They were then bent and welded into closed shapes. Prestretching was used to give the wire stirrups a distinct yield point, but it, also, gave rise to strain aging, which resulted in an increase in the yield strength with time. To account for the increase in strength, tensile tests were made on specimens of the wire on the day of the beam test.

The stirrups were welded to number 3 deformed bars, which served as transverse reinforcement for the flange. The bars of the reinforcement cage were tied together with iron wire ties. The strands and the deformed bars conformed to ASTM Specifications A416-74 and A615-78, respectively. The properties of the deformed bars, the strands, and the stirrups are given in Table 2.3. Typical stress-strain curves for the strands, stirrups, and concrete are shown in Figs. 2.3-2.9.

A single plywood form was used for all beams. The framework was assembled using bolts and form ties, which allowed the dimensions to be accurately maintained. The form was cleaned and oiled prior to casting each beam. When the reinforcing cage was placed in the formwork prior to concreting, the lead wires from the strain gages were carried out through the side of the formwork to enable connection of the gages to strain indicators during the tests. Three 1/4 inch diameter steel wires were bent into inverted U-shapes and embedded in the beams about 6 inches outside the support points to act as lifting devices.

The formwork was stripped from each beam three days after concrete placement, and the beam was covered with polythene sheet until a strength of about 3000 psi was attained. The beam was then moved and prepared for testing.

2.4 Loading Apparatus

The loading system (see Fig. 2.10) was designed to apply two concentrated loads to the test specimens. Two bearing plates were attached to the top of the beams, one-and-a-half feet on either side of the midspan, with Hydrostone high strength gypsum cement. Two wide-flange steel members, each weighing 300 pounds, were used as load spreader beams and were placed on the bearing plates. Each spreader beam was attached to two load rods. The load rods were strain-gaged and calibrated to act as load cells, so that the load in each rod could be determined during the test. The 1-inch diameter load rods were connected to Enerpac hydraulic jacks located below the structural test floor. Hydraulic pressure was applied and controlled using a Satec Pumping Console Assembly, an electrically powered hydraulic loading system.

2.5 Instrumentation

SR-4 foil strain gages (0.031 inch long) were bonded to the longitudinal reinforcement at midspan and to the stirrups at mid-height. The gages were, also, bonded to the strands in the overhangs to detect slip of the longitudinal reinforcement. Before attaching the gages, the surface of the steel was cleaned using Micromeasurement M-Prep Conditioner A, followed by M-Prep Neutralizer 5. The gages were bonded to the reinforcement after first applying M-Bond 200 catalyst to the bond surface of the gages and then M-Bond 200 adhesive to the surface of the reinforcement. A resilient protective coating, M-Coat G, was applied over each gage to provide waterproofing.

Precision paper backed wire strain gages, Type W240-120 (2.40 inches long), were attached to the concrete on the top of the beams within the shear span. The placing procedure included smoothing the locations with a grindstone and attaching the gages with Duco cement. For most of the beams, these concrete strain gages were installed at distances of 48, 54, and 60 inches on either side of midspan. The location and numbering of the concrete and stirrup strain gages are shown in Fig. 2.2. The stirrups in each half of a beam were numbered from the support toward midspan. A Vishay 220 Data Logging System, was used to obtain strain readings from all gages for eleven beams. Manually operated Model P350 Vishay strain indicators and switch boxes were used for two beams of the C group.

Deflections at the load points and midspan were recorded using 0.001 inch dial gages. Gages, numbers 1 and 3, measured deflections at the load points, and gage number 2 measured the deflection at the midspan. The midspan deflection was, also, measured using a TRANS-TEK Series 240 Displacement Transducer. Changes in the overall depth of the beam due to diagonal

cracking were measured using 0.0001 inch dial gages attached to specially designed frames (see Fig. 2.11). The frames were 28 inches square and were built using 1/2 inch square steel bars. Frames, numbers 1 and 2, on the left side of each beam, were placed at the locations of stirrups 5 and 6, respectively, while frames, numbers 3 and 4, on the right side, were placed at the locations of stirrups 6 and 5, respectively. The frames were, also, placed at these locations for the beams without stirrups. The frames were attached to the upper surface of the beams by bolting them to 1/2-inch thick plates, which were embedded in Hydrostone gypsum cement.

2.6 Test Procedure

Prior to testing, one side of each beam was white-washed with a gypsum cement slurry to enable the cracks to be seen clearly. Stirrup and flexural steel positions were marked on the beam.

The load was applied incrementally. After each increment of load had been added, deflections, strains, and changes in the depth of the beam were recorded. Cracks were marked on the beam. Cracks were identified by indicating the load at which they formed. The load increments varied. Generally, the increments were initially 2½ kips (2500 pounds) and reduced to 1½ kips until flexural cracking occurred. Above the flexural cracking load, 5 kip increments were used until just prior to the anticipated shear cracking load, when the increments were reduced to 1½ kips. After the formation of the initial shear cracks, 2½ kip load increments were used until failure occurred. Photographs of the beams were taken during the tests and after the failure.

2.7 Description of Behavior

Flexural cracks first formed near midspan. As the load increased, the

number of cracks in the shear-span increased, and they became inclined toward the load points. A further increase in load caused some of the inclined cracks to make an angle of 45 degrees or less at the level of the centroid of the uncracked transformed cross section (uncracked transformed neutral axis) to form the first "diagonal tension cracks." These cracks widened with an increase in load. At the formation of the first diagonal tension cracks, the average strains in the flexural reinforcements were 0.0023 in/in, 0.0027 in/in, and 0.0016 in/in for the beams, in groups A, B, and C, respectively.

In all beams, failure occurred at one side only and consisted of a diagonal tension failure of the flange. The critical diagonal tension crack which caused failure, propagated through the flange toward the loading point and, also, extended to the level of tensile reinforcement. In beams with stirrups, the critical diagonal tension crack was an existing diagonal crack, which opened under additional load. In beams without stirrups, on the other hand, the failure crack opened almost as soon as it was formed. Stirrups, intersected by the critical diagonal tension crack, yielded prior to failure.

Generally, changes in beam depth, as measured by the dial gages on the frames, were first recorded when the flexural cracks started inclining toward the load points. For beams without web reinforcement, the readings on the gages did not reach significant magnitudes before the onset of failure. Because of the danger of damage at failure, the dial gages were removed as the loads approached the ultimate, with the exception of the deflection gage at midspan. In every case for beams with stirrups, the onset of failure was indicated in advance when the frame dial readings became unstable.

2.8 Test Results

The nominal shear forces and stresses at ultimate are given in Table 2.4. Load-strain data from concrete and stirrup strains are shown graphically in Figs. 2.12-2.23 and Figs. 2.24-2.33, respectively. Graphs of load versus change in depth of beam are shown in Figs. 2.34-2.46. The crack patterns are reproduced in Figs. 2.47-2.51. Load-deflection curves are presented in Appendix B, while load-strain diagrams for the flexural reinforcement are shown in Appendix C.

CHAPTER 3

EVALUATION AND DISCUSSION OF TEST RESULTS

3.1 General

The test results described in Chapter 2 are used to determine shear cracking loads for the beams, and the applicability of the techniques used to identify shear cracking are discussed. The "cracking load" obtained using each technique is selected as the lowest of the values obtained for the left and right sides of each beam. The shear cracking load values from the various techniques are compared with each other and with predictions from equations according to the ACI Building Code (6), Zsutty (32), Placas and Regan (24), Rajagopalan and Ferguson (26), ACI Committee 426 (4), and Batchelor and Kwun (8).

A linear regression analysis is used to determine the effectiveness of web reinforcement as indicated by the increase in strength over the cracking load. A design approach is proposed based on the test results.

3.2 Determination of Shear Cracking Load

3.2.1 Visual Studies of Crack Patterns

This technique is based on the definition of the shear cracking load, which depends on the identification of a diagonal tension crack. Some researchers, such as Mathey and Watstein (20), studied rectangular beams and defined the shear cracking load as the load at which a diagonal tension crack, intersecting the level of tensile reinforcement at about 45 degrees, first crossed the neutral axis of the beam. From the crack patterns obtained in this study (Figs. 2.47-2.51), it is observed that only the critical diagonal tension cracks (i.e., which cause failure) make angles of 45 degrees or less with the tensile reinforcement. The use of this definition

of a shear crack, clearly overestimates the shear cracking load.

Haddadin, Hong and Mattock (14) studied T-beams and defined the shear cracking load as the load at which a diagonal tension crack made an angle of 45 degrees with the neutral axis of the beam. Using this definition for the beams in this study, the load at which the first diagonal tension crack makes an angle of 45 degrees or less with the neutral axis (centroid of the uncracked transformed cross section) is chosen as the shear cracking load. The load at which a diagonal tension crack is inclined at an angle of 45 degrees or less above the neutral axis is, also, recorded. The results obtained are tabulated in Table 3.1. The lowest values selected are based on the definition of the diagonal tension crack making an angle of 45 degrees with the neutral axis of the beam.

3.2.2 Concrete Strain in Compression Flange

The data obtained from the gages installed on top of the flange are shown graphically in Figs. 2.12-2.23. Generally, as the load is increased, the concrete compressive strains increase. Beyond shear cracking, the compressive strains in the cracked zone reduce and, in some cases, become tensile.

The load at which the reduction in compressive strain occurs is selected as the shear cracking load. The results are tabulated in Table 3.2.

3.2.3 Stirrup Strain

Stirrup strain data are shown graphically in Figs. 2.24-2.33. The stirrup gages began recording when flexural cracks started inclining toward the load points. This is reflected in the initial portions of the graphs. In order to eliminate the effect of flexural cracking on the shear cracking

load, the initial section along which a significant change in slope occurs in each graph is extended backwards to meet the load axis. The shear cracking load is recorded as the load at the point of intersection. In order to distinguish the point of intersection accurately, this determination was made using plots with an exaggerated horizontal scale (approximately five times that shown in Figs. 2.24-2.33). This procedure is illustrated in Fig. 3.1. The results are tabulated in Table 3.3.

3.2.4 Increase in Depth of Beam

Graphs of load against depth increase are shown in Figs. 2.34-2.46. The dial gages on the frames generally began recording when flexural cracks started inclining toward the load points. Thus, the initial portions of the graphs cannot be said to be due to shear cracking. The initial section along which a significant change in slope occurs in each graph is extended backwards to meet the load axis as is done in the case of the stirrup strain graphs. The results are tabulated in Table 3.4.

It is not possible to determine the shear cracking load from depth increase plots for beams without web reinforcement. This is because the relative displacements across a diagonal crack just before failure, were not recorded, since the dial gages were removed prior to failure to prevent damage.

3.3 Discussion of Results

This study is limited in scope, and the results should be viewed with these limitations in mind. Only thirteen beams were tested. For the two primary variables in the study, ρ_w and $\rho_v f_{vy}$, only three values of ρ_w and four values of $\rho_v f_{vy}$ were used. A single shear-span to depth ratio, a/d, was used for all beams. Because of the limited scope, the behavior of beams proportioned differently from the test beams cannot be predicted with certainty.

Another consideration is the fact that the use of T-beams may result in overestimating the role that the flange plays in resisting shear stresses in actual structures. This is because in real structures, the flange can be in tension in negative moment regions at supports, while the test beams were subjected to positive bending moments throughout.

On the other hand, the bond between the reinforcement and the concrete is likely to be higher in actual structures than in the test specimens, since the reinforcing steel in the test beams consisted of smooth wire and seven-wire strand.

In spite of these shortcomings, the tests were satisfactorily realistic to be of use in making design recommendations.

3.3.1 Shear Cracking

In comparing the different methods of determining shear cracking load, it is assumed that for the beams tested, the cracking stress, v_c, depends on the concrete strength and the amount of longitudinal reinforcement. Thus the reliability of a particular method of indicating the shear cracking load is measured by how close the values of v_c are to each other within a beam group. The contribution of stirrups to shear strength is assumed to be proportional to $\rho_v f_{vy}$ and independent of concrete strength and flexural reinforcing.

The values of cracking load and the corresponding stresses obtained for each technique are tabulated in Table 3.5.

Considering the cracking patterns, it might be expected that the load corresponding to diagonal tension cracking above the neutral axis would be higher than that for cracking at the neutral axis. The results shown in Table 3.1 are contrary to this expectation for some beams. This

indicates the inconsistent nature of the results obtained by studying crack patterns.

As a means of obtaining information on the redistribution of stresses following the formation of diagonal tension cracks, the strain gages attached to the compressive face of the concrete are able to give a good representation of beam behavior. This is seen from the results shown graphically in Figs. 2.12-2.23. Shear cracking loads are easily obtained from the graphs, and the results (Table 3.2) are generally consistent for both sides of the beams.

The results obtained from the stirrup strain gages meet expectations in terms of beam behavior. Initially, the recorded strains are very small. Beyond diagonal tension cracking, substantial increases occur in the strain readings. These trends are shown in Figs. 2.24-2.33. It can be seen from Table 3.5 that there is a good agreement between the results obtained from concrete and stirrup strain data.

The frames are useful in determining the increase in the depth of the beams. But as a means of obtaining the shear cracking load, the depth increase data, shown graphically in Figs. 2.34-2.46, do not give consistent results. These results tend to be slightly higher than those obtained from concrete and stirrup strain data for some beams. This indicates that the frames may not be as sensitive to shear cracking.

As expected (2,24), the values of shear cracking load are independent of the degree of shear reinforcing.

The concrete strength, f'_c, was not the same for all beams. In order to minimize the effect of this variation on the results, the shear stresses at cracking are normalized with respect to $(f'_c)^{1/2}$ and $(f'_c)^{1/3}$ in Figs.

3.2 and 3.3. It is seen from these figures that the results obtained from concrete and stirrup strains show less scatter than those obtained from changes in beam depth and studies of crack patterns.

Beam C00 (f'_c = 4270 psi), had a concrete slump of 1/2 inch and was one of two beams (beam C50 with slump of 1¼ inch was the other) tested only three days after concrete placement. The low value of shear cracking stress obtained for C00 with respect to other beams in Group C (see Figs. 3.2 and 3.3), may have been due to inadequate consolidation.

A detailed study of the data strongly indicates that, unlike flexural cracking, "shear cracking" does not represent the formation of a discrete crack or cracks. Instead, "shear cracking" represents a change in the way that the beam carries load within the shear span. Stresses are redistributed and shear deflection increases markedly. Crack patterns may be somewhat random, and the local angle of a crack does not appear to be of great interest. The most reliable measures of this change in behavior in this study, concrete and stirrup strains, may be reliable due to the fact that these strain readings reflect the behavior of a sizeable portion of the beam. The concrete gages pick up the softening due to diagonal cracks. The stirrups pick up load as the load carrying mechanisms change and are, thus, sensitive to the change in behavior. Since depth increase is a function of the stirrup stiffness, as well as the concrete, it may not be as sensitive as the stirrup gages.

Table 3.6 shows the calculated shear cracking stresses obtained using a number of equations proposed by other investigators. In Tables 3.7a and 3.7b, a comparison is made between the observed shear cracking stresses, v_c, using each of the four techniques, and the calculated shear cracking stresses obtained using Eqs. (1.1) through (1.6). For

the beams in this study ($a/d \simeq 4$), predictions of Eq. (1.2) by Zsutty (32) and Eq. (1.3) by Placas and Regan (25) are the same. It is observed from Tables 3.7(a) and (b) that the test results are generally higher than the predictions of Eq. (1.4) by Rajagopalan and Ferguson (26) and Eq. (1.6) by Batchelor and Kwun (8), while lower than ACI Eq. (1.1) (6) and Eqs. (1.2) and (1.3) by Zsutty and Placas and Regan, respectively. These trends are, also, shown in Figs. 3.2a through 3.2d where $v_c/(f'_c)^{1/2}$ is plotted against the longitudinal reinforcement ratio, ρ_w, and in Figs. 3.3a through 3.3d where $v_c/(f'_c)^{1/3}$ is plotted against ρ_w. The unconservative nature of the ACI equation for ρ_w less than one percent (11,16,18,20,26) is borne out by the results shown in Figs. 3.2. The fact that the results are consistently lower than the predictions of Zsutty, Eq. (1.2) (normally an accurate predictor of v_c), may be because most of the test results he used for his analysis were for beams with high ratios of longitudinal reinforcement. The lower bond strength between the flexural steel and the concrete in the current tests may have, also, had an effect. Eq. (1.6) by Batchelor and Kwun is more conservative than Eq. (1.4) by Rajagopalan and Ferguson within the range of longitudinal reinforcement ratios used. Both equations are safe lower bounds, especially when based on the results obtained from the concrete and stirrup strain data. The results are, also, compared with Eq. (1.5) proposed by ACI-ASCE Committee 426 (4). Eq. (1.5) is adequate for beams in groups A and B, but unconservative for beams in group C.

3.3.2 Stirrup Effectiveness

The increase in shear stress above the cracking stress, v_c, to the nominal shear stress, v_n, is used as a measure of the effectiveness of the web reinforcement. This is in line with the philosophy of the ACI Building

Code, ACI 318-77 (6). This increment of stress, $(v_n - v_c)$, is plotted against the nominal shear stress resisted by stirrups, $\rho_v f_{vy}$, for each technique used to determine v_c in Figs. 3.4a through 3.4d. The regression analyses indicate strongly (correlation coefficients, $r \geq 0.90$) that the trend of the results for all four techniques can be represented by straight lines with slopes of about 1.50. For this study, web reinforcement is therefore 1.5 times as effective as predicted by the modified truss analogy with a 45 degree crack. The region defined by the 95 percent confidence limits is large ($\simeq \pm 30$ psi) because of the small number of tests. The following equation represents the average results of this study:

$$v_n - v_c = 1.5\ \rho_v f_{vy} + C \qquad (C = 2\text{-}8 \text{ psi}) \qquad (3.1)$$

Bresler and Scordelis (10) and Haddadin, Hong, and Mattock (14) found that the contribution of web reinforcement to nominal strength was 1.8 and 1.75 times $\rho_v f_{vy}$, respectively. These higher values may have been due to the high longitudinal reinforcement ratios used in these studies. Also, Haddadin, Hong and Mattock supported their test beams on the side faces of the web. This may have induced somewhat flatter cracks, which would have intercepted more web reinforcement. On the other hand, Bresler and Scordelis supported their test beams on the bottom, indicating that the support conditions may not be of significance.

Table 3.8 compares the measured nominal shear stresses with the nominal stress values predicted by the ACI Building Code (6), $v_n = v_c + \rho_v f_{vy}$, for beams with stirrups. This comparison shows that using either Eq. (1.1) or

the simplified expression for v_c ($v_c = 2\sqrt{f'_c}$), results in slightly unconservative predictions of the nominal shear strength for only two beams, A25 and B25. For v_c obtained from Eq. (1.1), beams A25 and B50 are, respectively, 0.3 percent and 1 percent stronger than the predicted nominal shear strength, while beams A75 and C75 are 19 percent and 14 percent stronger, respectively. These trends indicate that although the concrete contribution to shear strength is less than predicted by the ACI Code, the lower concrete strength is compensated by the higher effectiveness of stirrups. The trend of the data, also, suggests that there may be limiting values of ρ_w and $\rho_v f_{vy}$ below which Eq. (1.1) cannot safely be used to calculate nominal shear strength. With the small number of test results in this study, it is not reasonable to propose the limiting values of ρ_w and $\rho_v f_{vy}$, above which Eq. (1.1) can be used. Tests covering a wider range of ρ_w and $\rho_v f_{vy}$ values are needed in order to accurately establish lower limits for these quantities.

A study of the crack patterns shows that further cracking occurs after initial shear cracking for all beams with stirrups. This implies that the stirrups improve the ductility of the beams, thus providing warning of impending failure (even for $\rho_v f_{vy} < 50$ psi). Based on the data analyzed in this investigation, therefore, the ACI 318-77 Building Code equations for nominal shear strength appear to provide reasonable predictions of the strength of beams with values of $\rho_v f_{vy}$ greater than 32 psi (minimum for beams with stirrups in this study) and with ρ_w greater than one-half percent.

3.3.3 Other Considerations

Haddadin, Hong, and Mattock (14) found from their tests that the increase in nominal shear strength of beams with low shear-span to depth ratios (a/d), over the strength of beams with high a/d ratios, was larger

than predicted by the ACI Code. A significant effect of the a/d ratio on shear strength over a wide range of longitudinal reinforcement ratio, ρ_w, is, also, reported by Batchelor and Kwun (8). The influence of the a/d (or $\frac{M}{Vd}$) ratio implies that in low moment regions (where longitudinal reinforcement may be terminated), the concrete contribution to shear strength is increased. While the present provisions of the ACI Code underestimate this increase, Eq. (1.4) by Rajagopalan and Ferguson (26) and Eq. (1.6) by Batchelor and Kwun (8) do not account for it at all.

To insure adequate ductility, the ACI Code requires that a minimum amount of shear reinforcement ($\rho_v f_{vy}$ = 50 psi) be provided where the factored shear stress, v_u, exceeds one half of ϕv_c, in which ϕ is a strength reduction factor (=0.85 for shear). Figs. 3.2a through 3.2d show that $v_c = \sqrt{f'_c}$ (i.e., one-half of $v_c = 2\sqrt{f'_c}$)is a very safe lower bound for the results of this study. Thus, this requirement for minimum shear reinforcement appears to be adequate for the design of beams without stirrups. Even though Eqs. (1.4) and (1.6) provide conservative estimates for v_c, their application to the requirement for minimum shear reinforcement may not be justified in view of the fact that they do not reflect the effect of the a/d ratio on shear strength.

3.4 Recommendations

3.4.1 Beams with Stirrups

This study of reinforced concrete beams with low ratios of longitudinal reinforcement has shown that, the effectiveness of stirrups in resisting shear stresses is higher than predicted by the ACI Code, while the shear stress carried by concrete is lower. The results further show that the lower strength of the concrete is compensated by the higher effectiveness

of the stirrups. Proposed equations by Rajagopalan and Ferguson (26), Eq. (1.4), and Batchelor and Kwun (8), Eq. (1.6), are safe lower bounds for the test results. But these equations are overconservative unless the actual strength of the stirrups is utilized. Eq. (1.5) by ACI-ASCE Committee 426 is slightly unconservative for beams in group C. Present ACI procedures for determining nominal shear strength are recommended for beams with stirrups ($\rho_v f_{vy} \geq 50$ psi, $\rho_w \geq 0.5$ percent), until such time as the additional strength of stirrups is utilized.

3.4.2 Beams without Stirrups

The test results indicate clearly that the ACI Code equations for v_c are unconservative for ρ_w less than one percent. This was a special concern of ACI Committee 426 when they recommended the use of Eq. (1.5). MacGregor and Gergely (18) specifically cited regions where a portion of the longitudinal reinforcement is terminated. The Code, however, requires that for beams without stirrups, the shear stress carried by concrete must be no larger than one-half of ϕv_c. This requirement gives a safe lower bound prediction for the results of this and other studies (8, 26). Eqs. (1.4)-(1.6) do not take advantage of the effect of the a/d ratio, which tends to increase v_c at locations of low moment (e.g. where longitudinal reinforcement may be terminated). It is, therefore, recommended that the present ACI Code provisions be retained for beams without stirrups.

3.4.3 Future Work

Additional tests should be carried out on beams in which the longitudinal reinforcement is terminated in order to determine the effect of ρ_w on their behavior in shear. Reinforced concrete beams in real structures are

continuous. Only simply supported beams have been tested in this investigation. Additional tests, therefore, also need to be conducted on continuous beams to give a better understanding of the behavior of actual structures.

CHAPTER 4

SUMMARY AND CONCLUSIONS

4.1 Summary

The shear behavior of thirteen lightly reinforced concrete T-beams is investigated. Four methods are used to determine the shear cracking load of the beams: visual studies of crack patterns; strain gages applied to the compressive face of the concrete; frames fixed to the top of the beams with dial gages to measure specimen depth; and strain gages applied to the web reinforcement.

Load versus strain and load versus deflection data are presented. The results obtained from the four methods are compared with each other and with predictive equations developed by others (2,4,6,8,25,26,28).

A linear regression analysis is used to determine the effectiveness of web reinforcement, as measured by the increase in strength over the cracking load. Design recommendations are made for beams with and without stirrups.

4.2 Conclusions

1) Based on the analysis of the data, the compressive concrete strains and stirrup strains are reliable measures of the shear cracking load and are better measures than depth increase or cracking patterns.

2) A study of the data obtained from concrete and stirrup strains indicates that, "shear cracking" represents a change in the way that a beam carries load within the shear span. Stresses are redistributed and shear deflection increases markedly.

3) Eq. (1.4) by Rajagopalan and Ferguson (26) and Eq. (1.6) by Batchelor and Kwun (8) are conservative for the tests reported. Eq. (1.5) by the ACI-ASCE Committee 426 (4) is slightly unconservative for beams in group C. Predictions of the ACI Code equation, Eq. (1.1) (6), and Eqs. (1.2) and (1.3) by Zsutty (32) and Placas and Regan (25), respectively, predict cracking loads that are higher than the test results. The test results confirm the findings of other investigators (8,11,16,18,20,26), who found that the present ACI equations for v_c are unconservative for beams without stirrups having a longitudinal reinforcement ratio, ρ_w, less than one percent.

4) Web reinforcement is found to be 1.5 times as effective as predicted by the modified truss analogy with a 45 degree crack.

5) The present ACI procedures for determining nominal shear strength (with $\rho_v f_{vy} \geq 50$ psi) are recommended for beams with stirrups having ρ_w greater than one-half percent.

6) It is recommended that the present ACI procedure limiting the shear stress to one-half of the calculated concrete shear strength be retained for the design of beams without stirrups.

4.3 Recommendations for Future Study

1) Additional tests need to be carried out to verify the suitability of Eq. (1.5) (by the ACI-ASCE Committee 426) and Eq. (1.6) (by Batchelor and Kwun) for adoption in the ACI Building Code and subsequent use in design.

2) The effect of the longitudinal reinforcement ratio, ρ_w, on the shear behavior of beams in which longitudinal reinforcement

is terminated, should be determined.

3) Tests need to be conducted on continuous beams to give a better understanding of the behavior of actual structures.

REFERENCES

1. Acharya, D. N., "The Influence of Shear Force on the Ultimate Strength of Flexural Members in Reinforced Concrete," Thesis presented to the University of London, England, 1963, in partial fulfillment of the requirement for the degree of MSc.

2. ACI-ASCE Committee 326, "Shear and Diagonal Tension," Journal of the American Concrete Institute, Proc. Vol. 59, No. 1, Jan. 1962, pp. 1-30, No. 2, Feb., 1962, pp. 277-333, No. 3, March, 1962, pp. 353-395.

3. ACI-ASCE Committee 426, "The Shear Strength of Reinforced Concrete Members," Journal of the Structural Division, ASCE, Vol. 99, No. ST6, June, 1973, pp. 1091-1176.

4. ACI-ASCE Committee 426, "Suggested Revisions to Shear Provisions of ACI Code 318-71," Journal of the American Concrete Institute, Proc. Vol. 74, No. 9, Sept., 1977, pp. 458-469.

5. Al-Alusi, A. F., "Diagonal Tension Strength of Reinforced Concrete T-beams with Varying Shear Span," Journal of the American Concrete Institute, Proc. Vol. 28, No. 11, May, 1957, pp. 1067-1077.

6. American Concrete Institute, Building Code Requirements for Reinforced Concrete (ACI 318-77), Detroit, Michigan, Nov., 1977.

7. Armishaw, J. W., Brunni, N. G., and Neville, A. M., "Distribution of Shear in Rectangular Beams," Concrete and Construction Engineer, Vol. 61, No. 4, April 1966, pp. 119-130, No. 5, May, 1966, pp. 157-161, 183.

8. Batchelor, B. deV. and Kwun, M. K.,"Preliminary Report on the Shear Strength of Reinforced Concrete Beams without Web Reinforcement," Paper accepted for publication in the Journal of the American Concrete Institute.

9. Bower, J. E. and Viest, I. M., "Shear Strength of Reinforced Concrete Beams without Web Reinforcement," Journal of the American Concrete Institute, Proc. Vol. 57, No. 1, July, 1960, pp. 73-98.

10. Bresler, B. and Scordelis, A. C., "Shear Strength of Reinforced Concrete Beams," Journal of the American Concrete Institute, Proc. Vol. 60, No. 1, Jan., 1963, pp. 51-72.

11. Diaz, de Cossio, R. and Leora, S., Discussion of "Basic Facts Concerning Shear Failure," by G. N. J. Kani, Journal of the American Concrete Institute, Proc. Vol. 63, No. 12, Dec., 1966, pp. 1511-1514.

12. Diaz de Cossio, R. and Siess, C. P., "Behavior and Strength in Shear of Beams and Frames without Web Reinforcement," Journal of the

American Concrete Institute, Proc. Vol. 56, No. 8, Feb., 1960, pp. 695-730

13. Ferguson, P. M., "Some Implications of Recent Diagonal Tension Tests," Journal of the American Concrete Institute, Proc. Vol. 28, No. 2, Aug., 1956, pp. 157-172.

14. Haddadin, M. J., Hong Sheu-tien, and Mattock, A. H., "A Study of the Effectiveness of Web Reinforced Concrete Beams Subject to Axial Forces," Reinforced Concrete Research Council, Project No. 27, University of Washington at Seattle, Sept., 1969.

15. Jones, R., "Ultimate Strength of Reinforced Concrete Beams in Shear," Magazine of Concrete Research, Vol. 8, No. 23, Aug., 1956, pp. 69-84.

16. Kani, G. N. J., "Basic Facts Concerning Shear Failure," Journal of the American Concrete Institute, Proc. Vol. 63, No. 6, June, 1966, pp. 675-692.

17. Krefeld, W. J. and Thurston, C. W., "Studies of the Shear and Diagonal Tension Strength of Simply Supported Reinforced Concrete Beams," Columbia University, New York, N. Y., June, 1962.

18. MacGregor, J. G. and Gergely, P., "Suggested Revisions to ACI Building Code Clauses Dealing with Shear in Beams," Journal of the American Concrete Institute, Proc. Vol. 74, No. 10, Oct., 1977, pp. 493-500.

19. Mathey, R. G. and Watstein, G., "Strains in Beams Having Diagonal Cracks," Journal of the American Concrete Institute, Proc. Vol. 55, No. 6, Dec., 1958, pp. 717-728.

20. Mathey, R. G. and Watstein, G., "Shear Strength of Beams without Web Reinforcement Containing Deformed Bars of Different Yield Strengths," Journal of the American Concrete Institute, Proc. Vol. 60, No. 2, Feb., 1963, pp. 183-208.

21. Mattock, A. H., "Diagonal Tension Cracking in Concrete Beams with Axial Forces," Journal of the Structural Division, ASCE, Vol. 95, No. ST9, Proc. 6776, Sept., 1969, pp. 1877-1900.

22. Moody, K. G., Viest, I. M., Elstner, R. C., and Hognestad, E., "Shear Strength of Reinforced Concrete Beams," Journal of the American Concrete Institute, Proc. Vol. 51, Dec., 1954, pp. 317-332.

23. Morrow, J., and Viest, I. M., "Shear Strength of Reinforced Concrete Frame Members Without Web Reinforcement," Journal of the American Concrete Institute, Proc. Vol. 53, No. 9, March, 1957, pp. 833-870.

24. Olesen, S.O., Sozen, M. A., and Siess, C. P., "Investigation of Prestressed Reinforced Concrete for Highway Bridges, Part IV: Strength in Shear of Beams with Web Reinforcement," Engineering Experiment Station Bulletin 493, Vol. 64, No. 134, University of Illinois at Urbana-Champaign, July, 1967.

25. Placas, A. and Regan, P. E., "Shear Failures of Reinforced Concrete Beams," Journal of the American Concrete Institute, Proc. Vol. 68, Oct., 1971, pp. 763-773.

26. Rajagopalan, K. S. and Ferguson, P. M., "Exploratory Shear Tests Emphasizing Percentage of Longitudinal Steel," Journal of the American Concrete Institute, Proc. Vol. 65, No. 8, Aug., 1968, pp. 634-638.

27. Subbiah, K. and Smith, R. B. L., "Influence of Shear on Moment of Resistance of Reinforced Concrete Beams," Structural Engineer, Vol. 36, No. 11, Nov., 1958, pp. 377-384, Vol. 37, No. 6, June, 1959, pp. 192-194.

28. Taub, J. and Neville, A. M., "Resistance to Shear of Reinforced Concrete Beams," Journal of the American Concrete Institute, Proc. Vol. 32, No. 2, Aug., 1960, pp. 193-200, No. 3, Sept., 1960, pp. 315-336, No. 4, Oct., 1960, pp. 443-463.

29. Taylor, R., "Some Shear Tests on Reinforced Concrete Beams without Shear Reinforcement," Magazine of Concrete Research, Vol. 12, No. 36, Nov., 1960, pp. 145-154.

30. Taylor, R., "Permissible Shearing Stresses in Reinforced Concrete Beams," Concrete and Construction Engineer, Vol. 58, No. 9, Sept., 1963, pp. 359-363.

31. Van Der Berg, F. J., "Shear Strength of Reinforced Concrete Beams without Web Reinforcement," Journal of the American Concrete Institute, Proc. Vol. 59, No. 10, Oct., 1962, pp. 1467-1477, No. 11, Nov., 1962, pp. 1587-1600, No. 12, Dec., 1962, pp. 1849-1862.

32. Zsutty, T. C., "Beam Shear Strength Prediction by Analysis of Existing Data," Journal of the American Concrete Institute, Proc. Vol. 65, No. 11, Nov., 1968, pp. 943-951.

Table 2.1 BEAM PROPERTIES

All Beams - b_w = 7.5 ins., a = 61 ins., s = 7 ins.

Group A - A_s: 5-½" diameter strands = 0.765 in^2

Group B - A_s: 5-7/16" diameter strands = 0.575 in^2

Group C - A_s: 5-0.6" diameter strands = 1.085 in^2

Beam	d (ins)	a/d	ρ_w	ρ_v	$\rho_v f_{vy}$ (psi)
A00	15.54	3.92	0.0066	0.0	0.0
A25	15.38	3.97	0.0066	0.00052	31.8
A25a	15.26	4.00	0.0067	0.00052	31.8
A50	15.42	3.96	0.0066	0.00104	74.0
A50a	15.49	3.94	0.0066	0.00103	75.0
A75	15.56	3.92	0.0066	0.00157	97.0
B00	15.70	3.88	0.0049	0.0	0.0
B25	15.52	3.93	0.0049	0.00052	32.4
B50	15.39	3.96	0.0050	0.00104	76.2
C00	15.41	3.96	0.0094	0.0	0.0
C25	15.33	3.98	0.0095	0.00052	32.4
C50	15.47	3.94	0.0094	0.00104	76.2
C75	15.57	3.92	0.0093	0.00157	103.0

TABLE 2.2 CONCRETE PROPERTIES

Beam	Mix Proportions by weight[1]	Slump (in)	Air Content (%)	f'_c[2] (psi)	f_r[3] (psi)	Age at testing (days)
A00	1.0:0.57:3.19:3.21	1.50	5.0	4740	667	7
A25	1.0:0.57:3.19:3.21	1.00	5.5	4720	496	16
A25a	1.0:0.52:2.86:2.88	0.75	2.0	4790	664	4
A50	1.0:0.57:3.19:3.21	1.50	6.5	3810	480	18
A50a	1.0:0.52:2.86:2.88	1.75	4.5	4060	512	6
A75	1.0:0.57:3.19:3.21	1.25	3.9	4670	550	6
B00	1.0:0.57:3.19:3.21	0.75	4.5	4640	567	11
B25	1.0:0.57:3.19:3.21	1.25	3.8	4470	525	18
B50	1.0:0.57:3.19:3.21	1.50	6.0	4390	585	13
C00	1.0:0.52:2.86:2.88	0.50	4.4	4270	604	3
C25	1.0:0.52:2.86:2.88	0.75	3.3	4100	462	5
C50	1.0:0.45:2.37:2.37	1.25	6.5	4300	650	3
C75	1.0:0.52:2.86:2.88	1.00	3.2	4260	585	9

(1) Ratio of cement to water to fine aggregate to coarse aggregate, based on air content of 5%.

(2) f'_c - compressive strengtn from 6 x 12 inch cylinders.

(3) f_r - modulus of rupture from 6 x 6 x 21 inch flexural specimens, third point loading on an 18 inch span.

TABLE 2.3 REINFORCEMENT PROPERTIES

Beams	Bar Size	Yield Point (ksi)	Ultimate strength (ksi)
Group A	1/2" dia. strand	259.5	279.4
Group B	7/16" dia. strand	255.7	284.3
Group C	0.6" dia. strand	256.0	278.7
All Beams	#3	69.6	116.4
All Beams	#4	66.2	108.0
A25, A25a	0.132" dia. stirrup	61.0	78.8
B25,C25	0.132" dia. stirrup	62.1	81.8
A50	0.186" dia. stirrup	71.4	78.2
A50a	0.186" dia. stirrup	72.5	81.0
B50,C50	0.186" dia. stirrup	73.6	81.0
A75	0.229" dia. stirrup	61.9	78.7
C75	0.229" dia. stirrup	65.7	81.3

TABLE 2.4 MEASURED NOMINAL SHEAR STRENGTH

Beam	V_n(test) (kips)	v_n (test) (psi)
A00	14.56	126
A25	19.27	167
A25a	20.77	182
A50	25.95	225
A50a	24.66	213
A75	31.97	275
B00	16.03	136
B25	17.67	153
B50	24.05	208
C00	13.27	115
C25	18.65	166
C50	30.15	261
C75	31.02	266

TABLE 3.1 SHEAR CRACKING LOADS DETERMINED FROM CRACK PATTERNS

Beam	V_c (kips)				V_c (kips)	v_c (psi)
	left side		right side		lowest values	
	at N.A.	above N.A.	at N.A.	above N.A.	crack at N.A.	definition
A00	14.1	12.9	10.3	12.9	10.3	89
A25	15.5	15.5	12.9	10.3	12.9	112
A25a	14.4	13.1	13.1	10.5	13.1	114
A50	14.1	14.1	14.1	14.1	14.1	122
A50a	13.2	10.6	13.2	10.6	13.2	114
A75	16.1	12.9	12.9	12.9	12.9	110
B00	11.7	7.9	11.7	7.9	11.7	100
B25	13.3	13.3	12.1	13.3	12.1	104
B50	13.9	13.9	11.3	11.3	11.3	98
C00	13.4	13.4	8.3	10.9	8.3	73
C25	13.2	13.2	13.2	13.2	13.2	114
C50	13.1	13.1	14.4	14.4	13.1	115
C75	10.9	10.9	10.9	13.4	10.9	94

TABLE 3.2 SHEAR CRACKING LOADS DETERMINED FROM CONCRETE STRAIN DATA

Beams	V_c (kips)						V_c(kips)	v_c(psi)
	Gages on left side			Gages on right side			Lowest values	
	#17	#18	#19	#14	#15	#16		
A00	*	12.9	12.9	*	12.9	12.9	12.9	111
A25	*	*	*	*	*	12.9	12.9	112
A25a	14.4	14.4	14.4	- -	13.1	13.1	13.1	114
A50	13.5	13.5	- -	- -	- -	13.5	13.5	116
A50a	13.2	13.2	13.2	13.2	- -	13.2	13.2	114
A75	14.2	15.5	- -	16.1	13.6	12.9	12.9	110
B00	10.5	11.7	10.5	- -	10.5	12.5	10.5	89
B25	10.8	10.8	- -	12.1	- -	12.1	10.8	93
B50	11.3	11.3	11.3	11.3	11.3	11.3	11.3	98
C00	10.9	10.9	10.9	10.9	10.9	10.9	10.9	96
C25	*	13.2	13.2	13.2	*	*	13.2	114
C50	14.4	13.1	13.1	14.4	13.1	13.1	13.1	115
C75	*	13.4	*	*	13.4	*	13.4	116

NOTES: - - Bad gage
* Gage was not installed.

TABLE 3.3 SHEAR CRACKING LOADS DETERMINED FROM STIRRUP STRAIN DATA

Beam	V_c (kips)								V_c(kips) Lowest values	v_c(psi)
	Gages on left side				Gages on right side					
	#5	#6	#7	#8	#9	#10	#11	#12		
A25	15.1	- -	15.1	- -	12.9	13.4	16.8	16.8	12.9	112
A25a	13.8	15.0	14.4	15.7	15.7	13.1	13.1	13.1	13.1	114
A50	16.1	12.9	13.5	15.4	15.4	12.9	- -	12.9	12.9	112
A50a	15.2	- -	14.5	13.2	14.5	15.8	15.8	13.2	13.2	114
A75	14.2	12.9	16.1	16.7	15.5	15.5	16.7	13.6	12.9	110
B25	10.8	13.3	12.1	13.3	- -	- -	10.8	- -	10.8	93
B50	15.1	12.5	11.3	13.9	18.4	13.9	13.9	16.5	11.3	98
C25	13.2	13.2	13.2	15.6	13.2	10.6	13.2	13.2	13.2	115
C50	13.1	13.1	13.1	13.1	13.1	- -	- -	13.1	13.1	115
C75	13.4	14.7	13.4	14.7	16.0	14.7	14.7	13.4	13.4	116

NOTE: - - Bad gage

TABLE 3.4 SHEAR CRACKING LOADS DETERMINED FROM DEPTH INCREASE
BEAMS WITH WEB REINFORCEMENT

Beam	V_c (kips)				V_c(kips)	v_c(psi)
	Frames on left side		Frames on right side		Lowest values	
	#1	#2	#3	#4		
A25	14.3	14.3	14.3	15.5	14.3	124
A25a	13.1	13.1	13.1	13.1	13.1	114
A50	14.1	14.8	15.4	16.1	14.1	122
A50a	15.2	15.2	13.2	13.2	13.2	114
A75	13.6	17.6	17.6	15.6	13.6	116
B25	13.3	13.3	- -	14.4	13.3	114
B50	15.1	15.1	16.5	15.1	15.1	131
C25	13.2	13.2	13.2	13.2	13.2	115
C50	13.1	13.1	13.1	13.1	13.1	115
C75	14.7	13.4	14.7	13.4	13.4	116

NOTE: - - No reading on dial gage.

TABLE 3.5 SHEAR CRACKING LOADS AND STRESSES

Beam \ Method	Crack Patterns		Stirrup Strain		Concrete Strain		Depth Increase	
	V_c (kips)	v_c (psi)	V_c (kips)	v_c (psi)	V_c (kips)	v_c (psi)	V_c (kips)	v_c (psi)
A00	10.3	89	- -	- -	12.9	111	- -	- -
A25	12.9	112	12.9	112	12.9	112	14.3	124
A25a	13.1	114	13.1	114	13.1	114	13.1	114
A50	14.1	122	12.9	112	13.5	116	14.1	122
A50a	13.2	114	13.2	114	13.2	114	13.2	114
A75	12.9	110	12.9	110	12.9	110	13.6	116
B00	11.7	100	- -	- -	10.5	89	- -	- -
B25	12.1	104	10.8	93	10.8	93	13.3	114
B50	11.3	98	11.3	98	11.3	98	15.1	131
C00	8.3	73	- -	- -	10.9	96	- -	- -
C25	13.2	114	13.2	115	13.2	114	13.2	115
C50	13.1	115	13.1	115	13.1	115	13.1	115
C75	10.9	94	13.4	116	13.4	116	13.4	116

TABLE 3.6 CALCULATED SHEAR CRACKING STRESSES

Beam	Shear cracking stress, v_c (psi)				
	Eq. (1.1)[1]	Eqs. (1.2&1.3)[2]	Eq. (1.4)[3]	Eq. (1.5)[4]	Eq. (1.6)[5]
A00	135	118	101	110	91
A25	135	118	100	109	91
A25a	136	118	101	111	92
A50	122	109	90	98	82
A50a	125	112	93	101	84
A75	134	117	100	109	90
B00	133	99	89	95	77
B25	130	105	87	93	76
B50	129	104	86	93	76
C00	130	128	114	126	108
C25	128	126	112	124	105
C50	131	128	115	126	108
C75	130	128	114	125	107

(1) Equation (1.1) according to ACI Building Code (ACI 318-77).
(2) Equation (1.2) by Zsutty and (1.3) by Placas and Regan.
(3) Equation (1.4) by Rajagopalan and Ferguson.
(4) Equation (1.5) by ACI-ASCE Committee 426
(5) Equation (1.6) by Batchelor and Kwun.

Table 3.7a Comparison of Test and Calculated Shear Cracking Stresses

Beam	v_c(psi)(Test)[1]	Measured v_c from Concrete Strain: $\frac{v_c(\text{Test})}{v_c(\text{Eq.1.1})}$	$\frac{v_c(\text{Test})}{v_c(\text{Eq.1.2 \&1.3})}$	$\frac{v_c(\text{Test})}{v_c(\text{Eq.1.4})}$	$\frac{v_c(\text{Test})}{v_c(\text{Eq.1.5})}$	$\frac{v_c(\text{Test})}{v_c(\text{Eq.1.6})}$	v_c(psi)(Test)[2]	Measured v_c from Crack Patterns: $\frac{v_c(\text{Test})}{v_c(\text{Eq.1.1})}$	$\frac{v_c(\text{Test})}{v_c(\text{Eq.1.2 \&1.3})}$	$\frac{v_c(\text{Test})}{v_c(\text{Eq.1.4})}$	$\frac{v_c(\text{Test})}{v_c(\text{Eq.1.5})}$	$\frac{v_c(\text{Test})}{v_c(\text{Eq.1.6})}$
A00	111	0.82	0.94	1.10	1.01	1.22	89	0.66	0.75	0.88	0.81	0.98
A25	112	0.83	0.95	1.12	1.02	1.23	112	0.83	0.95	1.12	1.02	1.23
A25a	114	0.84	0.97	1.13	1.03	1.24	114	0.84	0.97	1.13	1.03	1.24
A50	116	0.95	1.06	1.29	1.18	1.41	122	1.00	1.12	1.36	1.24	1.49
A50a	114	0.91	1.02	1.23	1.12	1.36	114	0.91	1.02	1.23	1.12	1.36
A75	110	0.82	0.94	1.10	1.01	1.22	110	0.82	0.94	1.10	1.01	1.22
B00	89	0.67	0.90	1.00	0.94	1.16	100	0.75	1.01	1.12	1.06	1.30
B25	93	0.72	0.89	1.07	1.00	1.22	104	0.80	0.99	1.20	1.12	1.37
B50	98	0.76	0.94	1.14	1.06	1.29	98	0.76	0.94	1.14	1.06	1.29
C00	96	0.74	0.75	0.84	0.76	0.89	73	0.56	0.57	0.64	0.58	0.68
C25	114	0.89	0.90	1.02	0.92	1.09	114	0.89	0.90	1.02	0.92	1.09
C50	115	0.88	0.90	1.00	0.91	1.06	115	0.88	0.90	1.00	0.91	1.06
C75	116	0.89	0.91	1.02	0.93	1.08	94	0.72	0.73	0.82	0.75	0.88
Mean		0.82	0.93	1.08	0.99	1.19		0.80	0.91	1.06	0.97	1.17
Standard Deviation, σ		0.082	0.073	0.113	0.105	0.137		0.114	0.145	0.189	0.176	0.223
Coeff. of Variation, V_e		10%	7.8%	10.4%	10.6%	11.5%		14.2%	15.9%	17.8%	18.2%	19.1%

Table 3.7b Comparison of Test and Calculated Shear Cracking Stresses

Beam	Measured v_c from Stirrup Strain					Measured v_c from Depth Increase					
	v_c(psi)$_{(Test)}$[1]	$\frac{v_c(Test)}{v_c(Eq.1.1)}$	$\frac{v_c(Test)}{v_c(Eq.1.2\ \&1.3)}$	$\frac{v_c(Test)}{v_c(Eq.\ 1.4)}$	$\frac{v_c(Test)}{v_c(Eq.1.5)}$	$\frac{v_c(Test)}{v_c(Eq.1.6)}$	v_c(psi)$_{(Test)}$[2]	$\frac{v_c(Test)}{v_c(Fq.1.1)}$	$\frac{v_c(Test)}{v_c(Eq.1.2\ \&1.3)}$	$\frac{v_c(Test)}{v_c(Eq.1.4)}$	$\frac{v_c(Test)}{v_c(Ea.1.5)}$	$\frac{v_c(Test)}{v_c(Eq.1.6)}$
A25	112	0.83	0.95	1.12	1.02	1.23	124	0.92	1.05	1.24	1.13	1.36
A25a	114	0.84	0.97	1.13	1.03	1.24	114	0.84	0.97	1.13	1.03	1.24
A50	112	0.92	1.03	1.24	1.14	1.37	122	1.00	1.12	1.36	1.24	1.49
A50a	114	0.91	1.02	1.23	1.12	1.36	114	0.91	1.02	1.23	1.12	1.36
A75	110	0.82	0.94	1.10	1.01	1.22	116	0.87	0.99	1.16	1.07	1.29
B25	93	0.72	0.89	1.07	1.00	1.22	114	0.88	1.09	1.31	1.23	1.50
B50	98	0.76	0.94	1.14	1.06	1.29	131	1.02	1.26	1.52	1.41	1.72
C25	115	0.90	0.91	1.02	0.93	1.10	115	0.90	0.91	1.03	0.93	1.10
C50	115	0.88	0.90	1.00	0.91	1.06	115	0.88	0.90	1.00	0.91	1.06
C75	116	0.89	0.91	1.02	0.93	1.08	116	0.89	0.91	1.02	0.93	1.08
Mean		0.85	0.95	1.11	1.02	1.22		0.91	1.02	1.20	1.10	1.32
Standard Deviation, σ		0.067	0.048	0.083	0.078	0.109		0.057	0.113	0.167	0.161	0.212
Coeff. of Variation, V_e		7.9%	5%	7.5%	7.7%	8.9%		6.3%	11.1%	13.9%	14.6%	16.1%

TABLE 3.8 COMPARISON OF TEST AND CALCULATED NOMINAL SHEAR STRESSES

Beam	v_n(test) (psi)	$v_n = v_c + \rho_v f_{vy}$ (1) (psi)	$\frac{v_n\ (test)}{v_n^{(1)}}$	$v_n = v_c + \rho_v f_{vy}$ (2) (psi)	$\frac{v_n\ (test)}{v_n^{(2)}}$
A00	126	135.0	0.93	137.7	0.91
A25	167	166.5	1.003	169.2	0.99
A25a	182	163.3	1.11	170.2	1.07
A50	225	195.4	1.15	197.5	1.14
A50a	213	200.3	1.06	202.4	1.05
A75	275	231.1	1.19	233.7	1.18
B00	136	132.6	1.02	136.2	1.00
B25	153	162.5	0.94	166.1	0.92
B50	208	205.2	1.01	208.7	1.00
C00	115	130.1	0.88	130.7	0.88
C25	166	160.0	1.04	160.5	1.03
C50	261	206.8	1.26	207.3	1.26
C75	266	232.9	1.14	233.5	1.14

(1) $v_c = 1.9\sqrt{f'_c} + 2500\rho_w V_u d/M_u \leq 3.5\sqrt{f'_c}$ (1.1)

(2) $v_c = 2\sqrt{f'_c}$

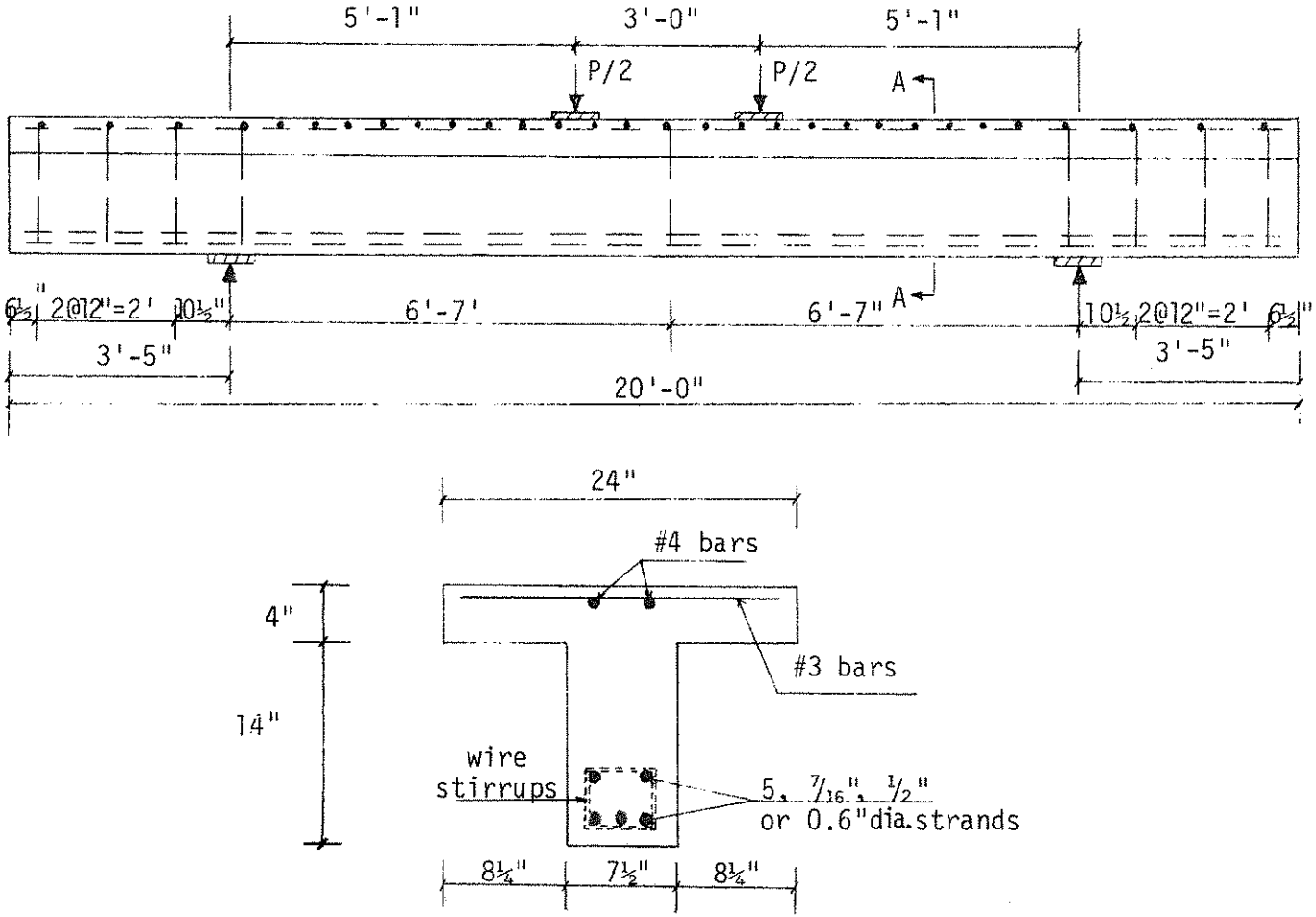

SECTION A-A

Figure 2.1. Beams without Stirrups

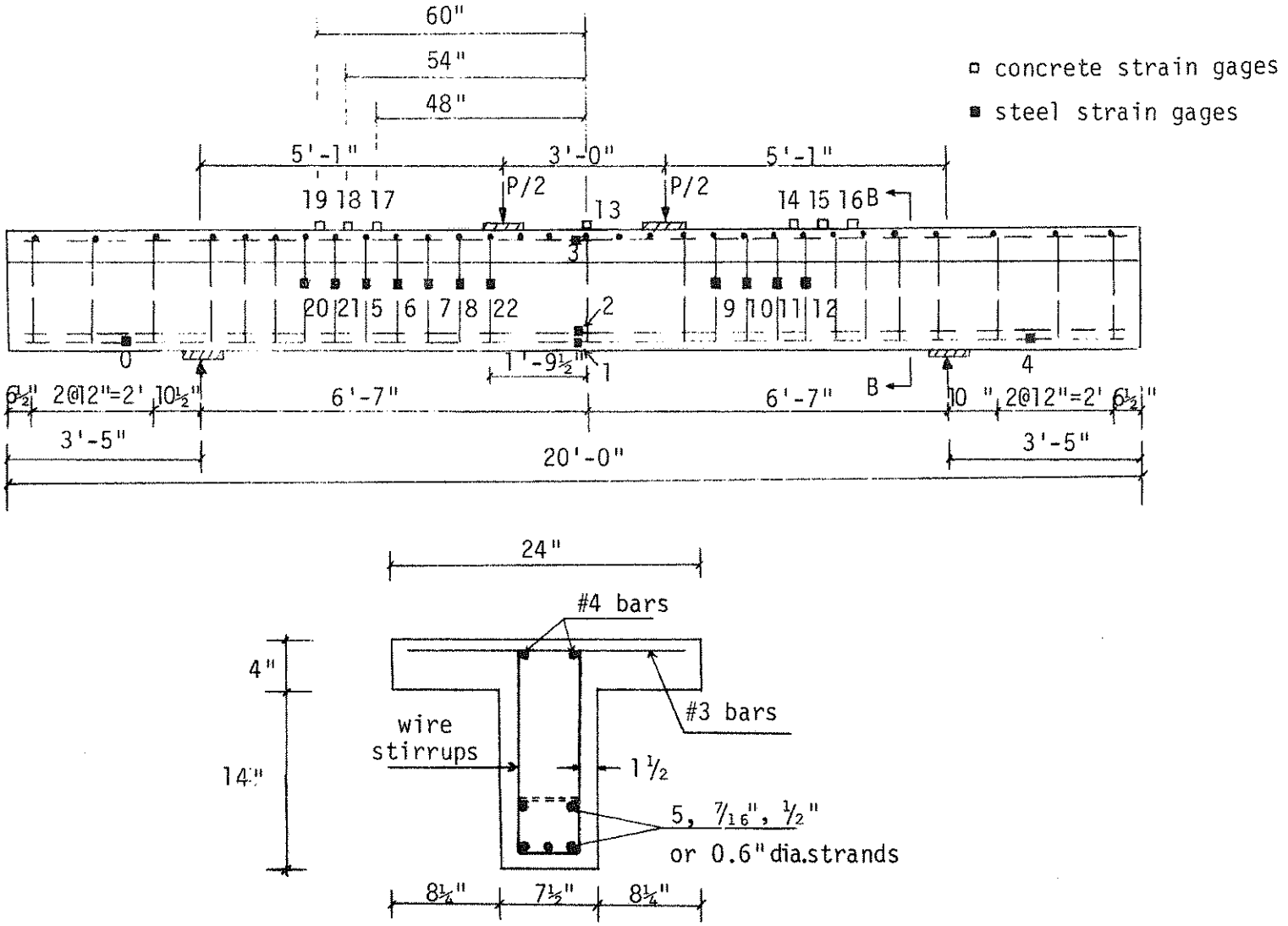

SECTION B-B

Figure 2.2. Beams with Stirrups

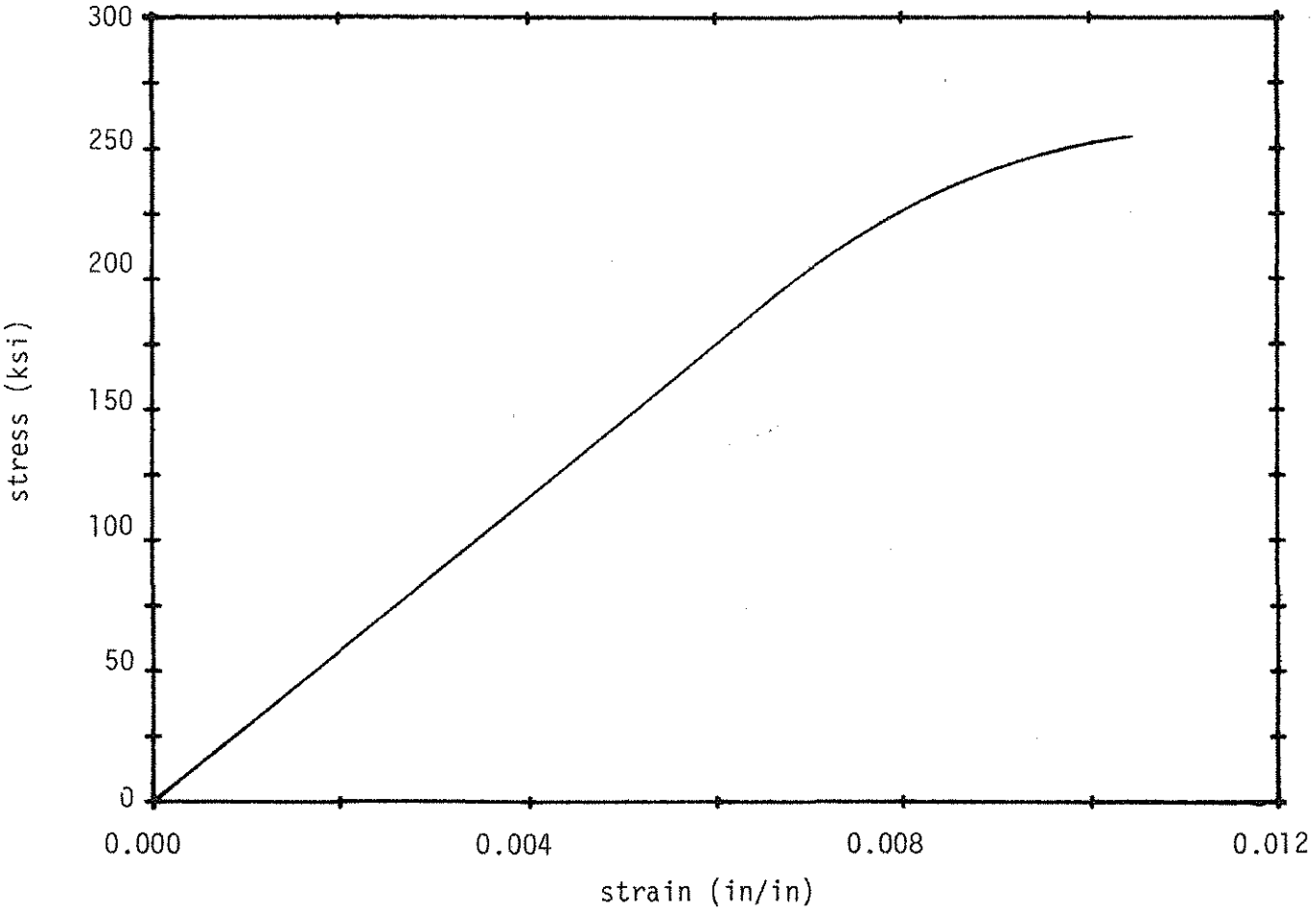

Figure 2.3. Stress-Strain Curve for 7/16 Inch Diameter Strand.

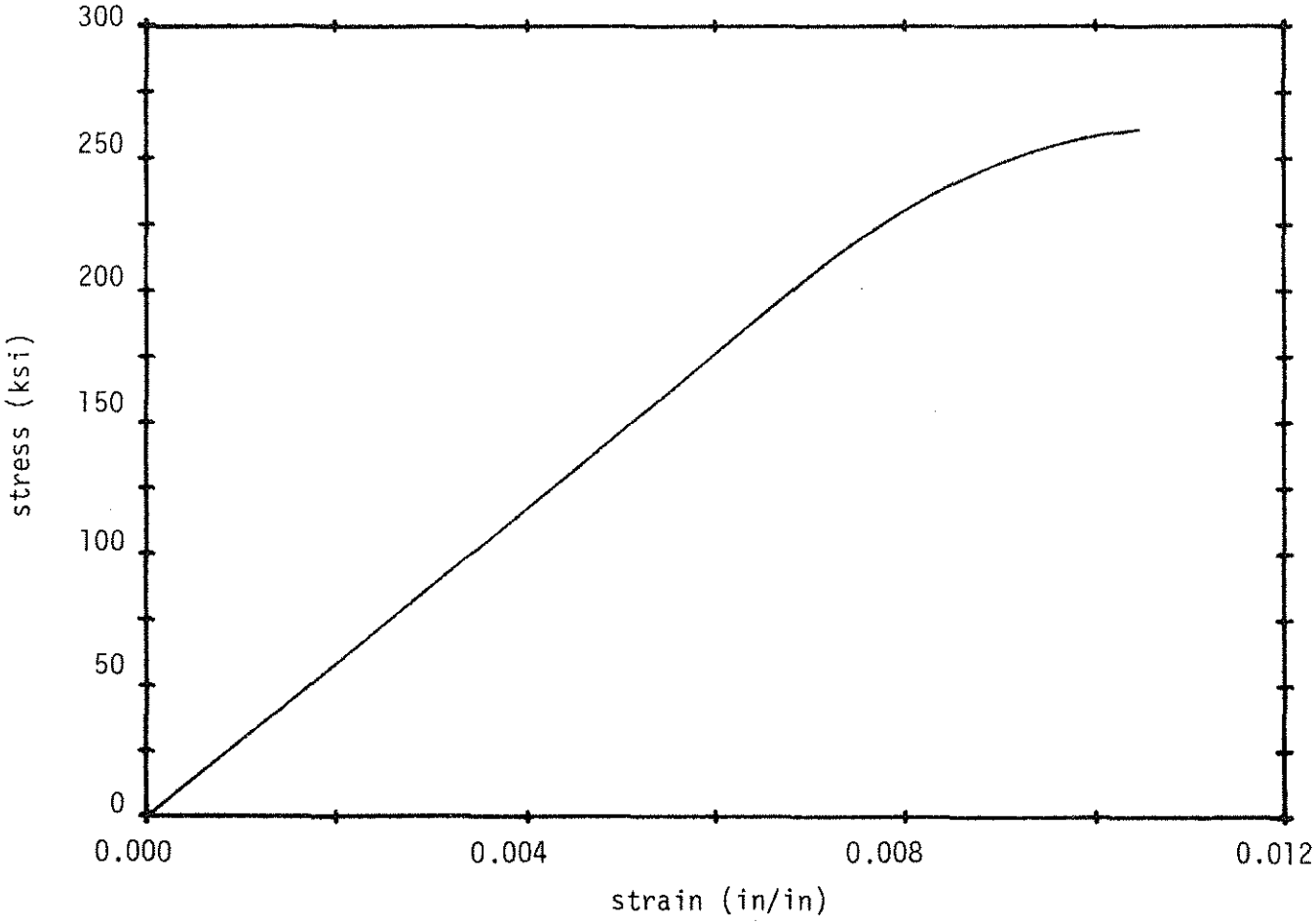

Figure 2.4. Stress-Strain Curve for 1/2 Inch Diameter Strand.

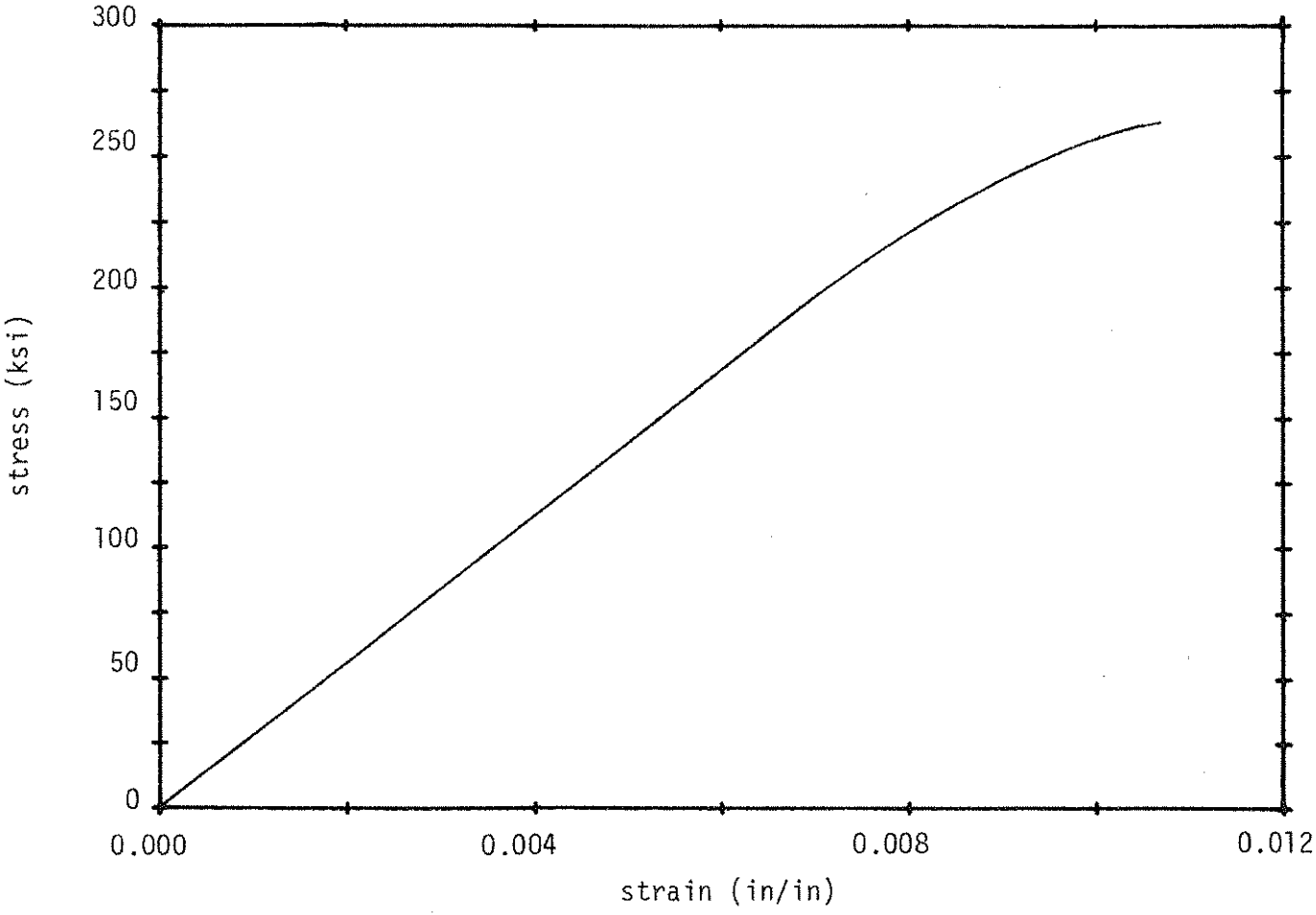

Figure 2.5. Stress-Strain Curve for 0.6 Inch Diameter Strand

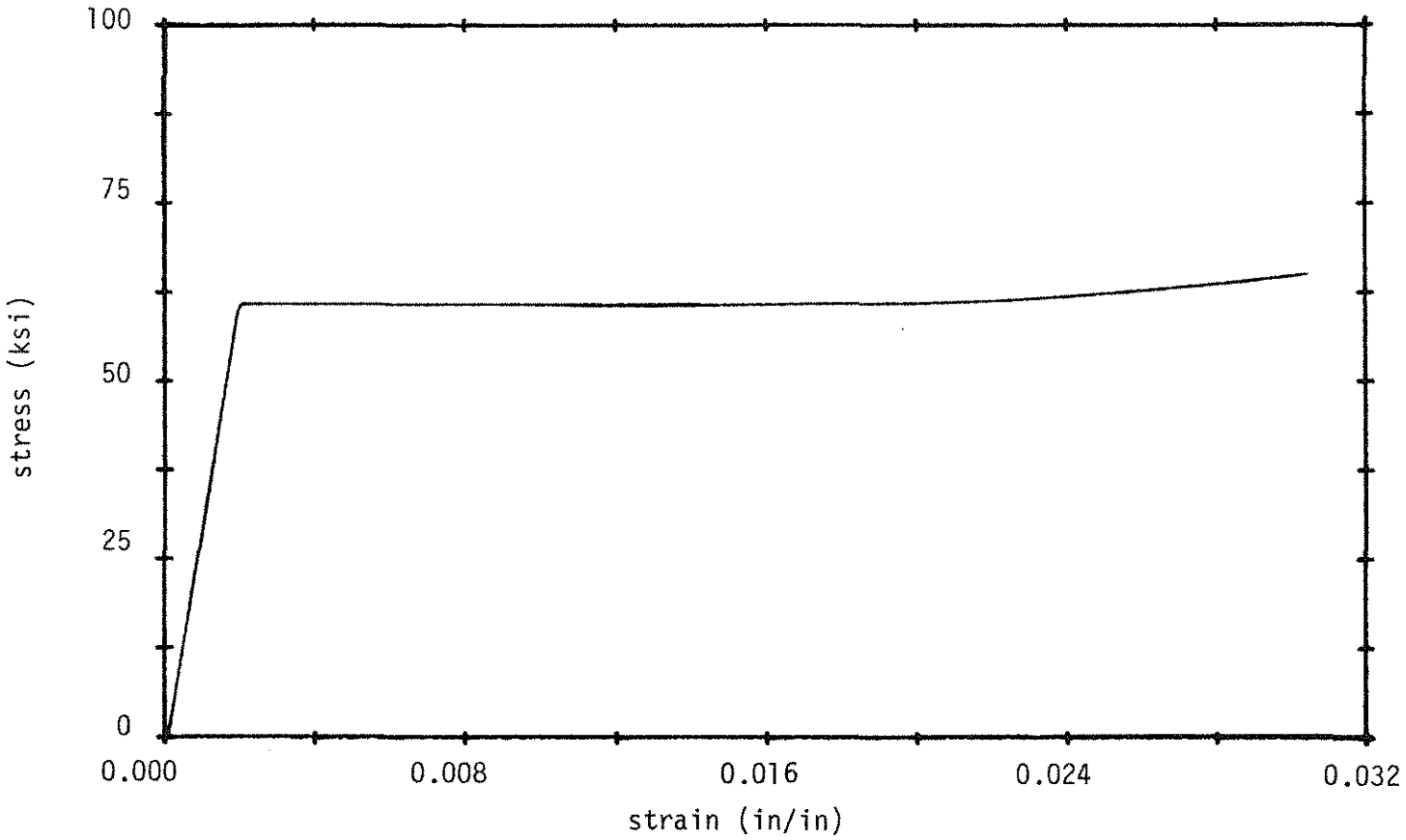

Figure 2.6. Typical Stress-Strain Curve for Series "25" Stirrups.

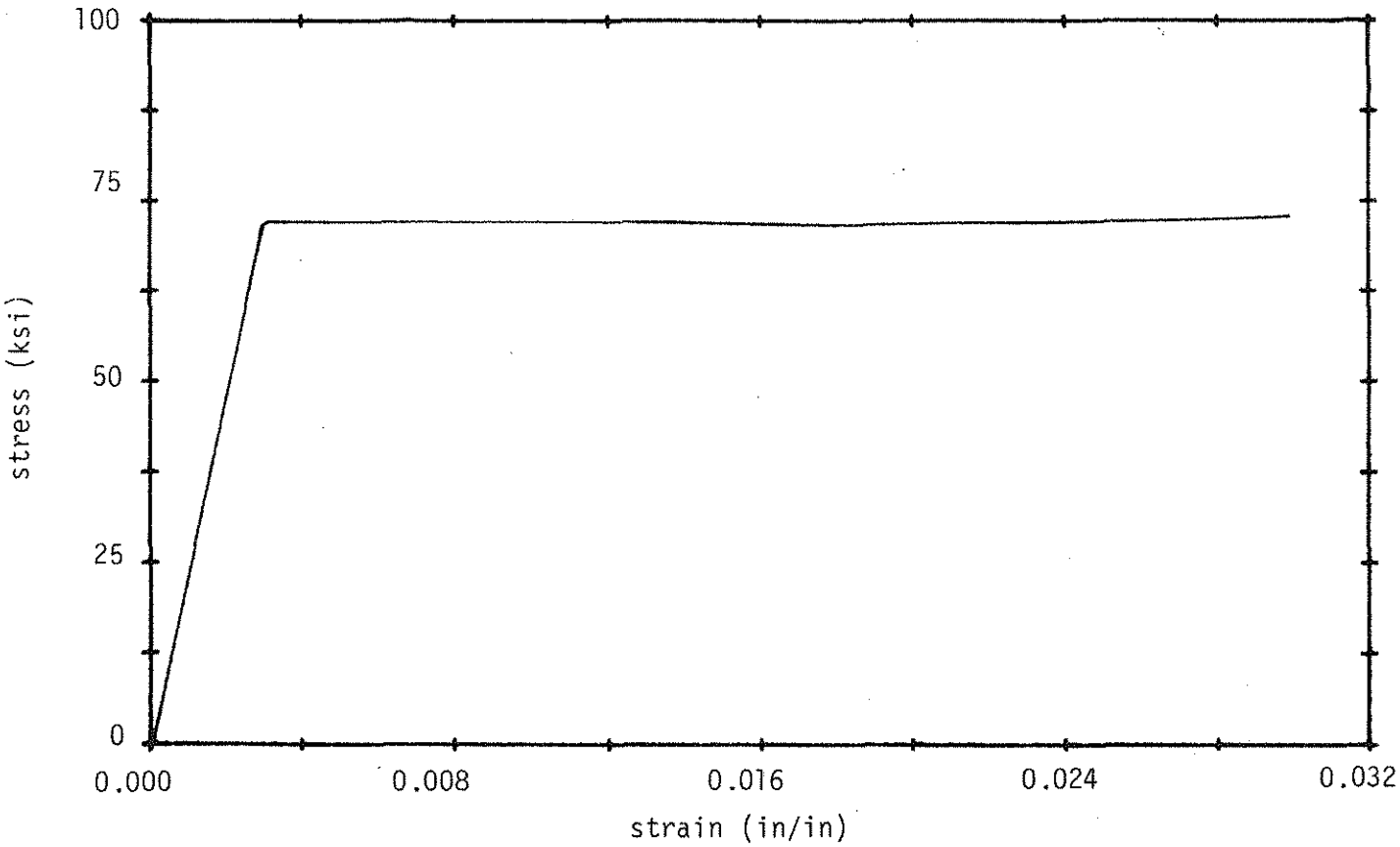

Figure 2.7. Typical Stress-Strain Curve for Series "50" Stirrups.

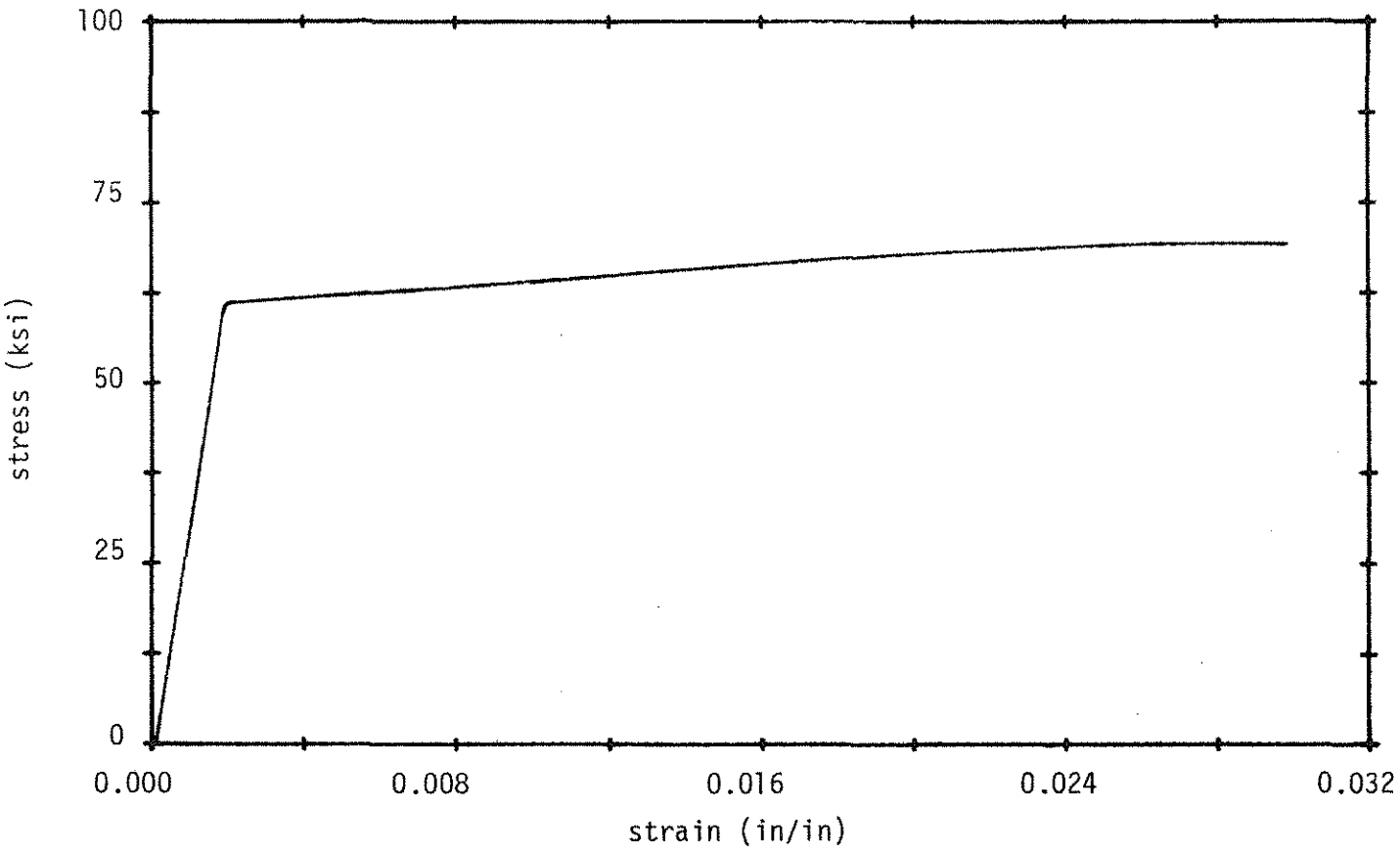

Figure 2.8. Typical Stress-Strain Curve for Series "75" Stirrups.

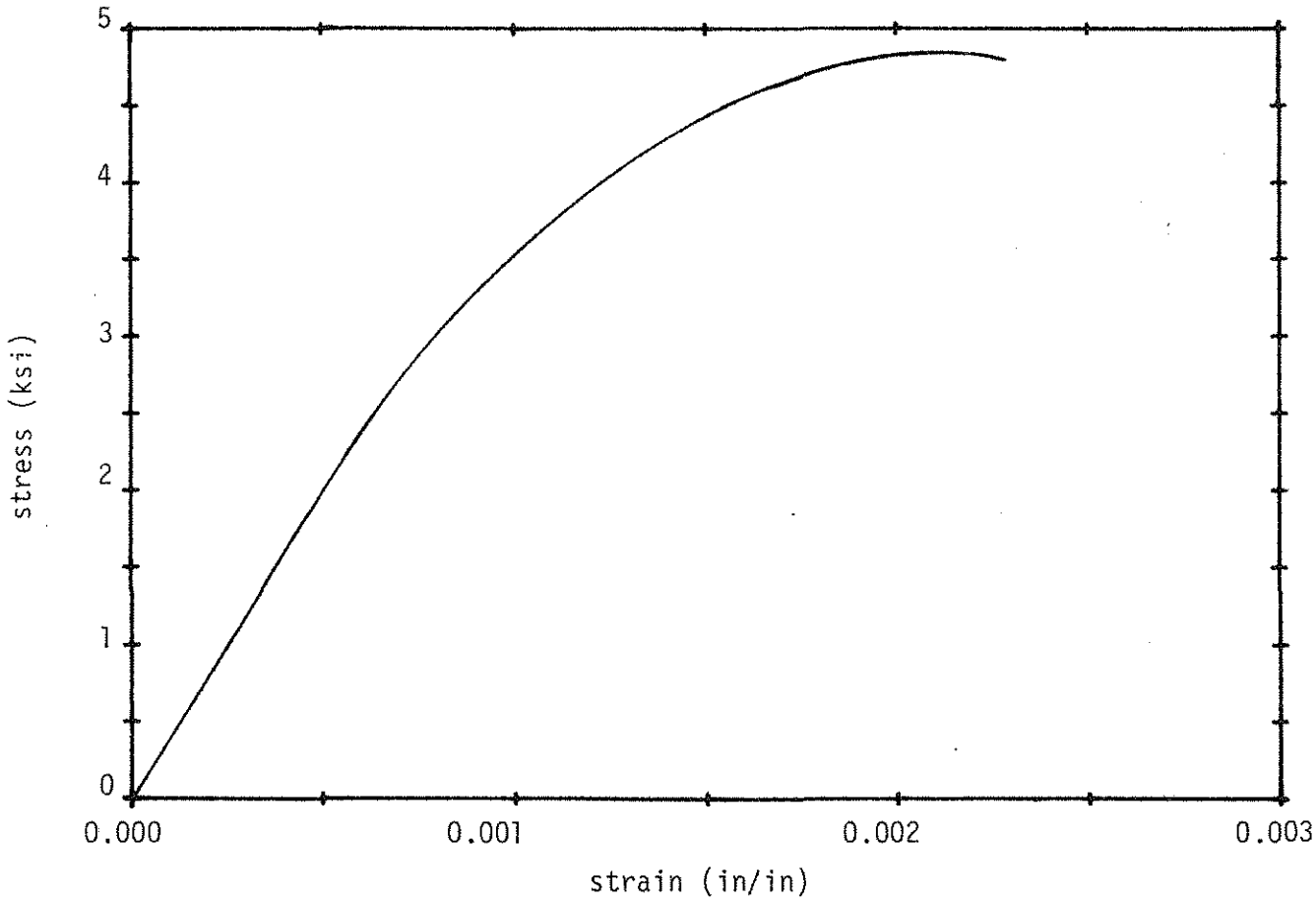

Figure 2.9. Concrete Stress-Strain Curve.

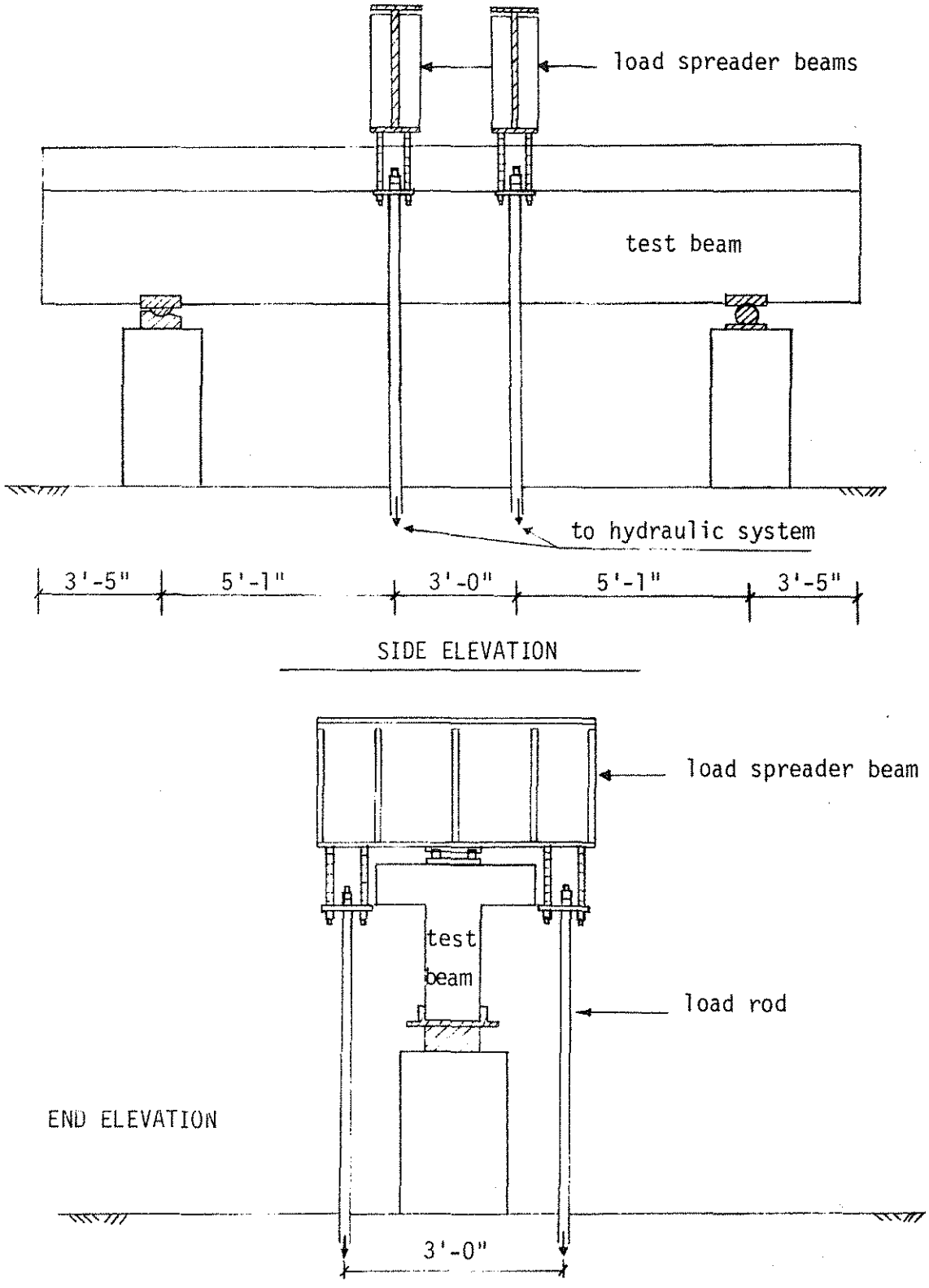

Figure 2.10. Loading Arrangement.

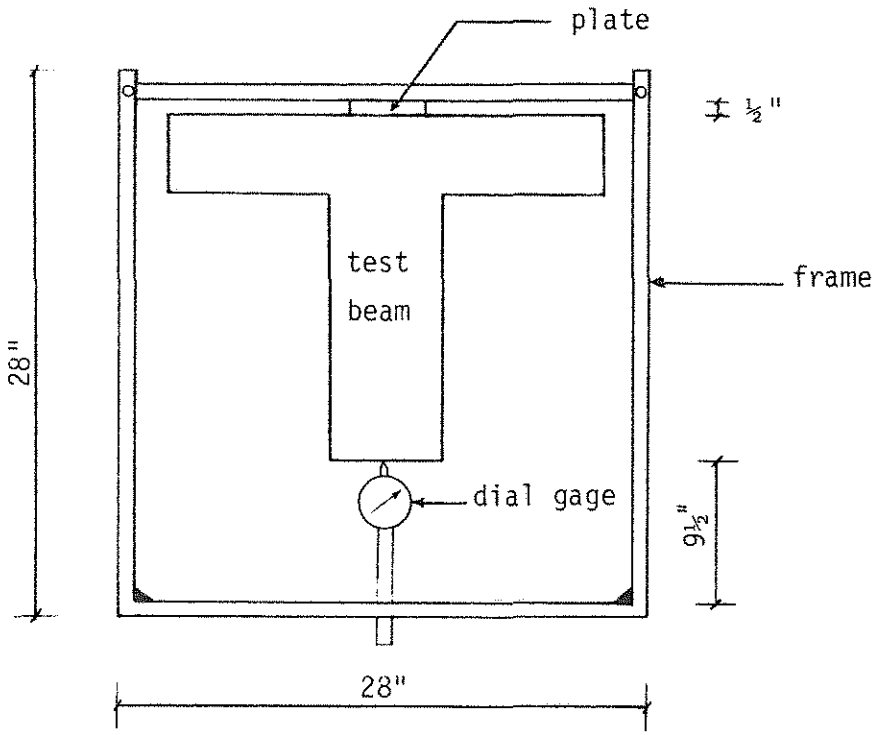

Figure 2.11. Beam-Frame Arrangement.

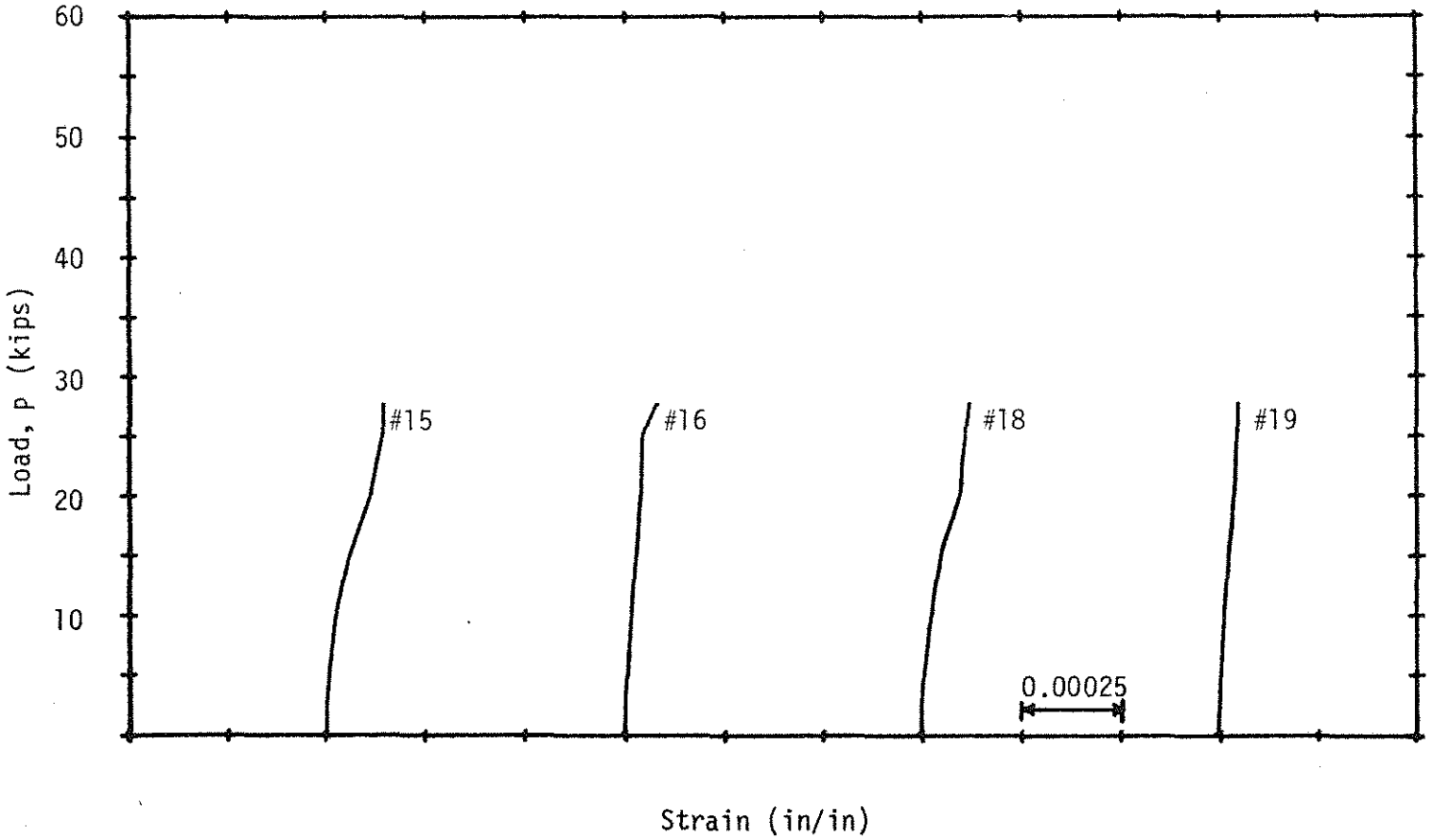

Figure 2.12. Load-Concrete Strain Diagram; Beam A00.

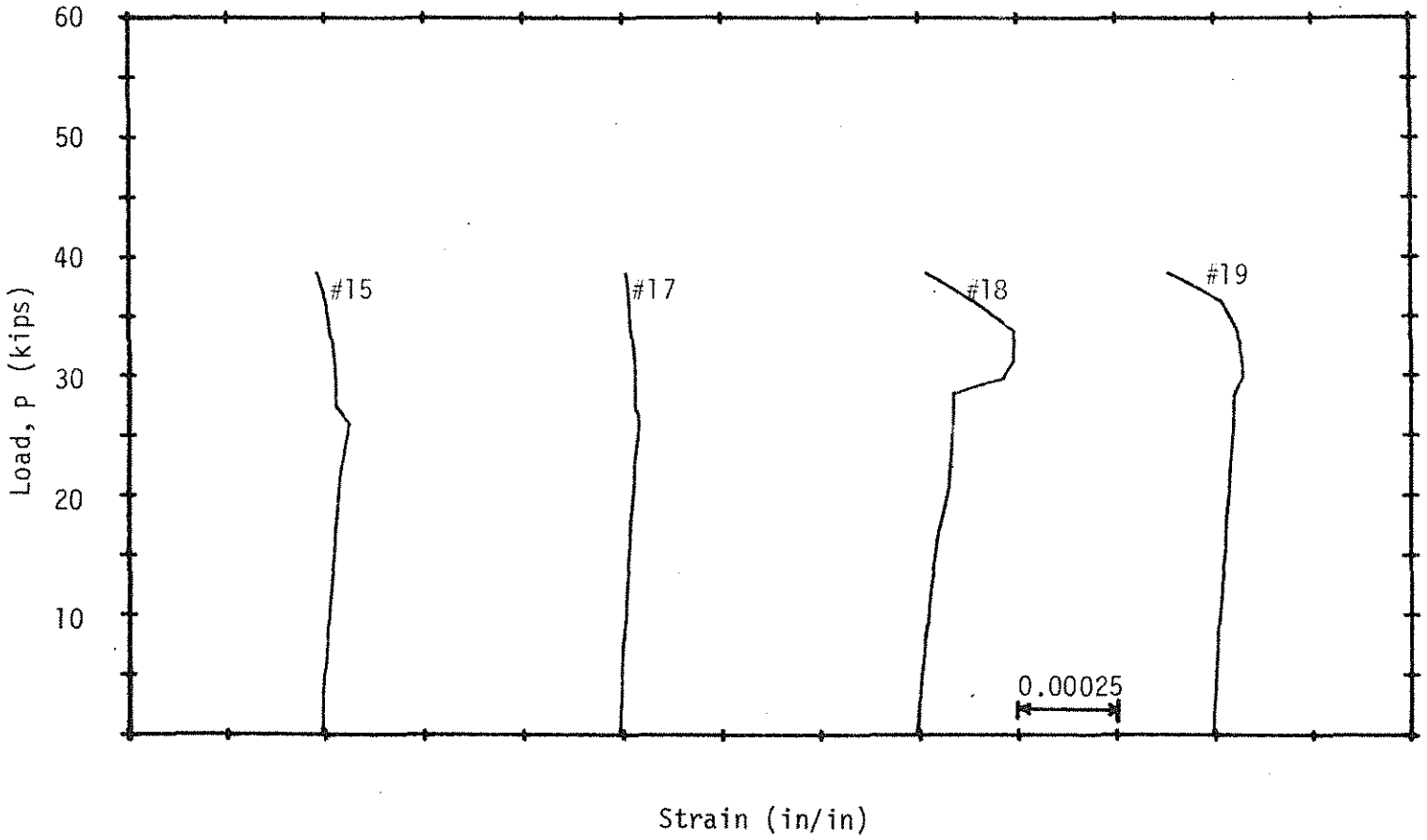

Figure 2.13. Load-Concrete Strain Diagram; Beam A25a.

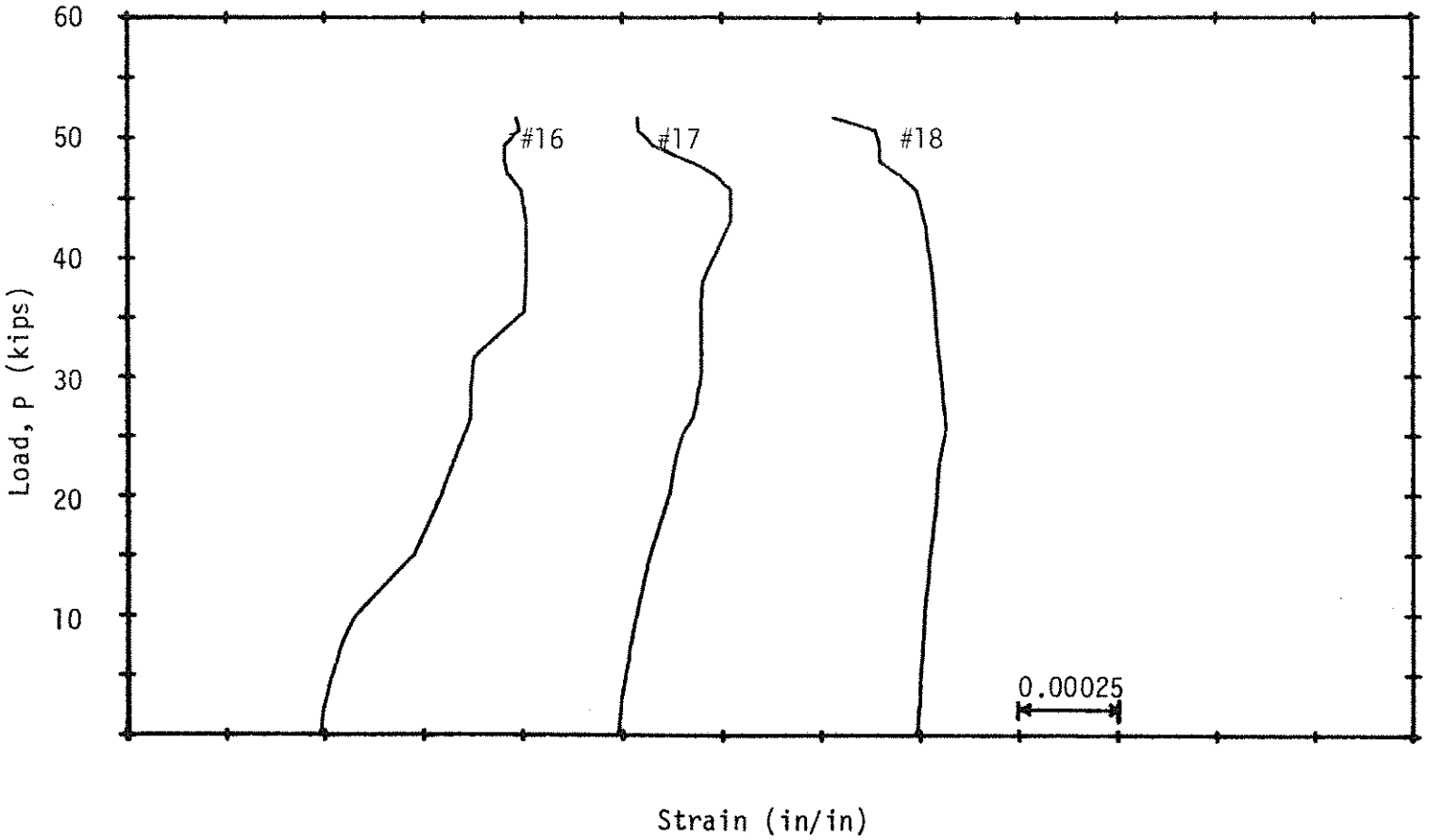

Figure 2.14. Load-Concrete Strain Diagram; Beam A50.

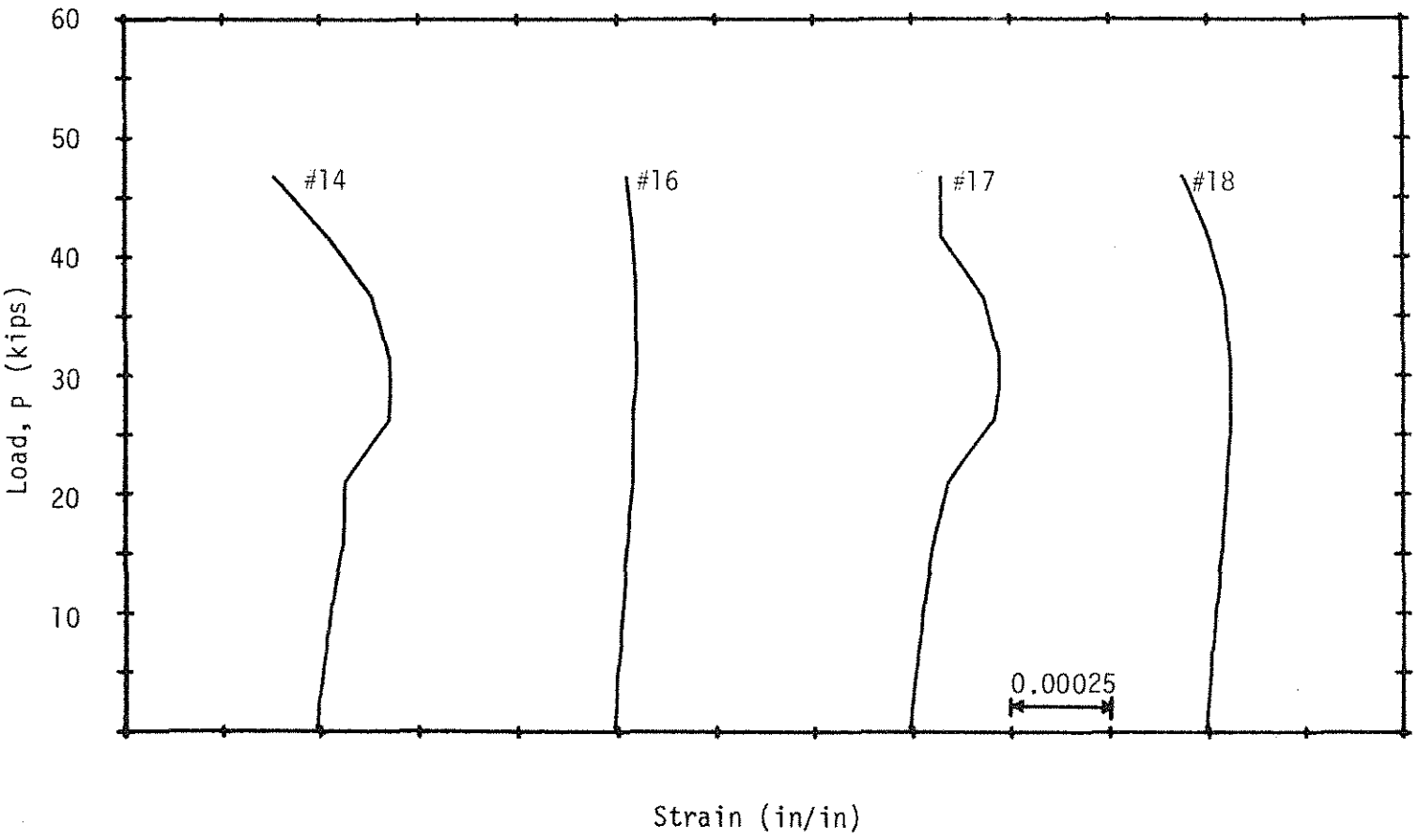

Figure 2.15. Load-Concrete Strain Diagram; Beam A50a.

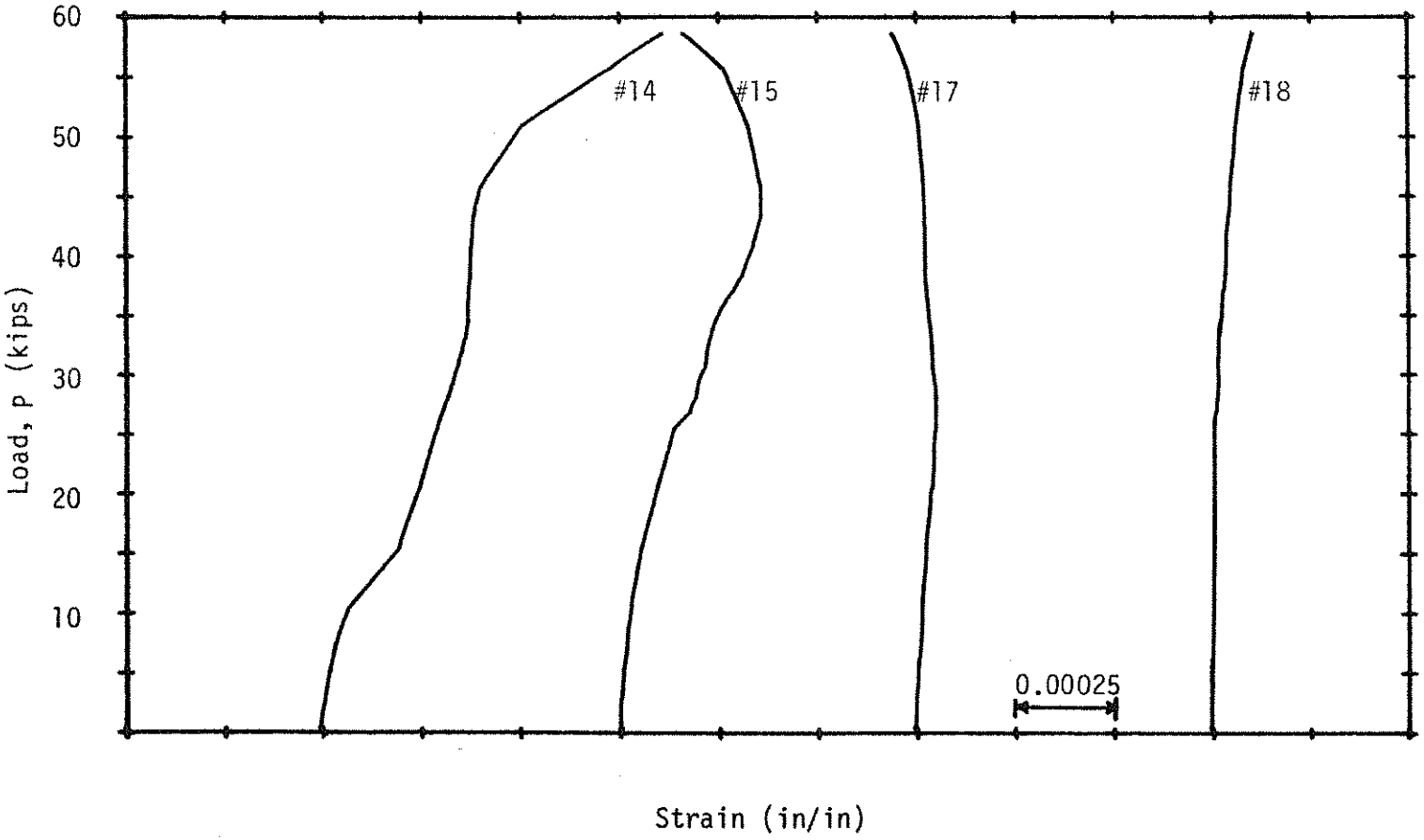

Figure 2.16. Load-Concrete Strain Diagram; Beam A75.

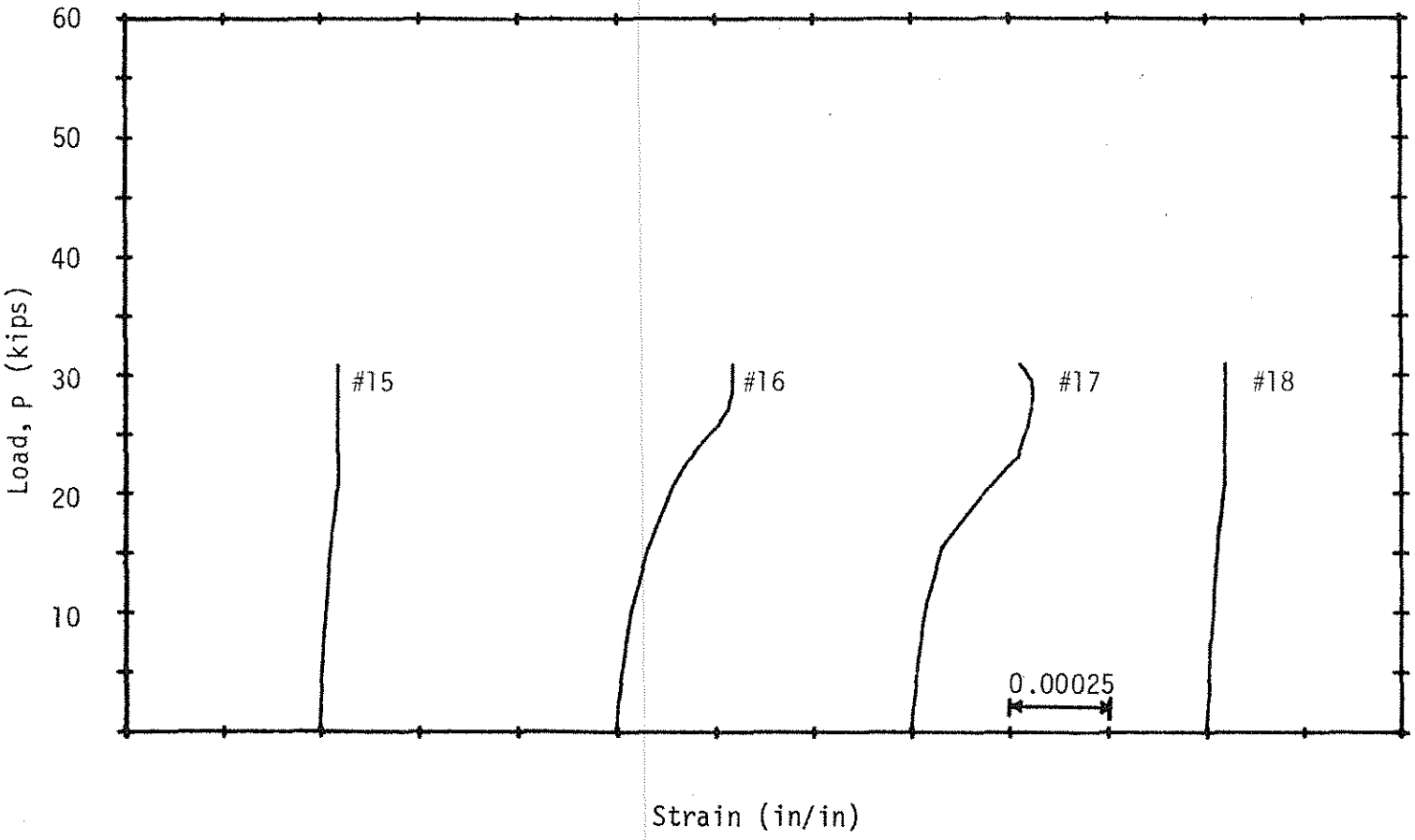

Figure 2.17. Load-Concrete Strain Diagram; Beam B00.

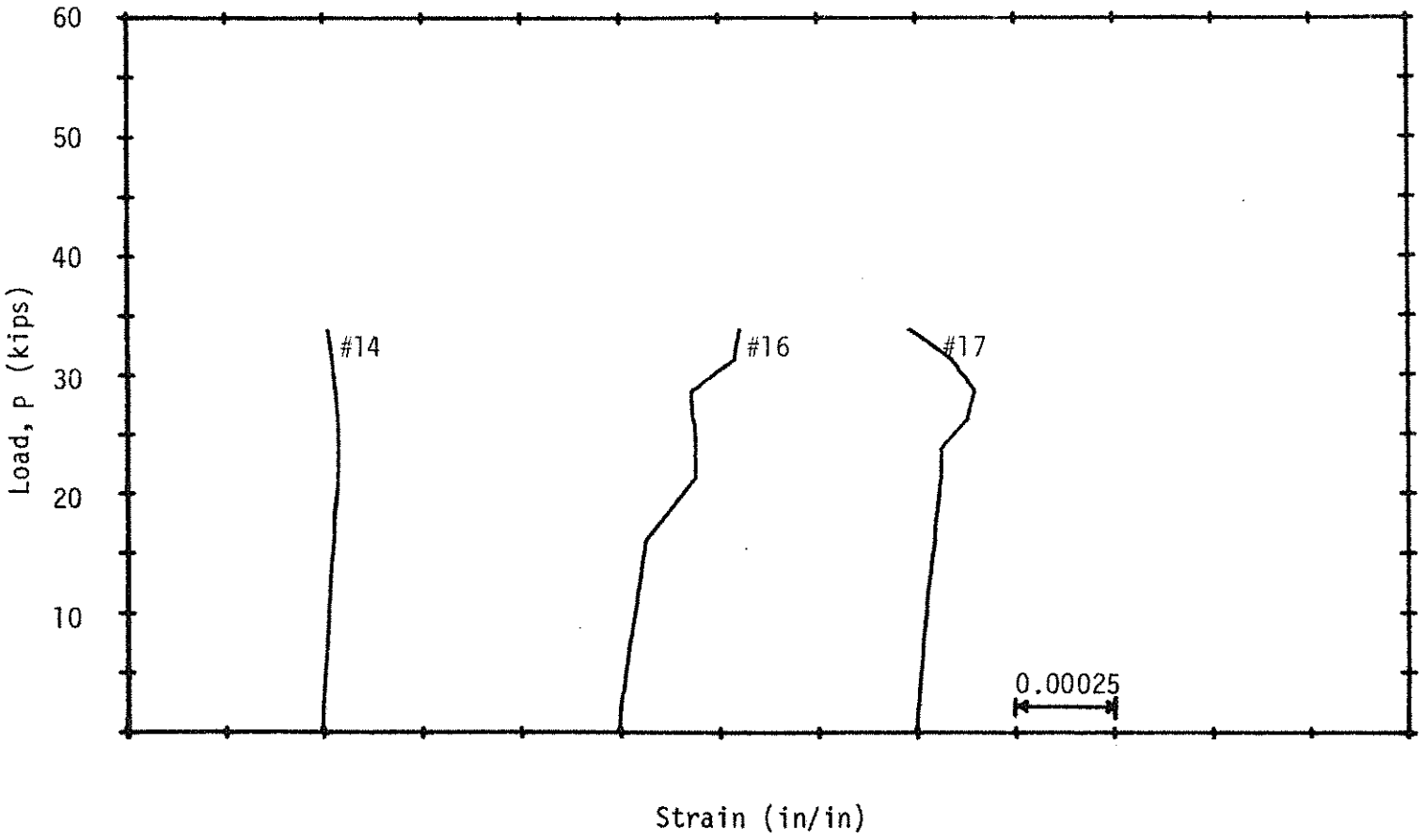

Figure 2.18. Load-Concrete Strain Diagram; Beam B25.

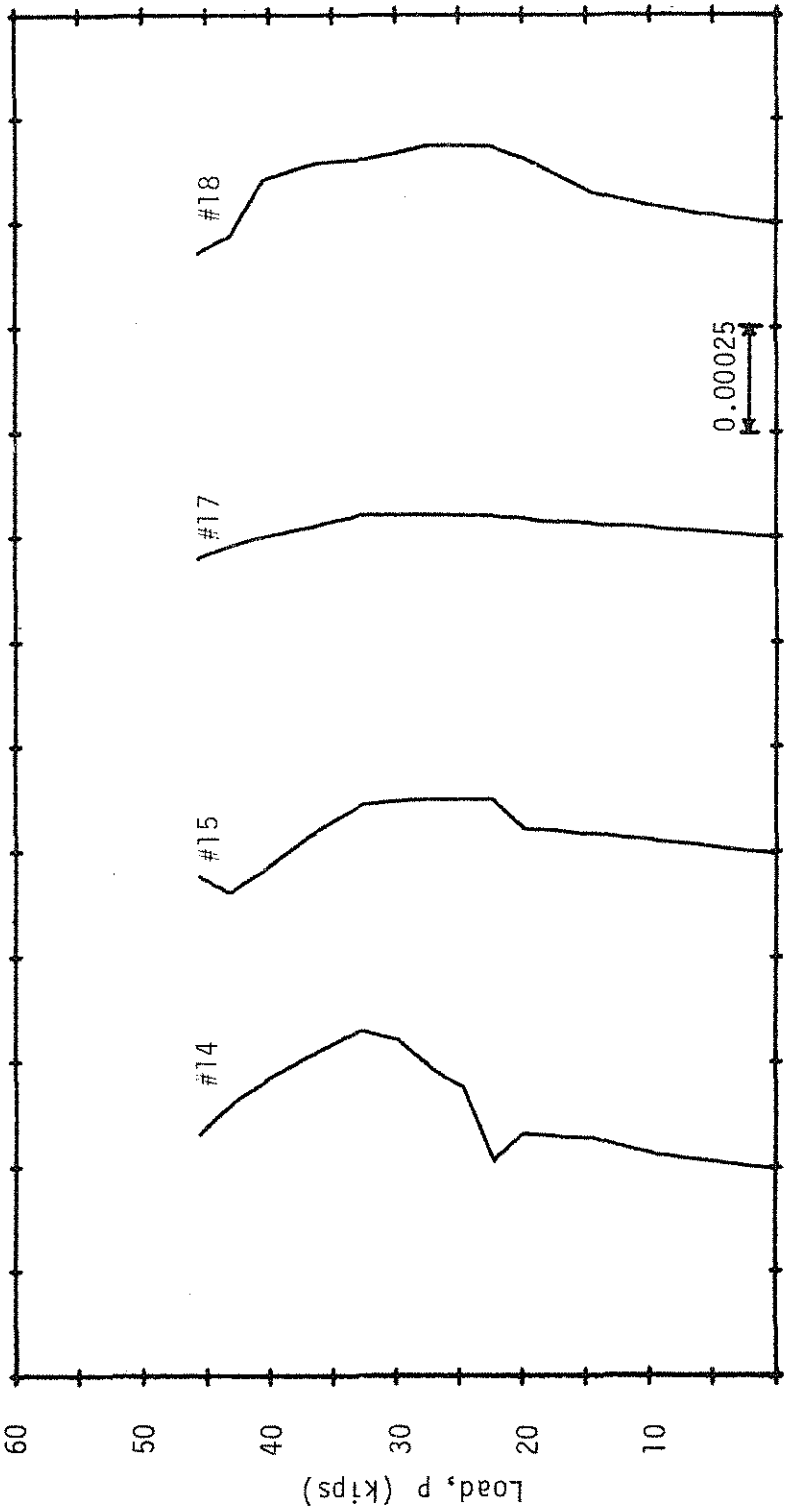

Figure 2.19. Load-Concrete Strain Diagram; Beam B50.

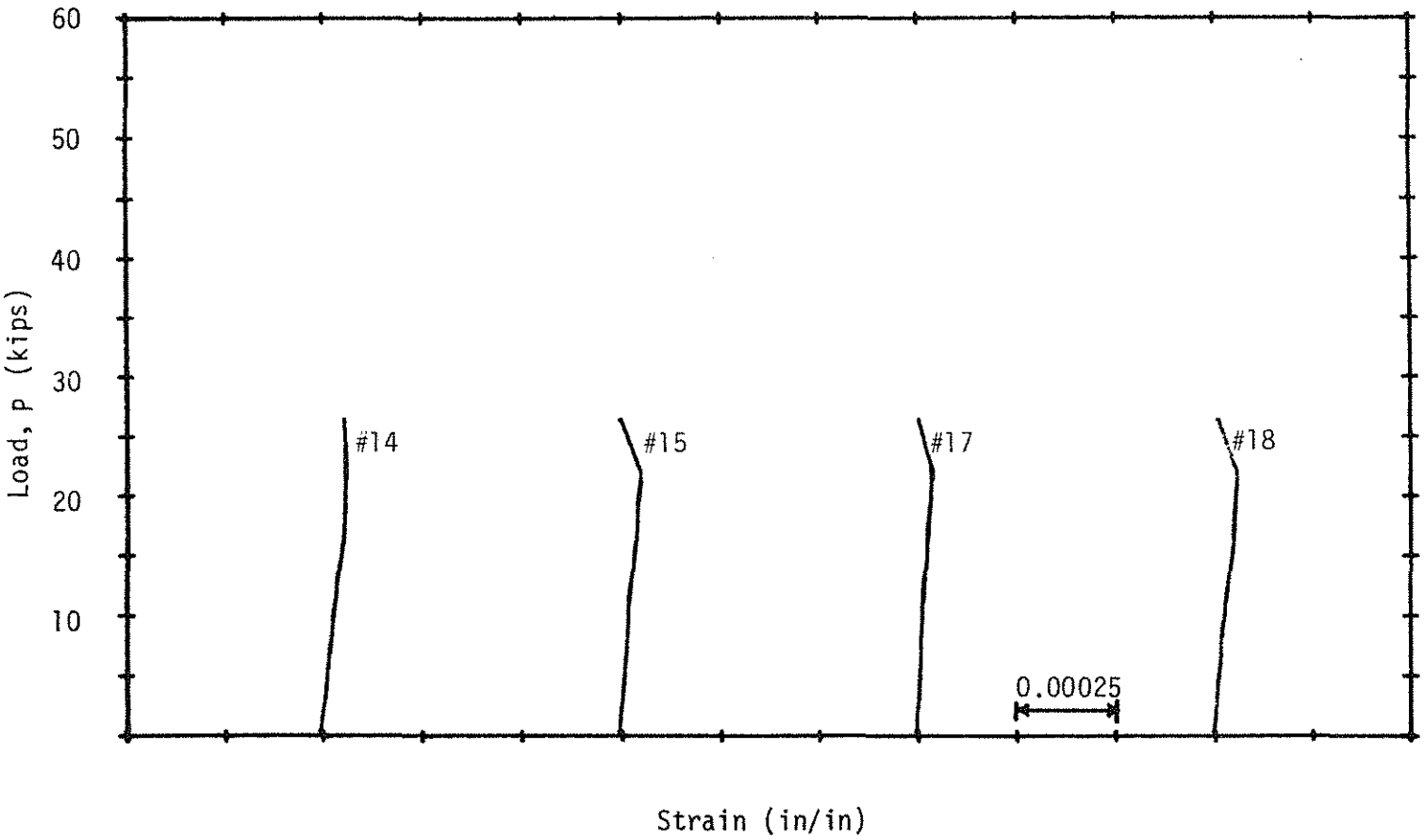

Figure 2.20. Load-Concrete Strain Diagram; Beam C00.

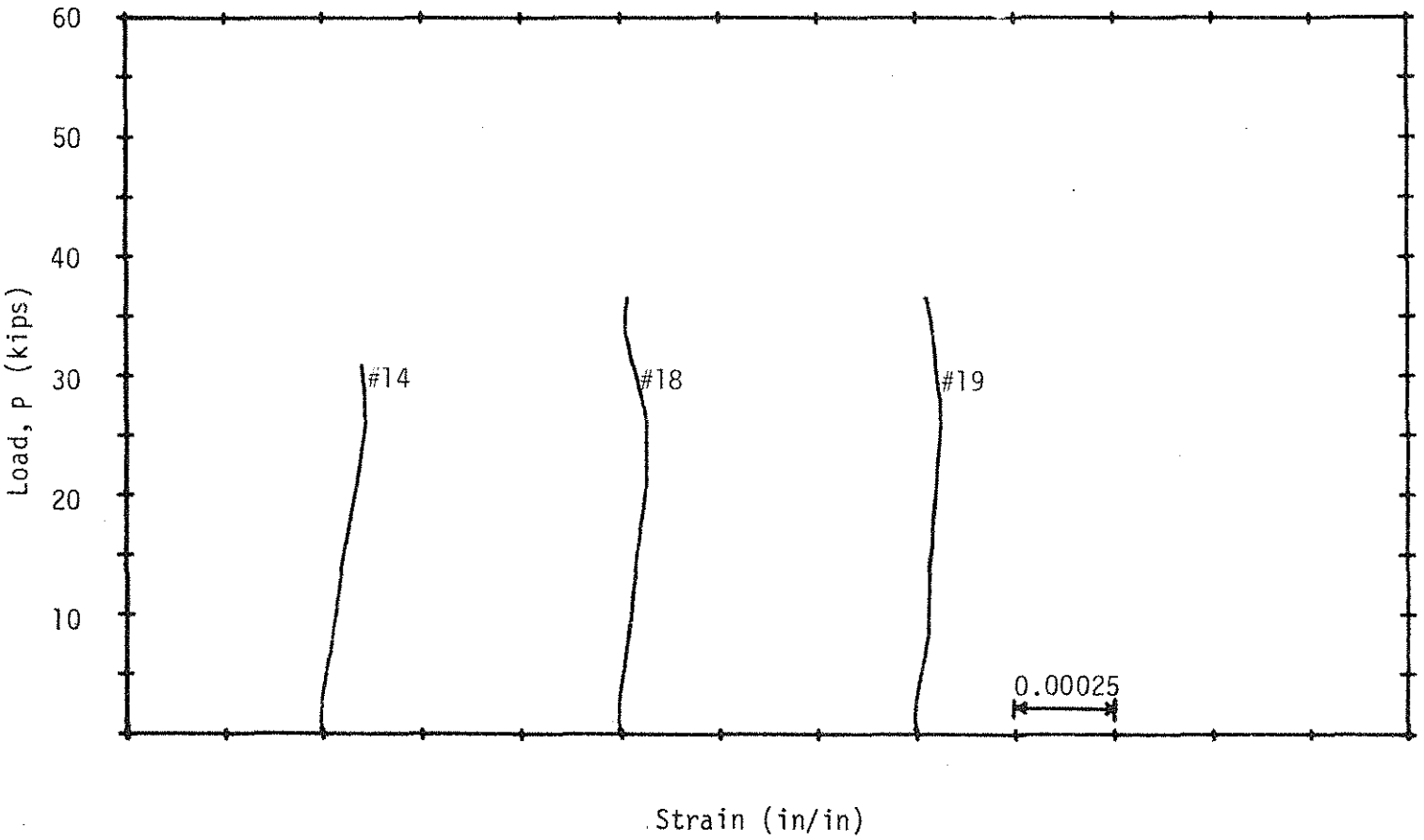

Figure 2.21. Load-Concrete Strain Diagram; Beam C25.

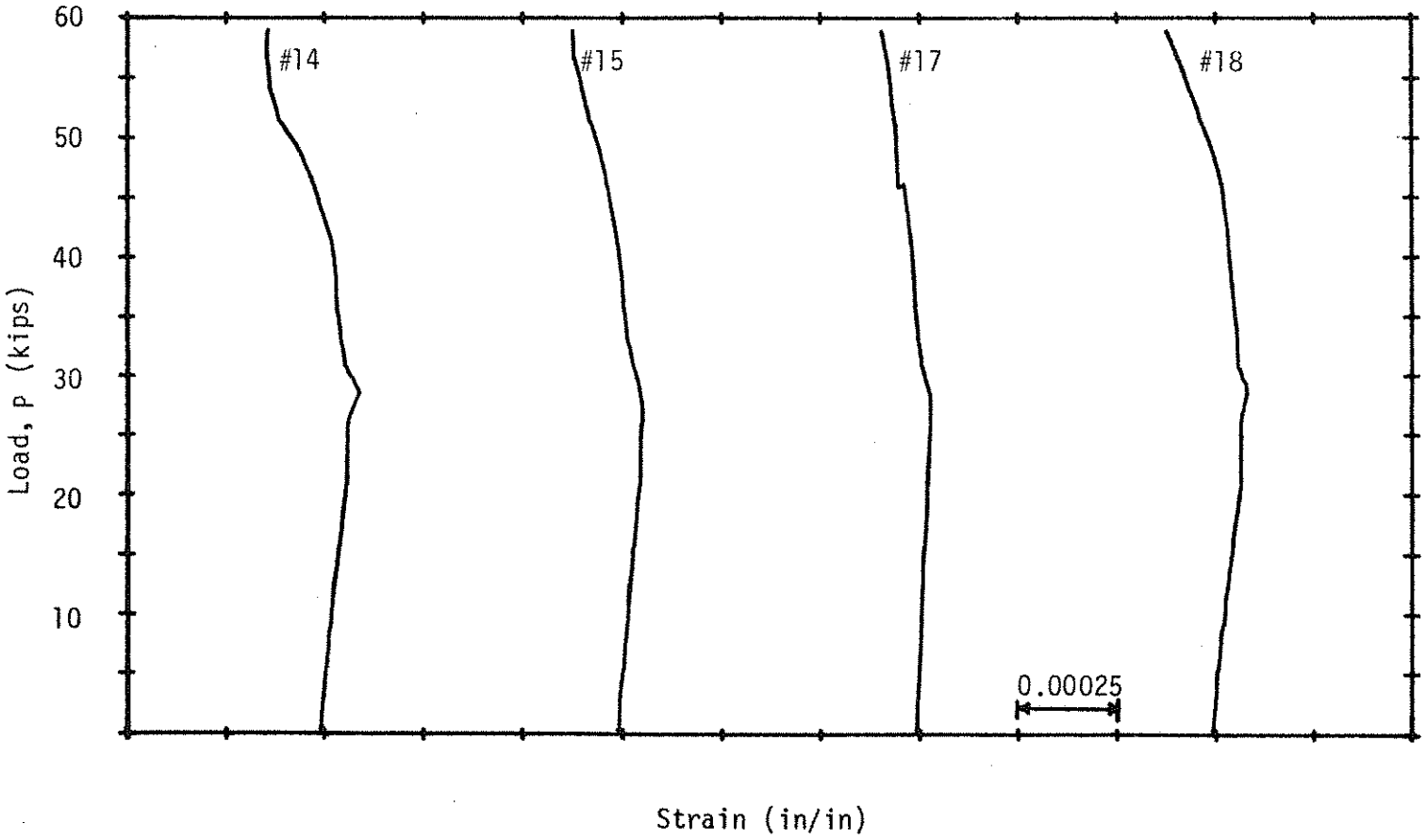

Figure 2.22. Load-Concrete Strain Diagram; Beam C50.

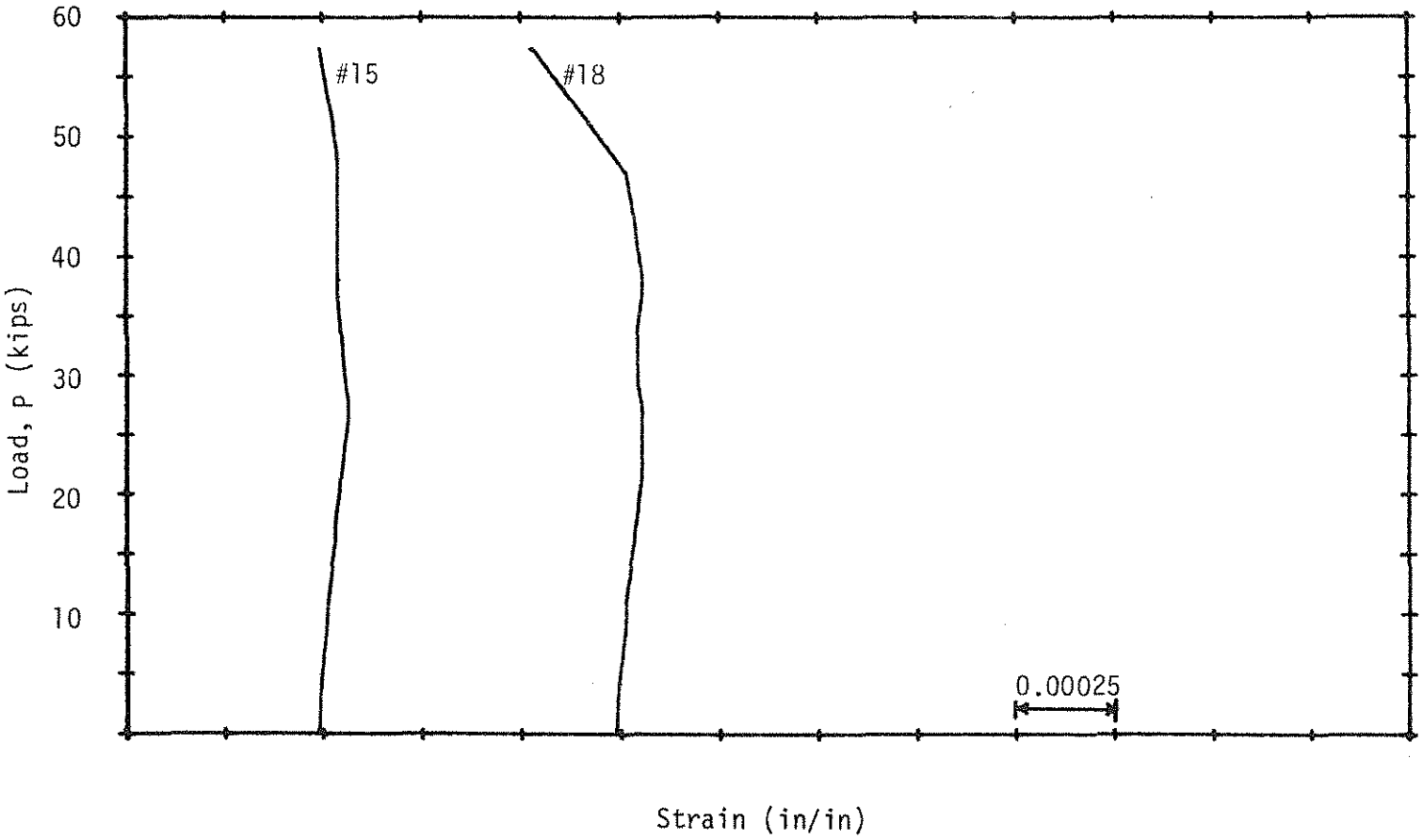

Figure 2.23. Load-Concrete Strain Diagram; Beam C75.

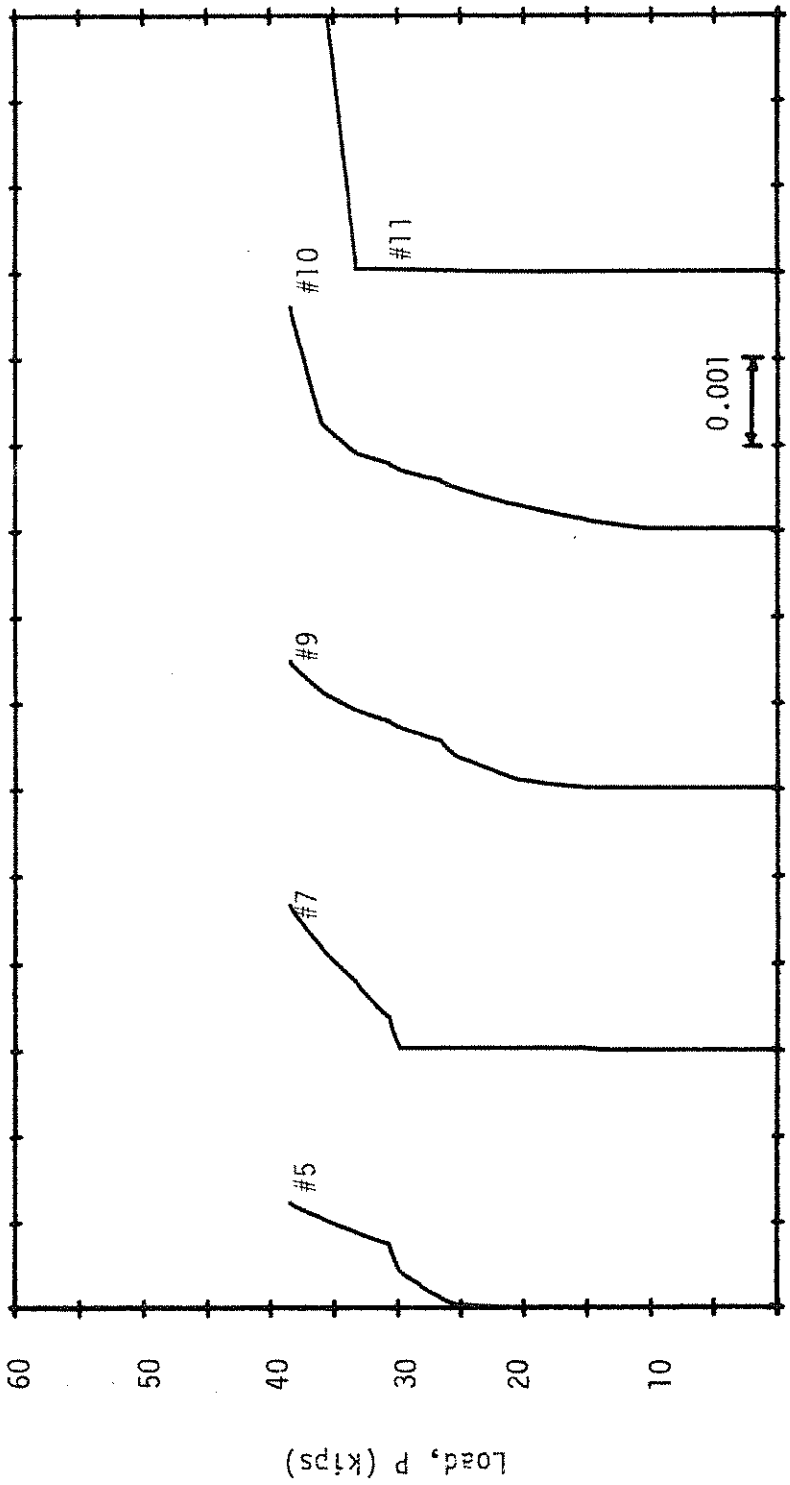

Figure 2.24. Load-Stirrup Strain Diagrams; Beam A25.

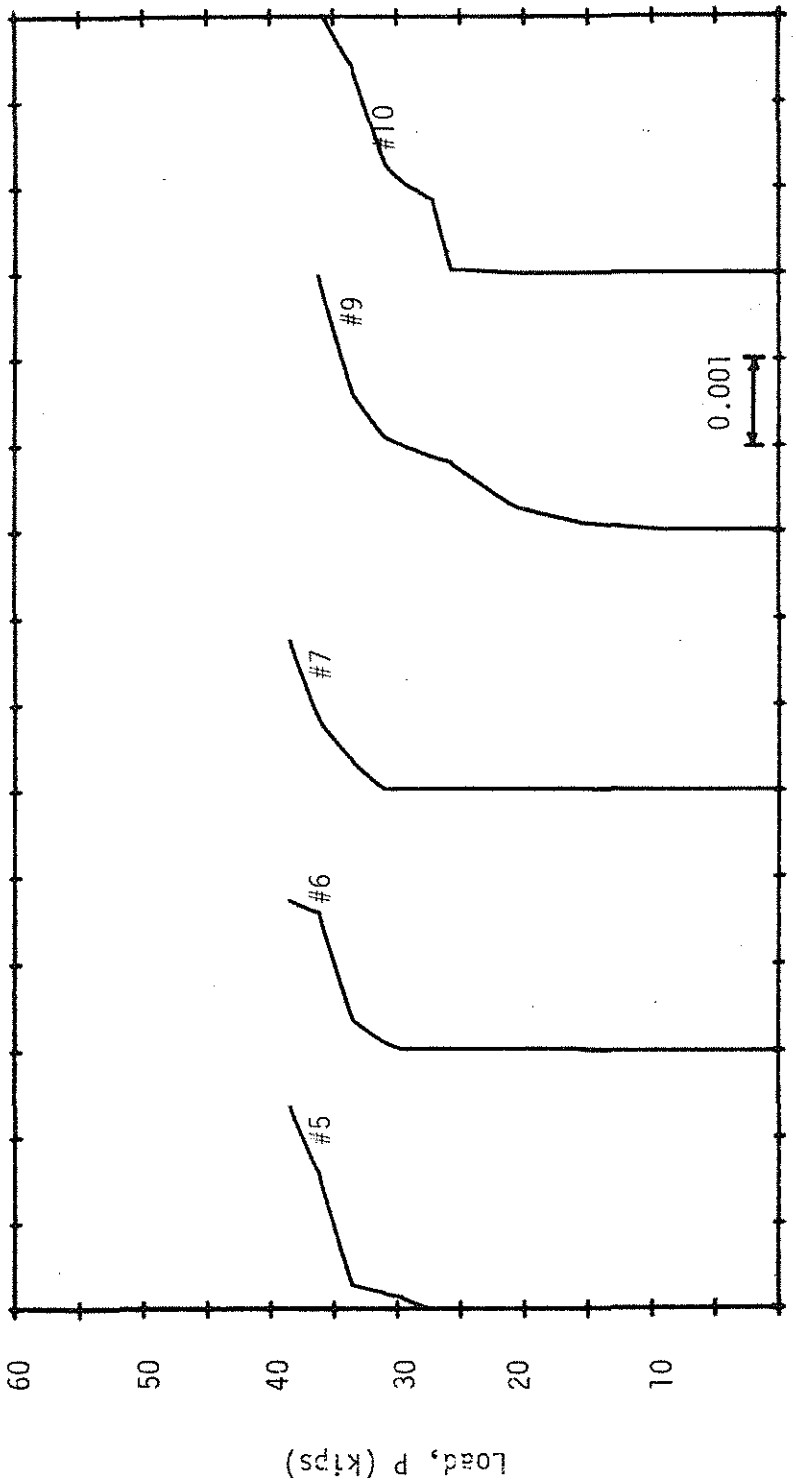

Figure 2.25. Load-Stirrup Strain Diagrams; Beam A25a.

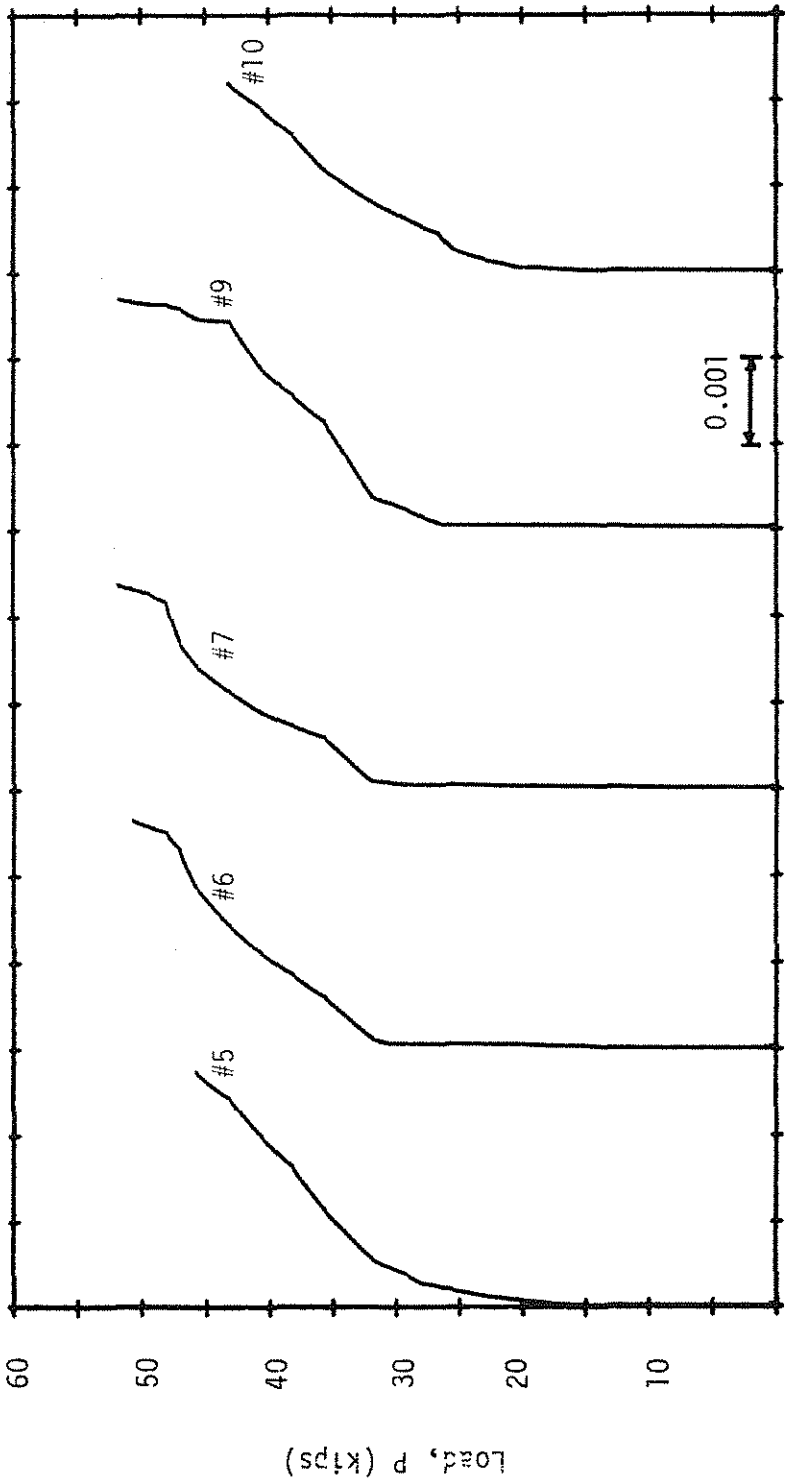

Figure 2.26. Load-Stirrup Strain Diagrams; Beam A50.

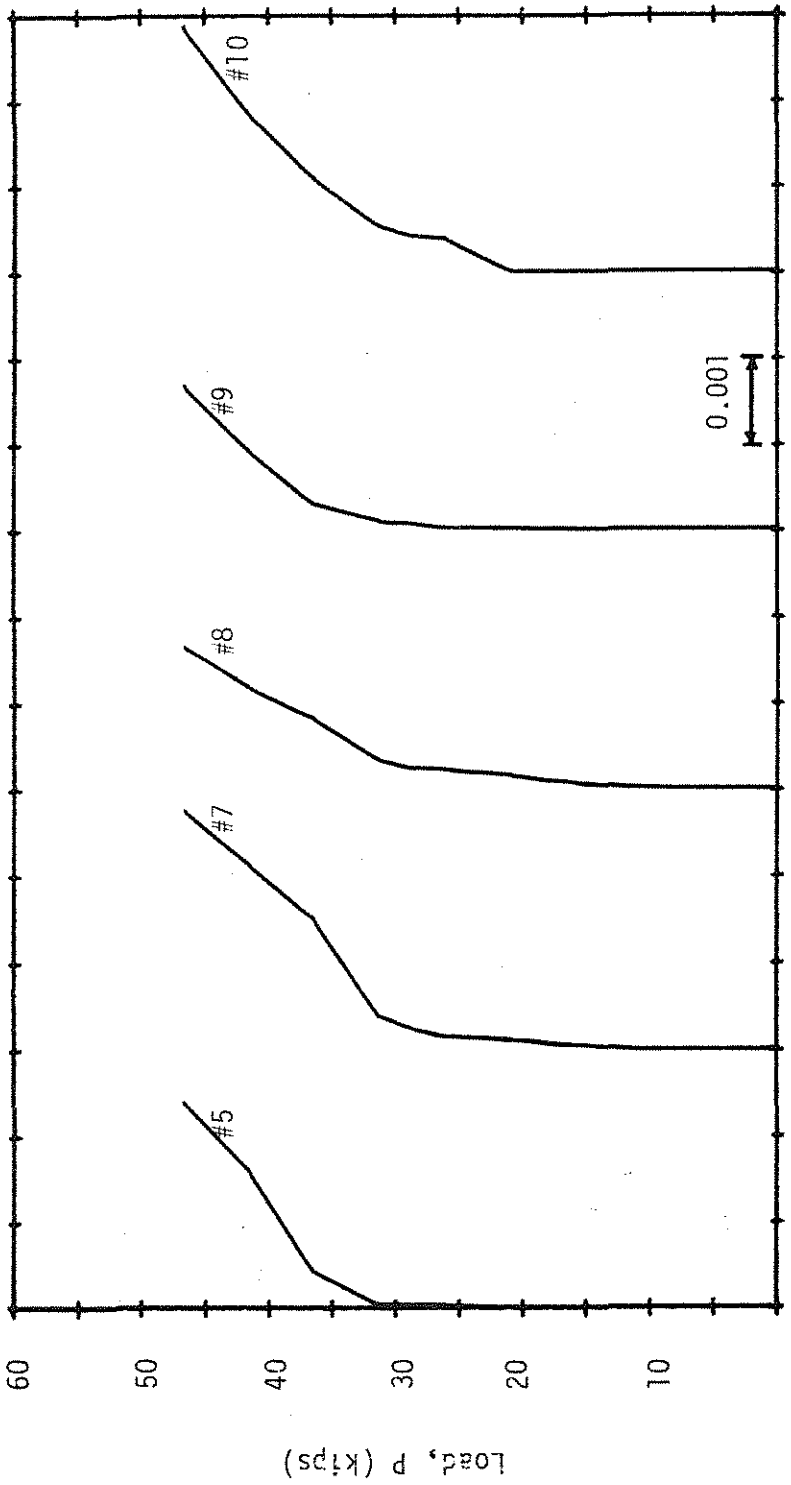

Figure 2.27. Load-Stirrup Strain Diagrams; Beam A50a.

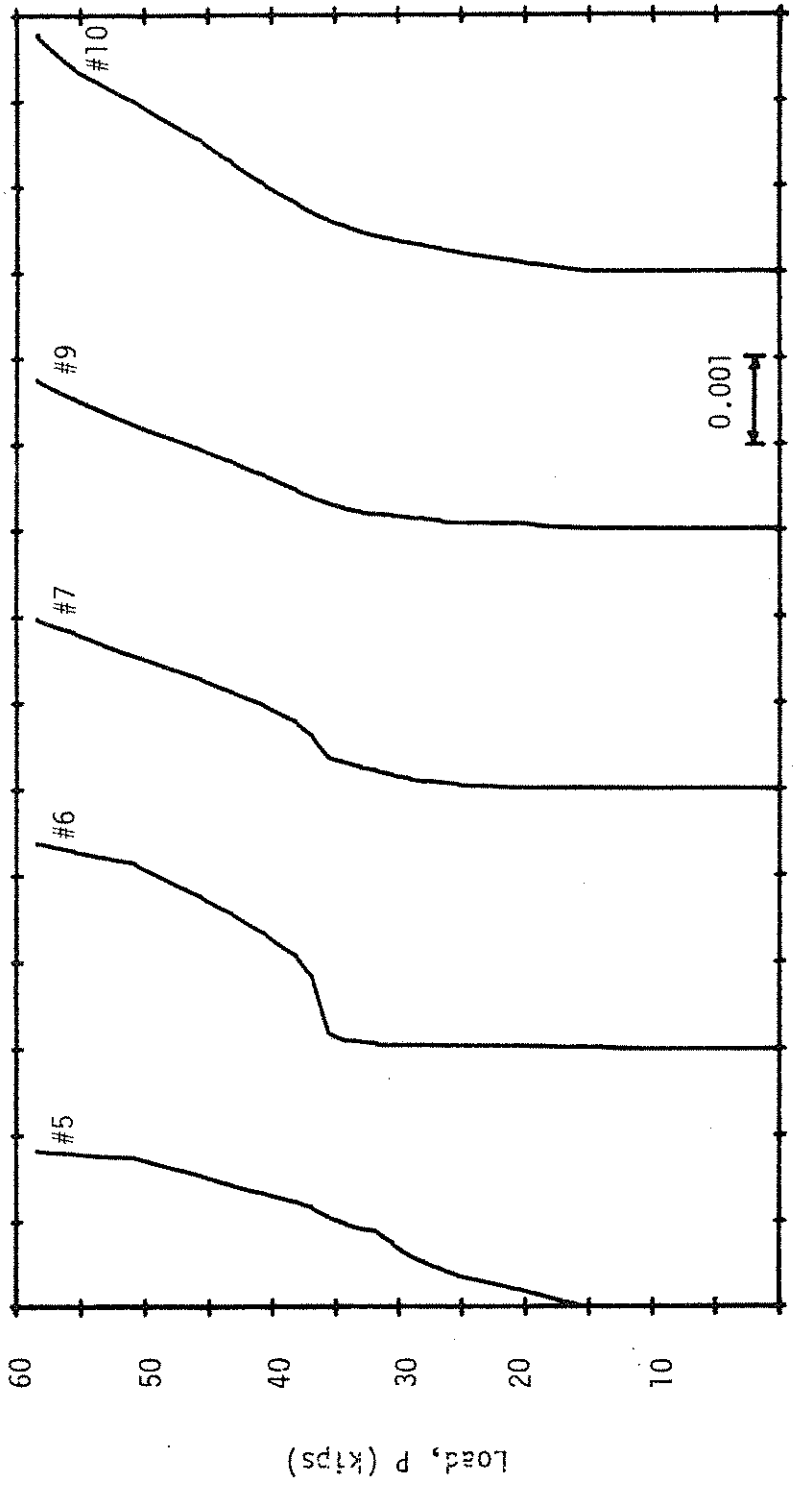

Figure 2.28. Load-Stirrup Strain Diagrams; Beam A75.

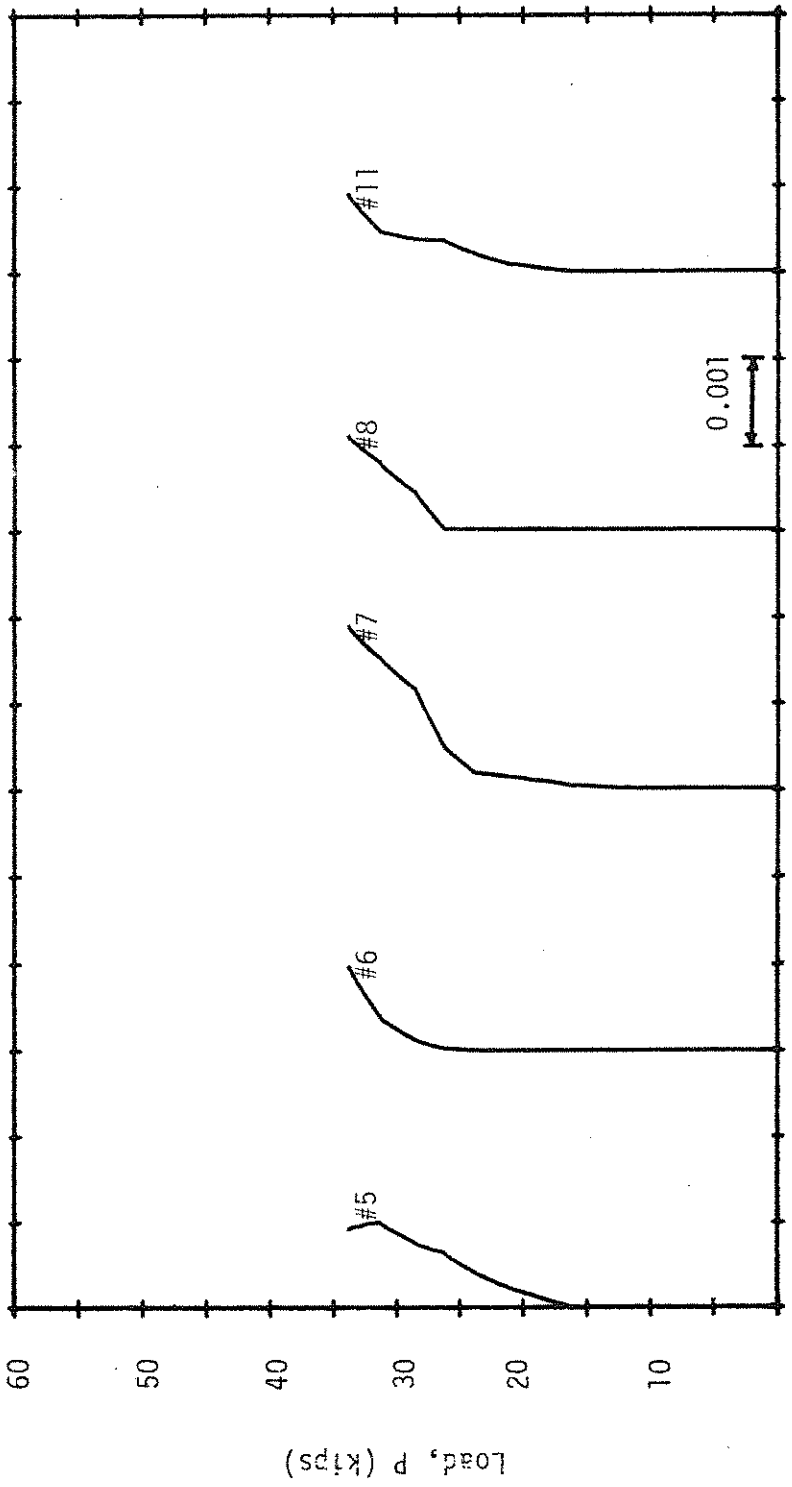

Figure 2.29. Load-Stirrup Strain Diagrams; Beam B25.

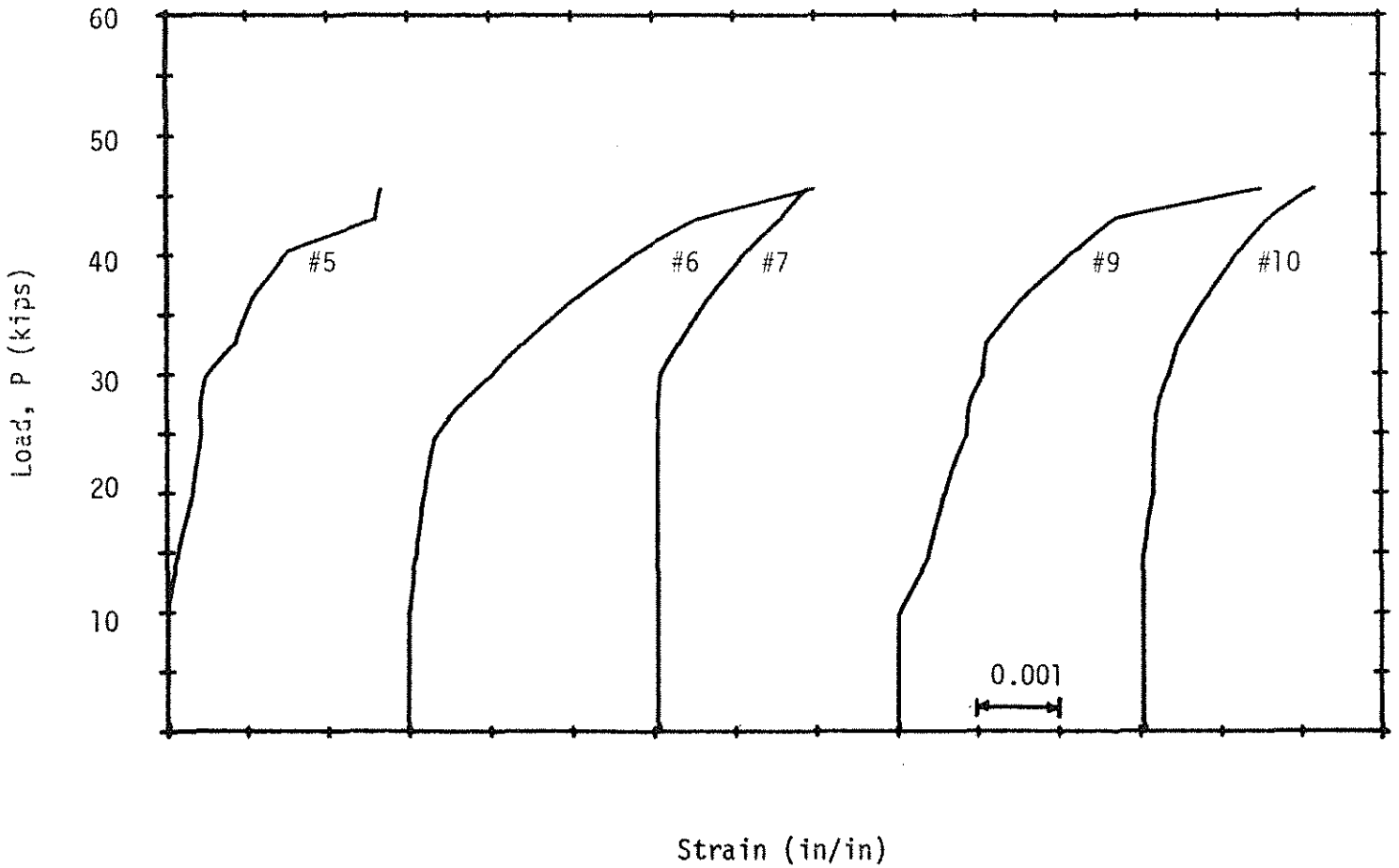

Figure 2.30. Load-Stirrup Strain Diagrams; Beam B50.

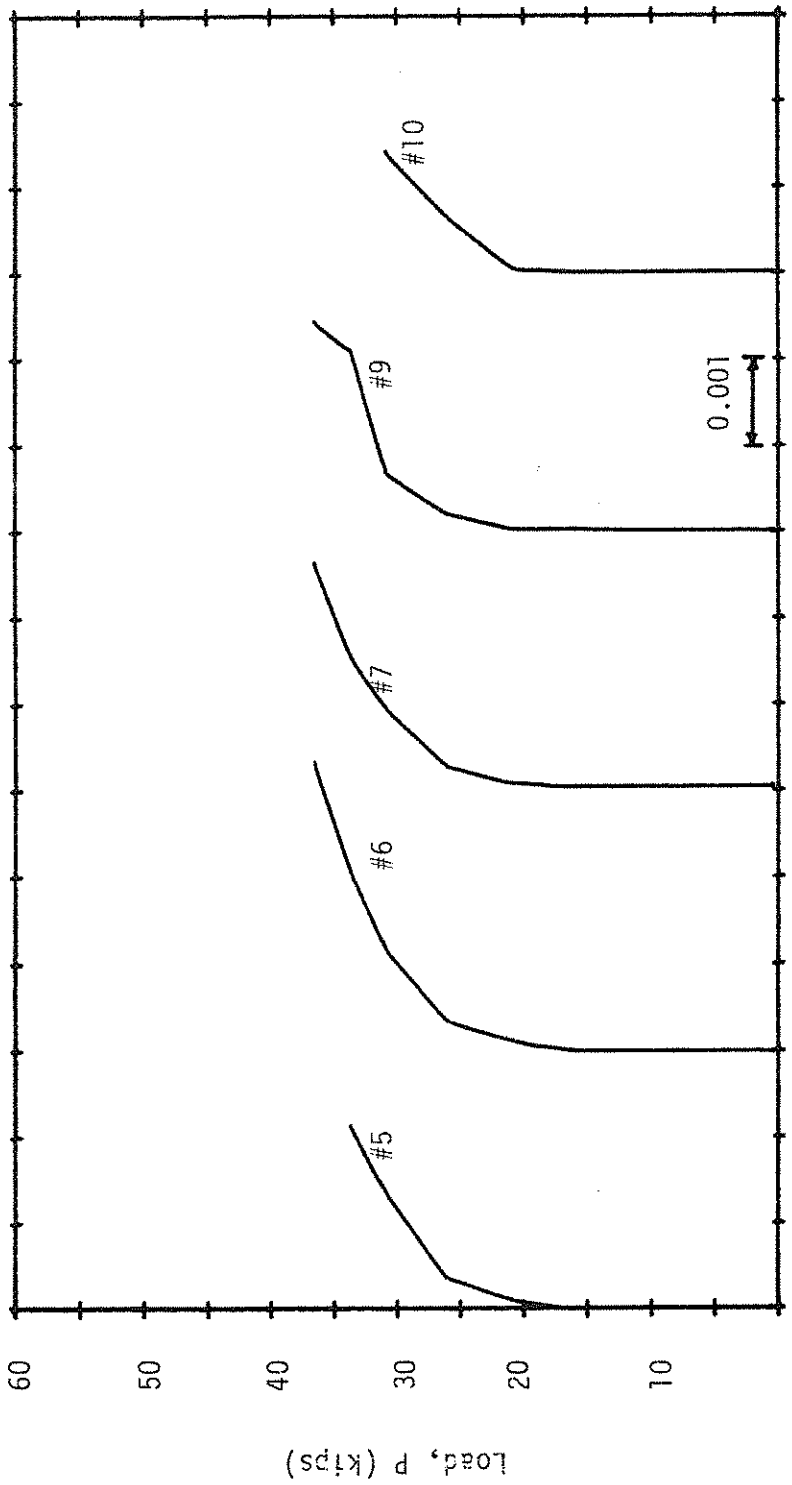

Figure 2.31. Load-Stirrup Strain Diagrams; Beam C25.

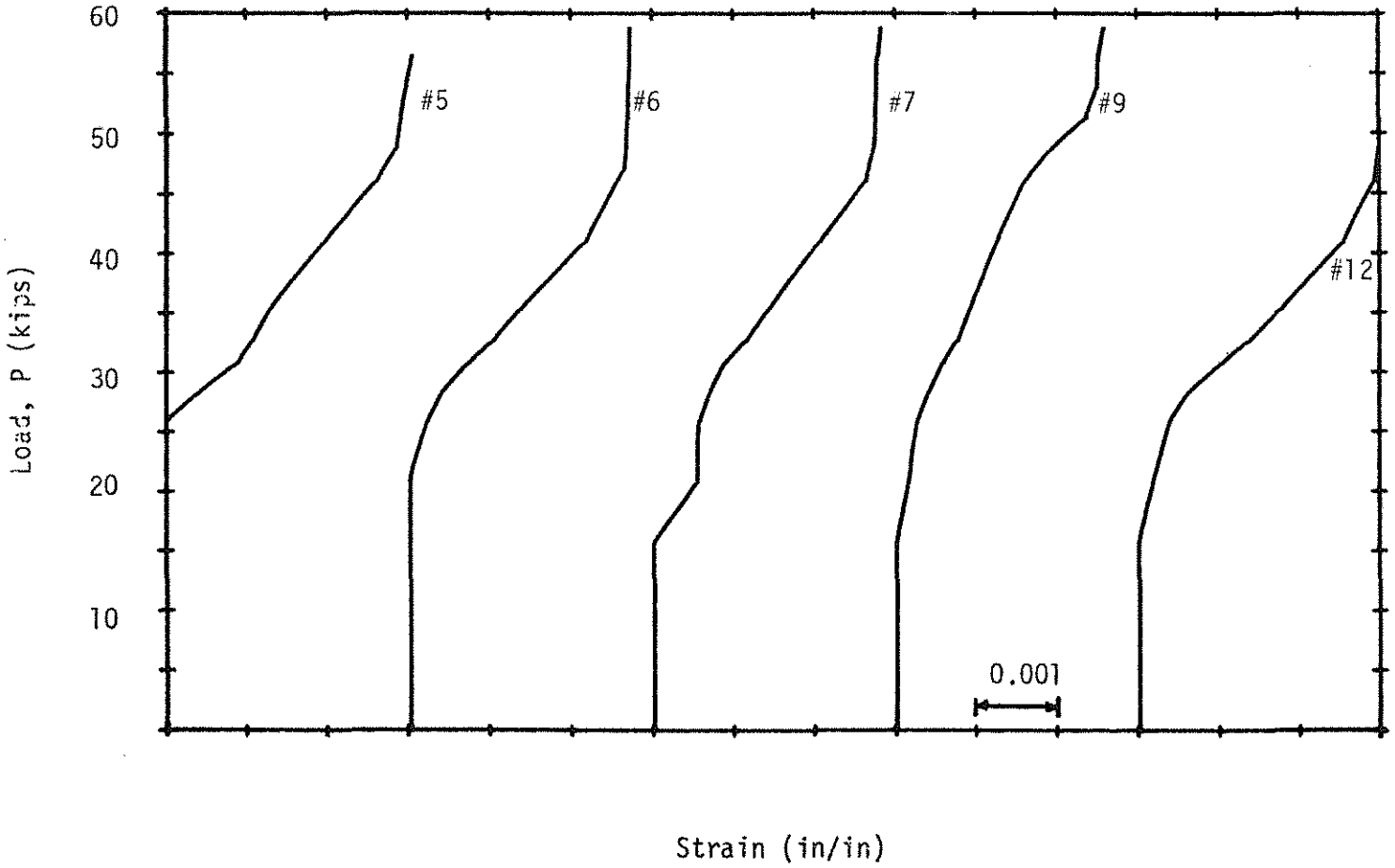

Figure 2.32. Load-Stirrup Strain Diagrams; Beam C50.

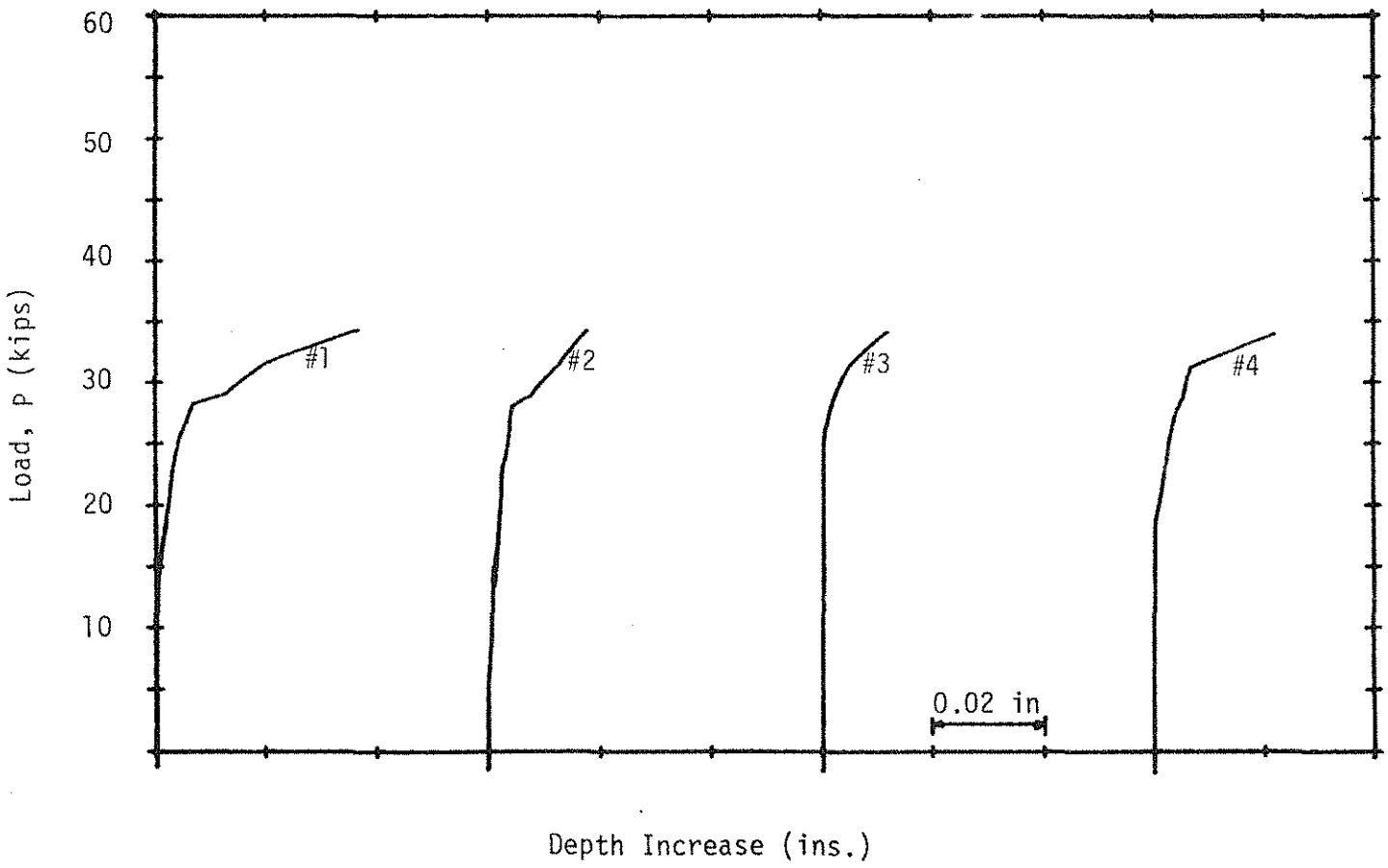

Figure 2.35. Load-Depth Increase Diagrams; Beam A25.

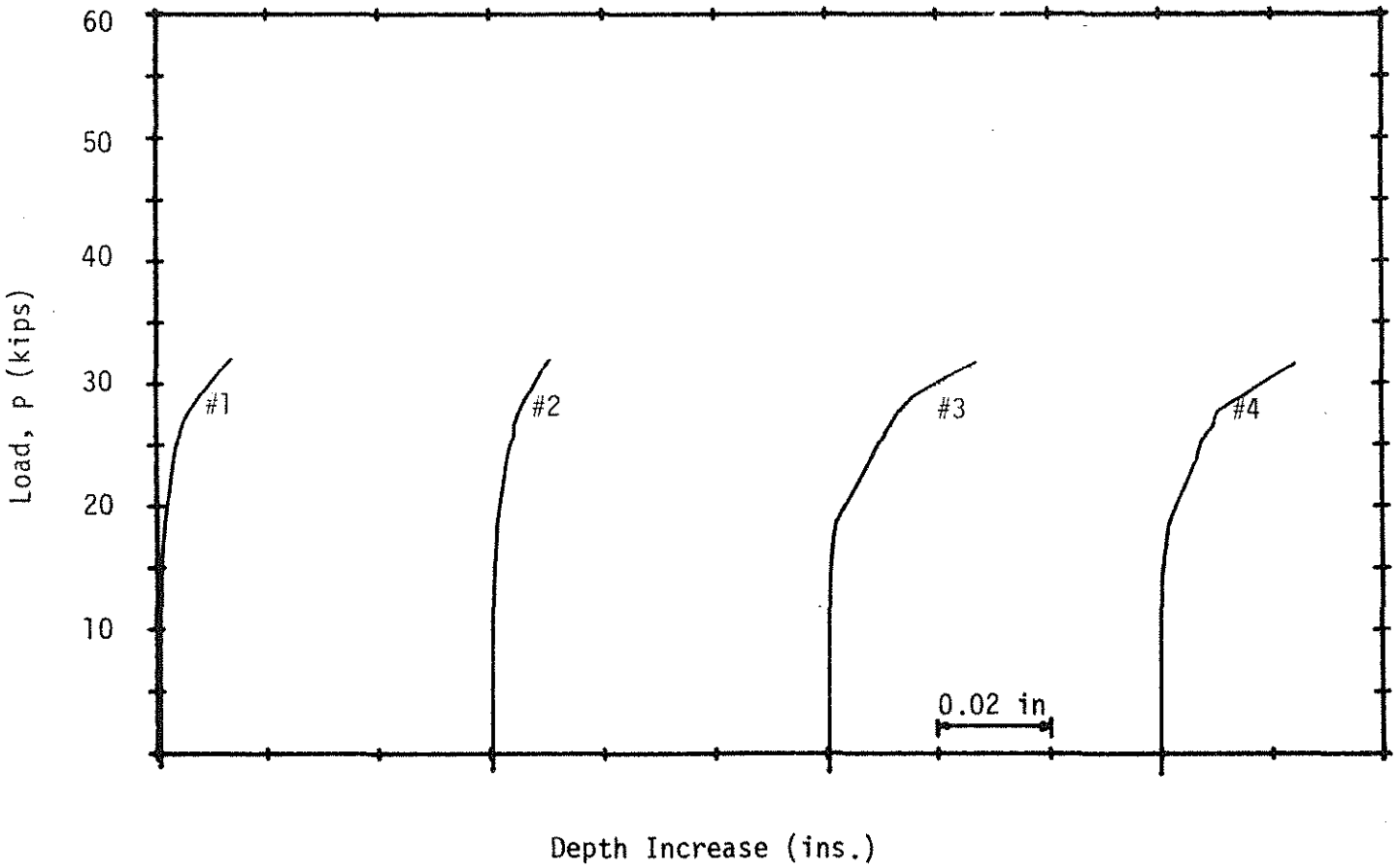

Figure 2.36. Load-Depth Increase Diagrams; Beam A25a.

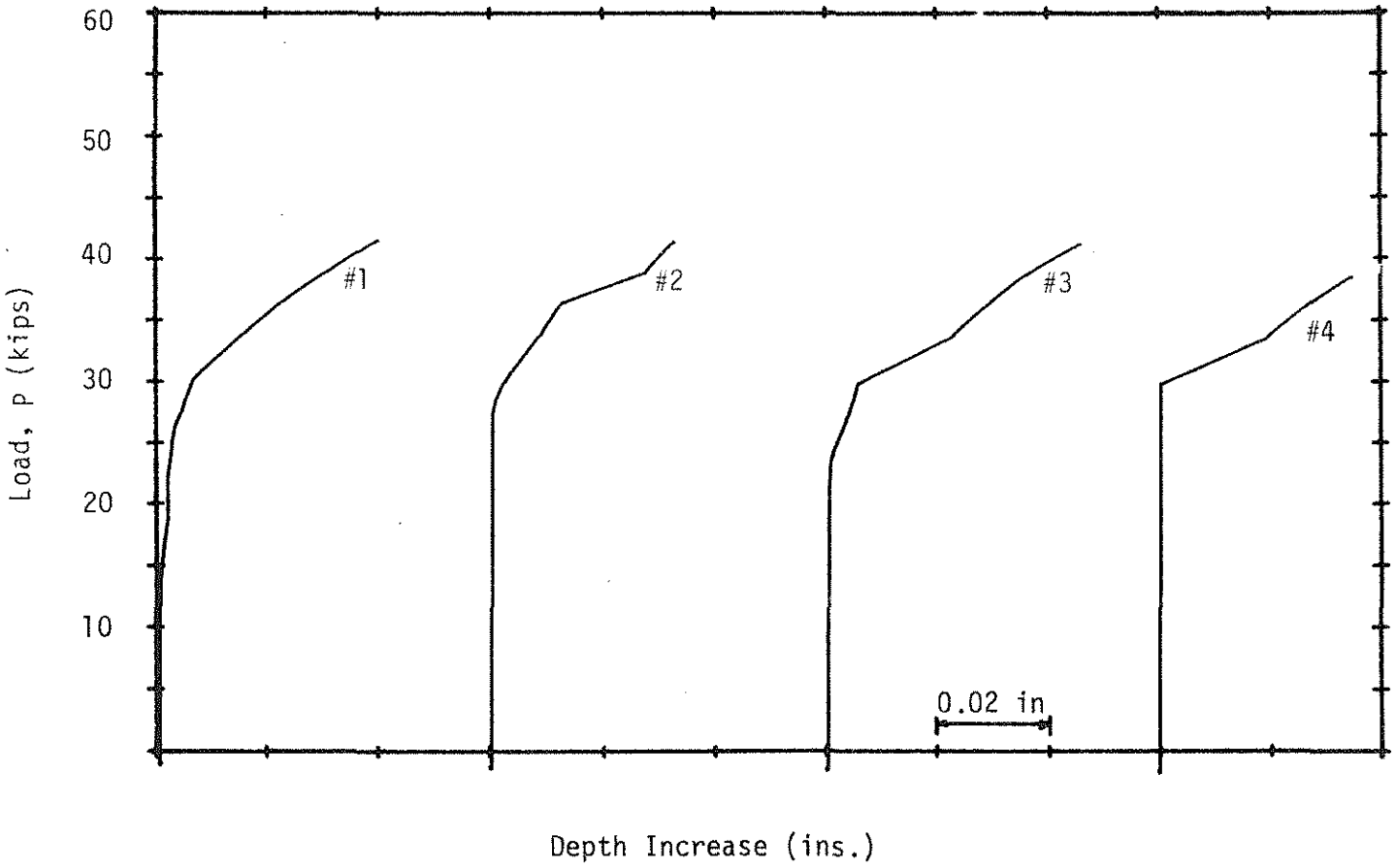

Figure 2.37. Load-Depth Increase Diagrams; Beam A50.

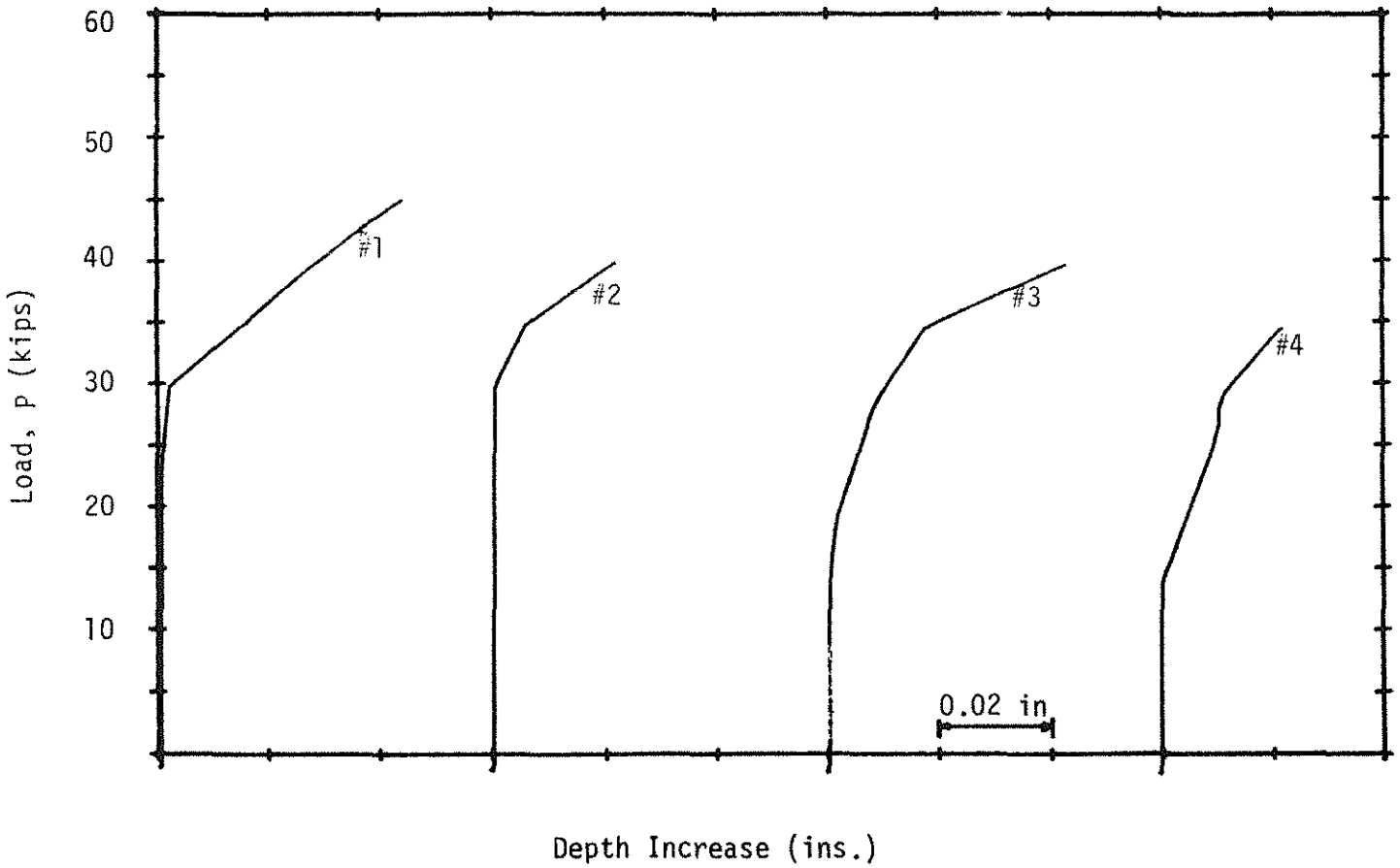

Figure 2.38. Load-Depth Increase Diagrams; Beam A50a.

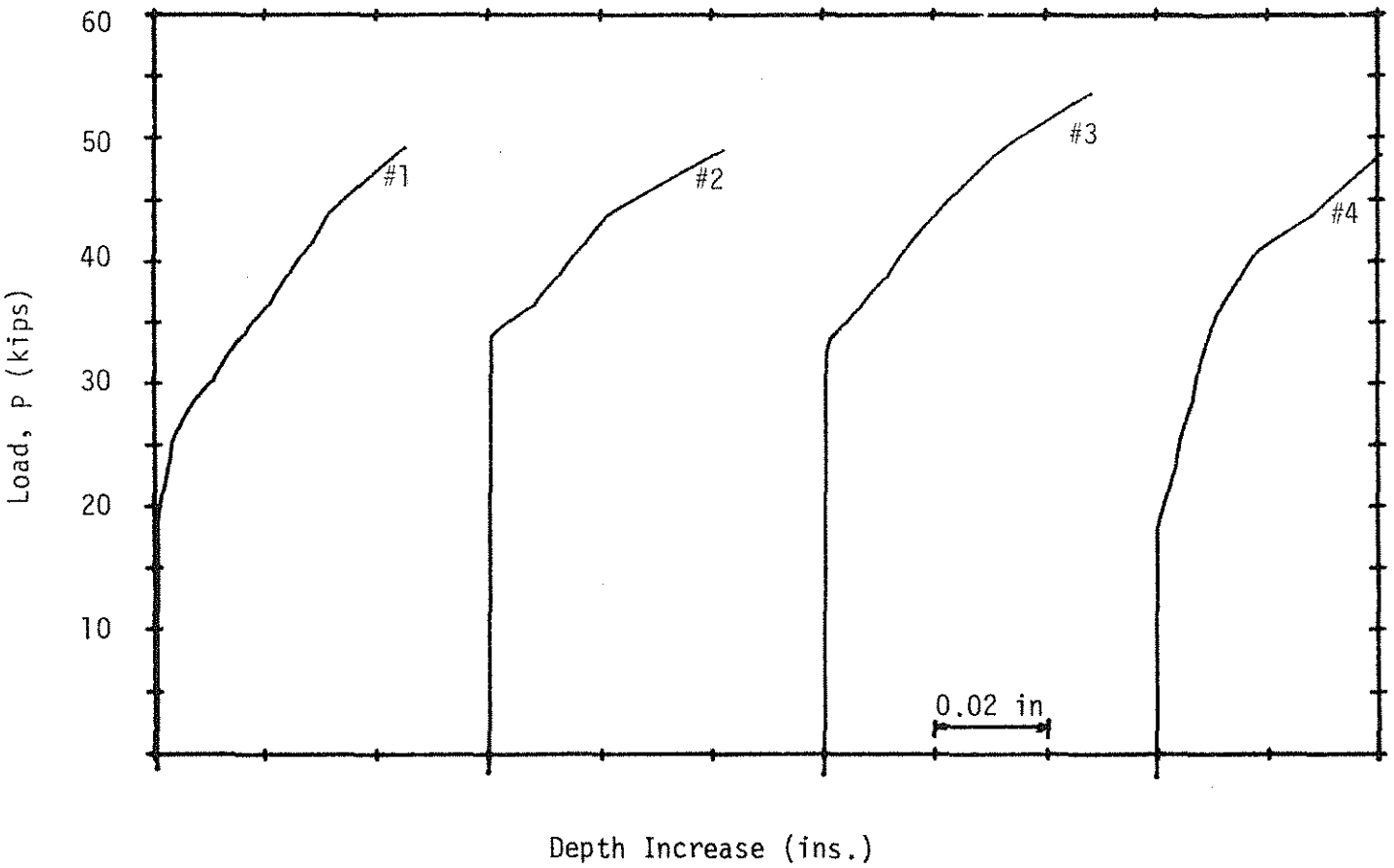

Figure 2.39. Load-Depth Increase Diagrams; Beam A75.

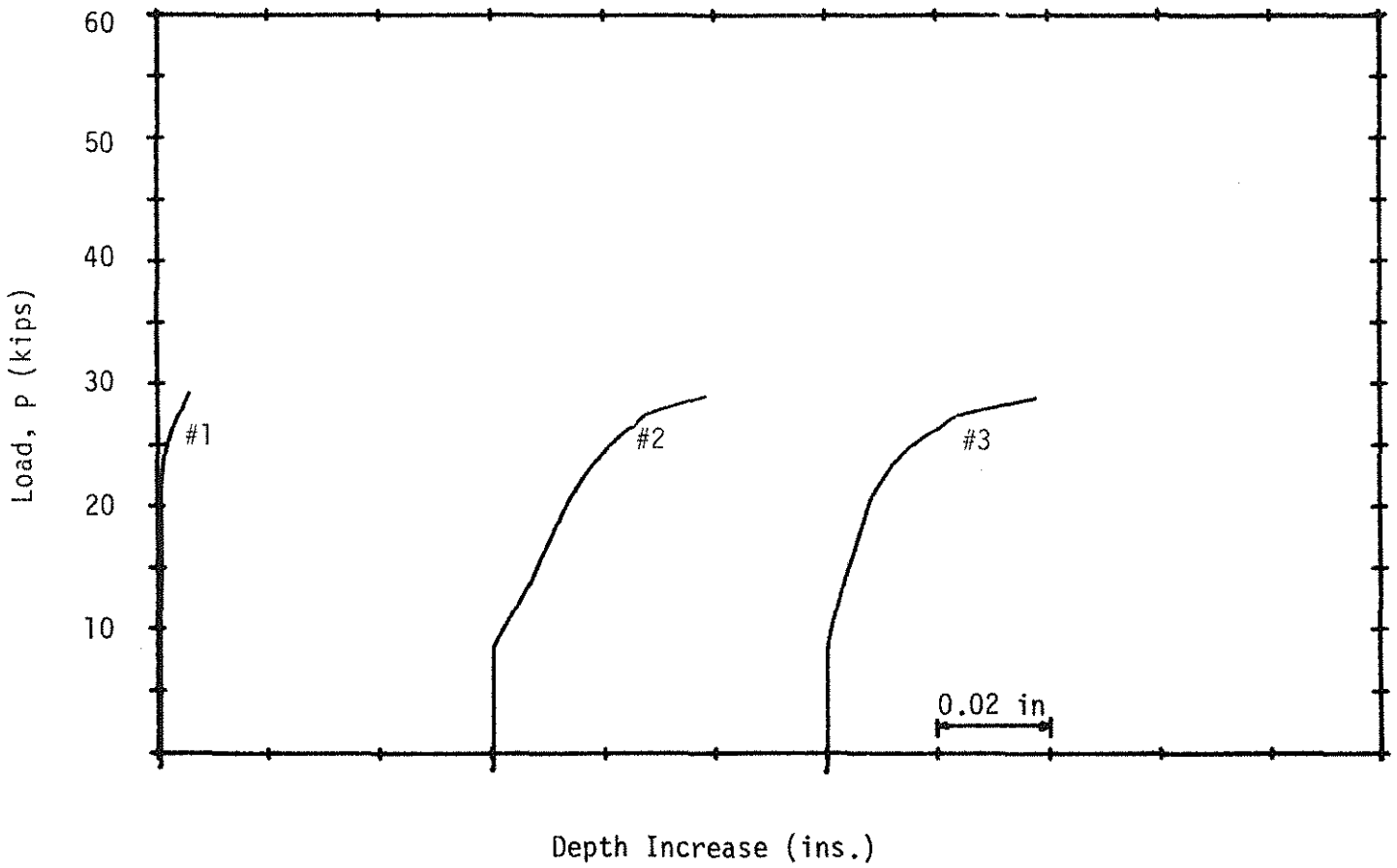

Figure 2.40. Load-Depth Increase Diagrams; Beam B00.

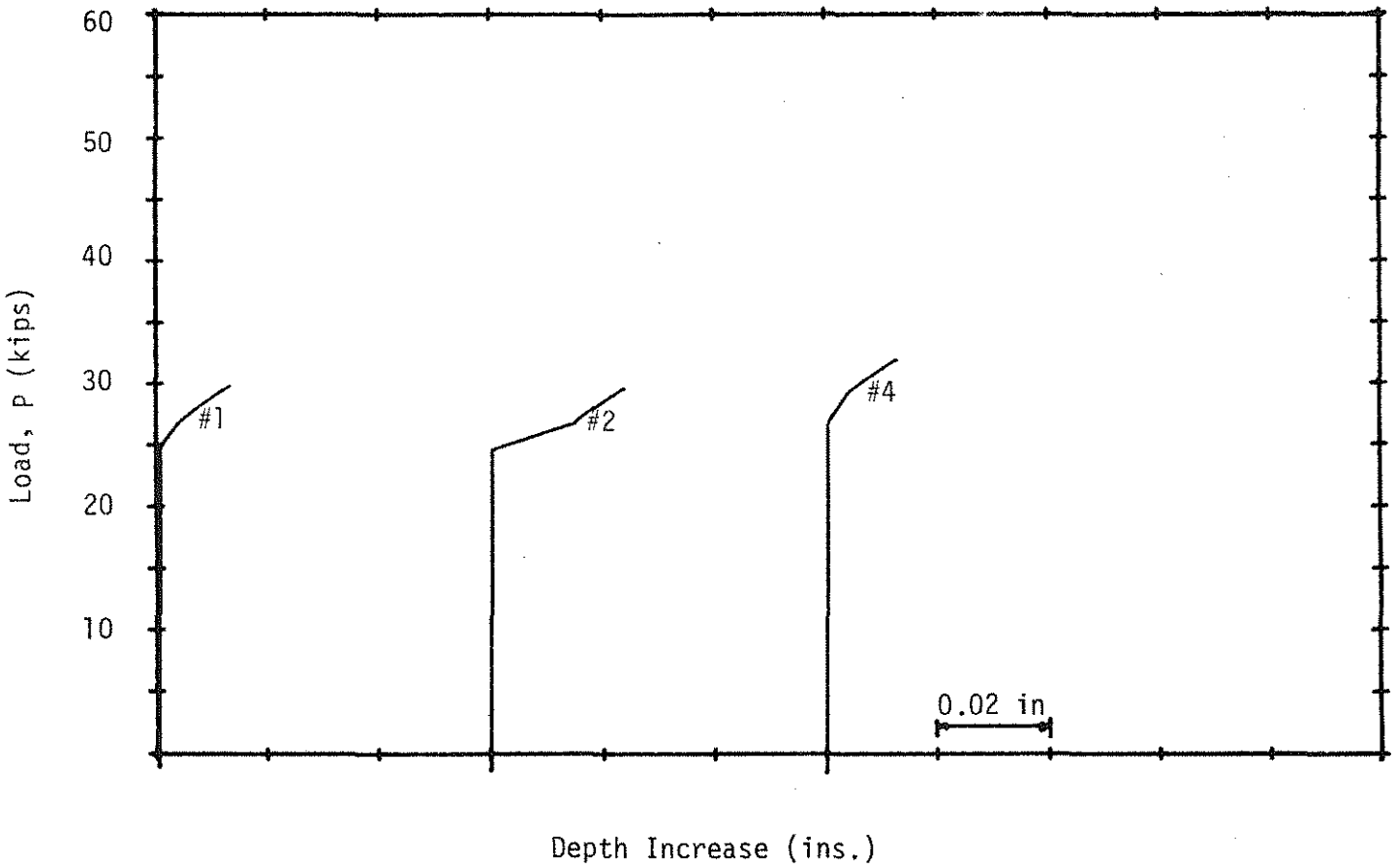

Figure 2.41. Load-Depth Increase Diagrams; Beam B25.

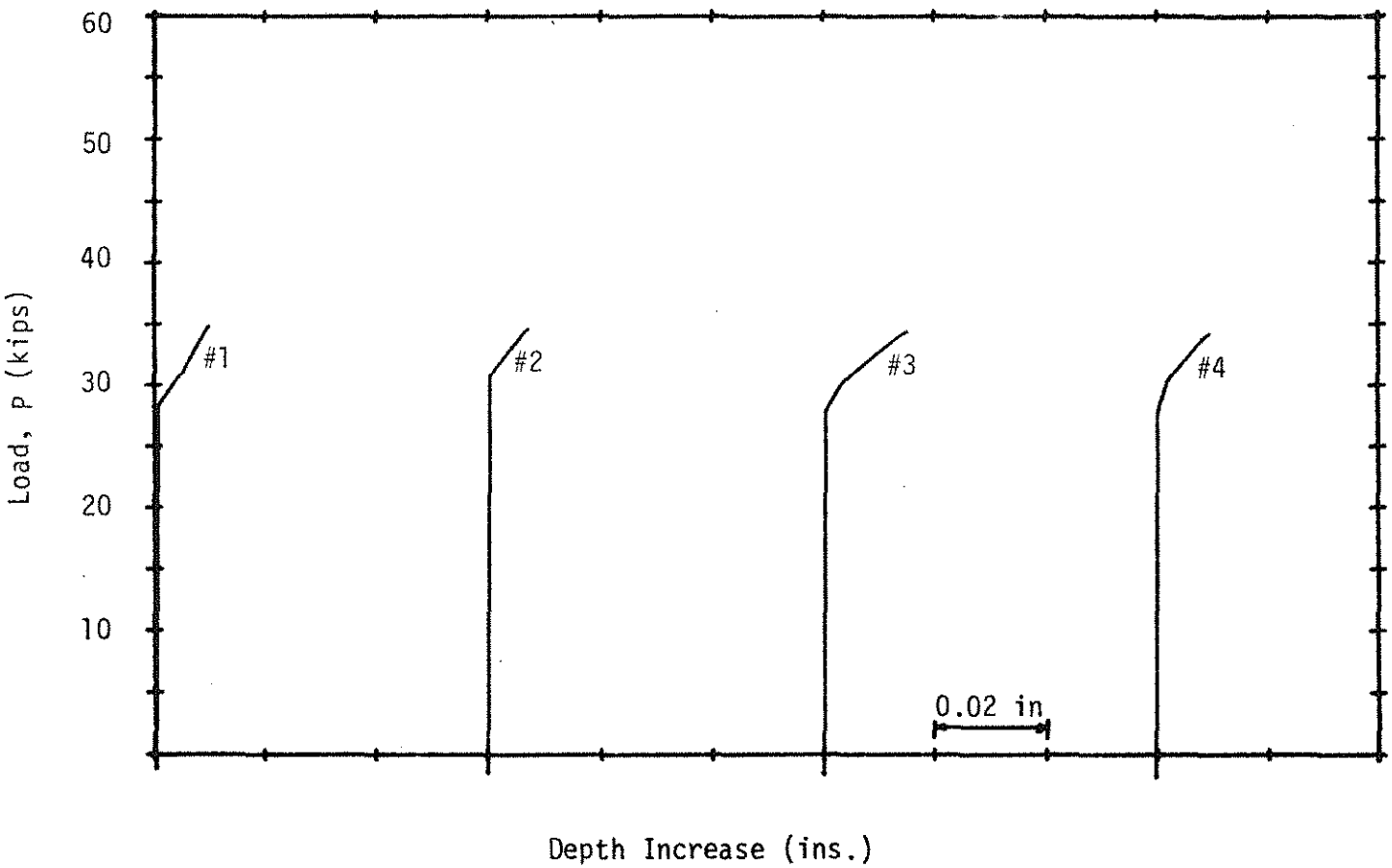

Figure 2.42. Load-Depth Increase Diagrams; Beam B50.

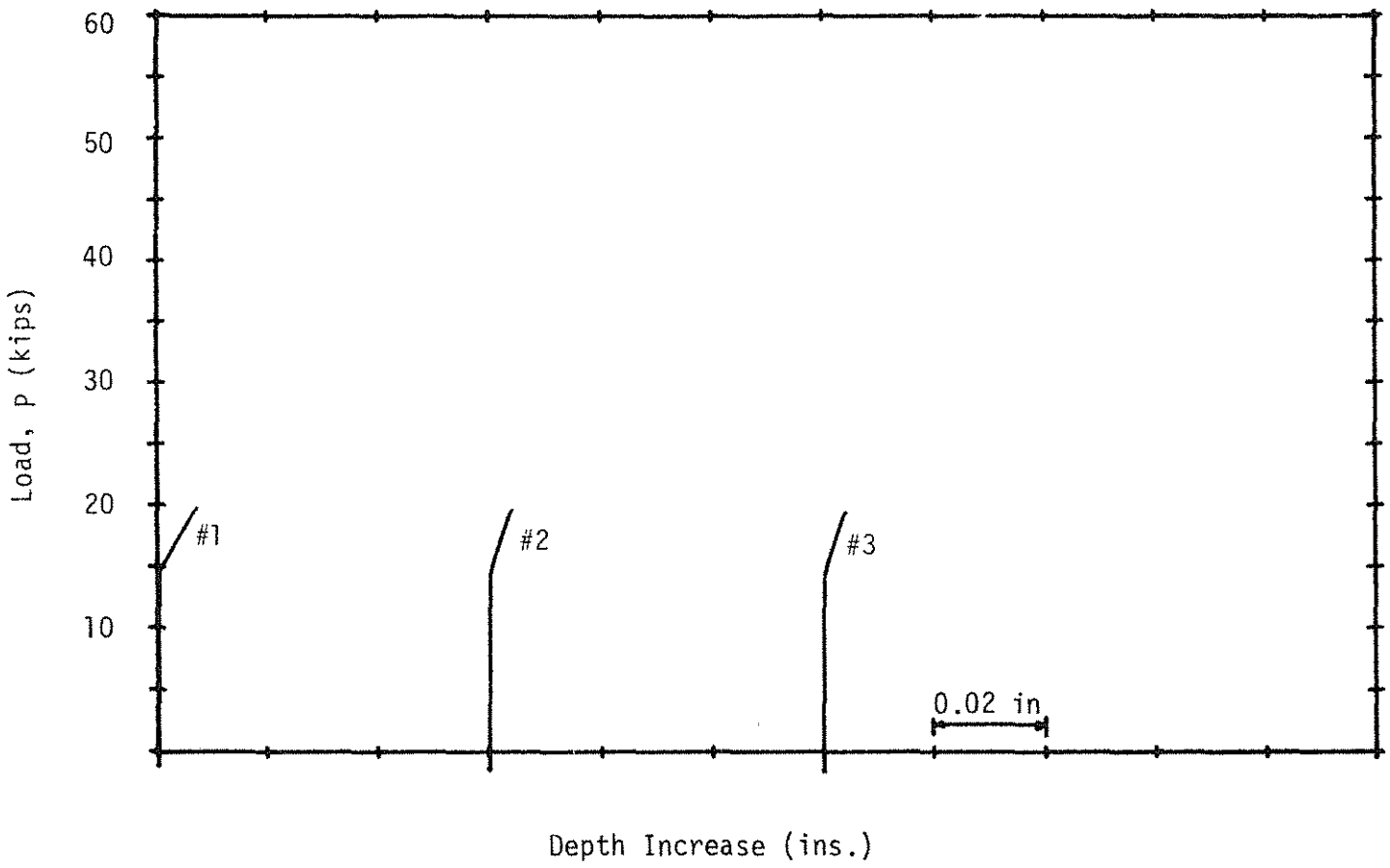

Figure 2.43. Load-Depth Increase Diagrams; Beam C00.

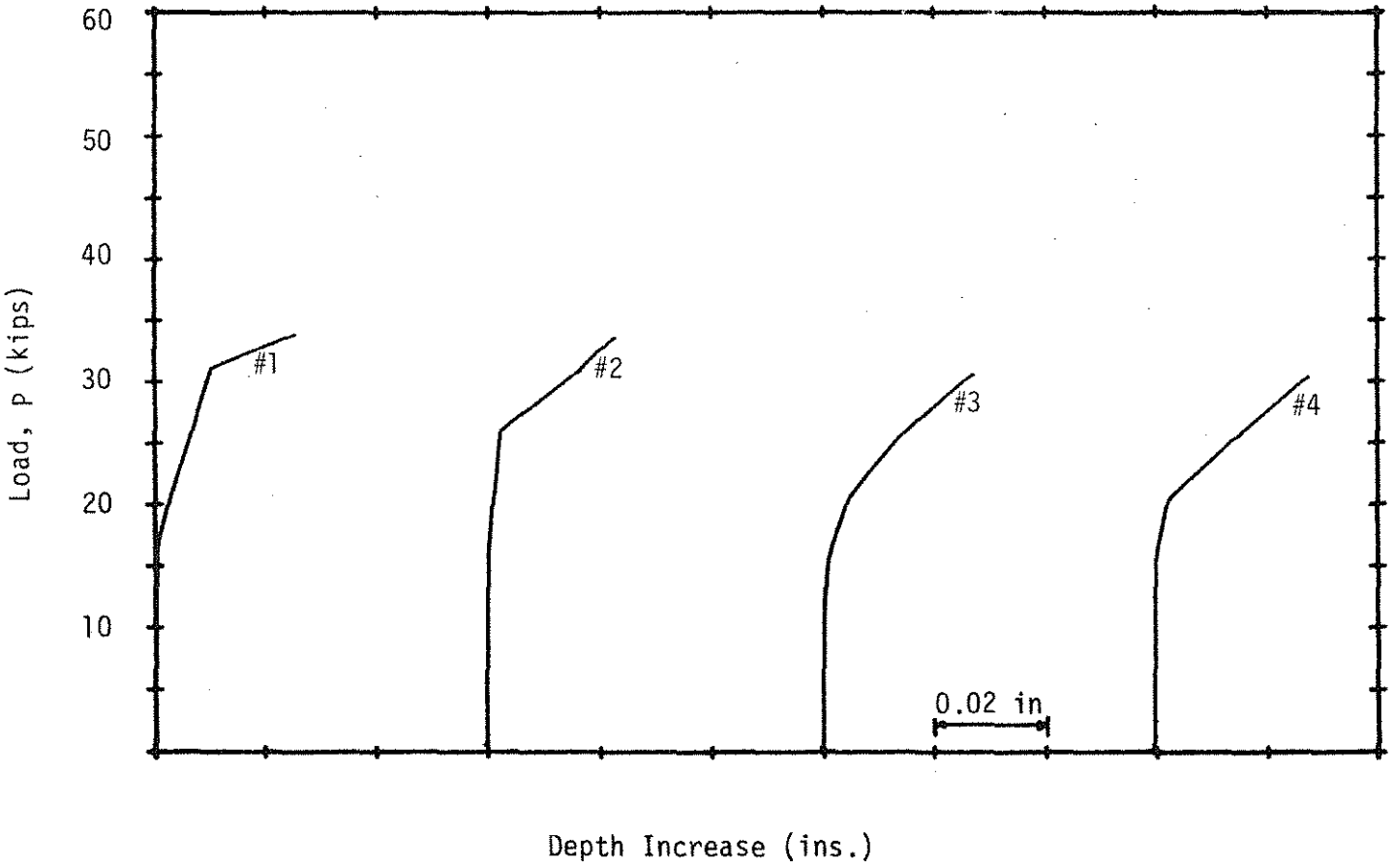

Figure 2.44. Load-Depth Increase Diagrams; Beam C25.

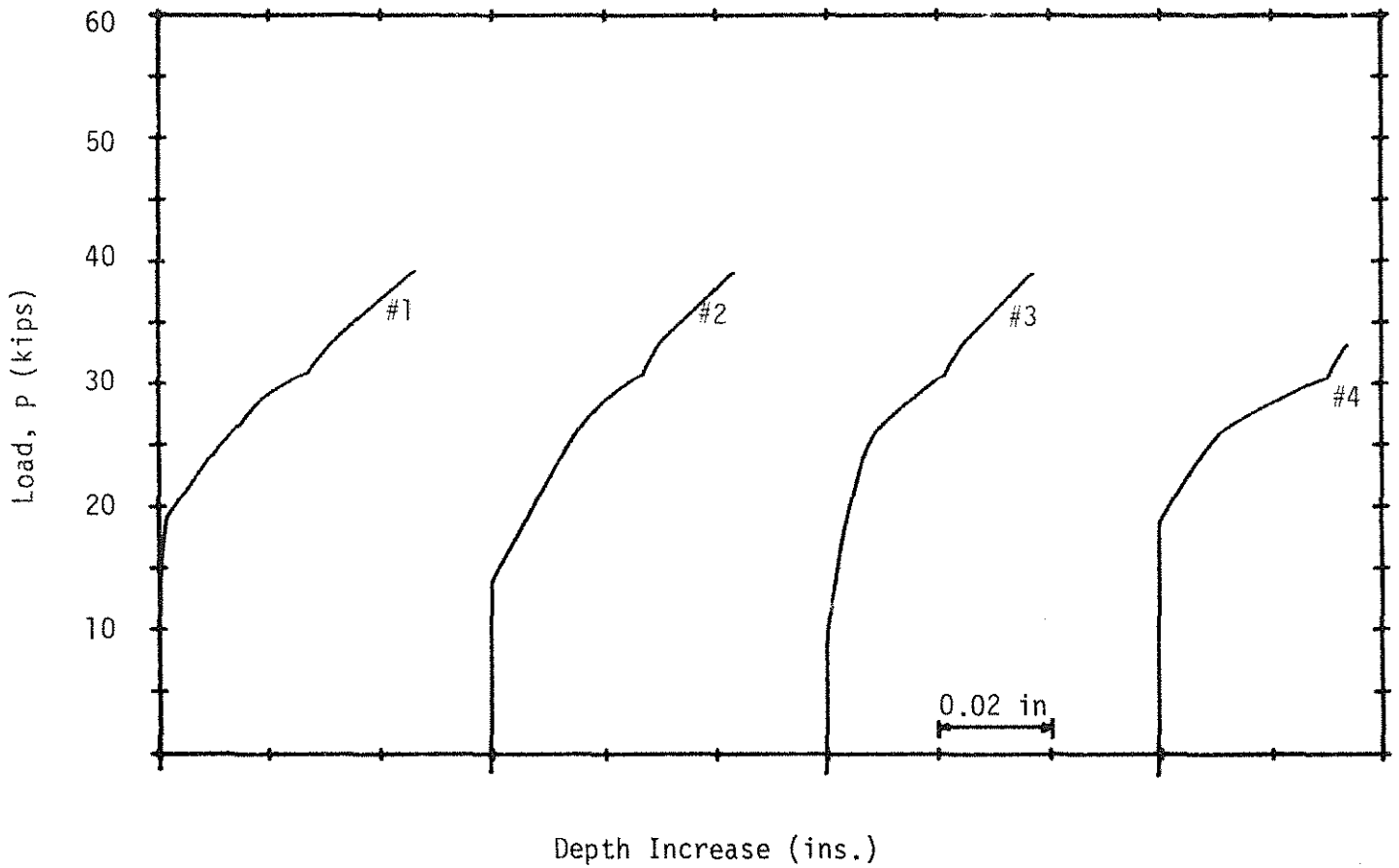

Figure 2.45. Load-Depth Increase Diagrams; Beam C50.

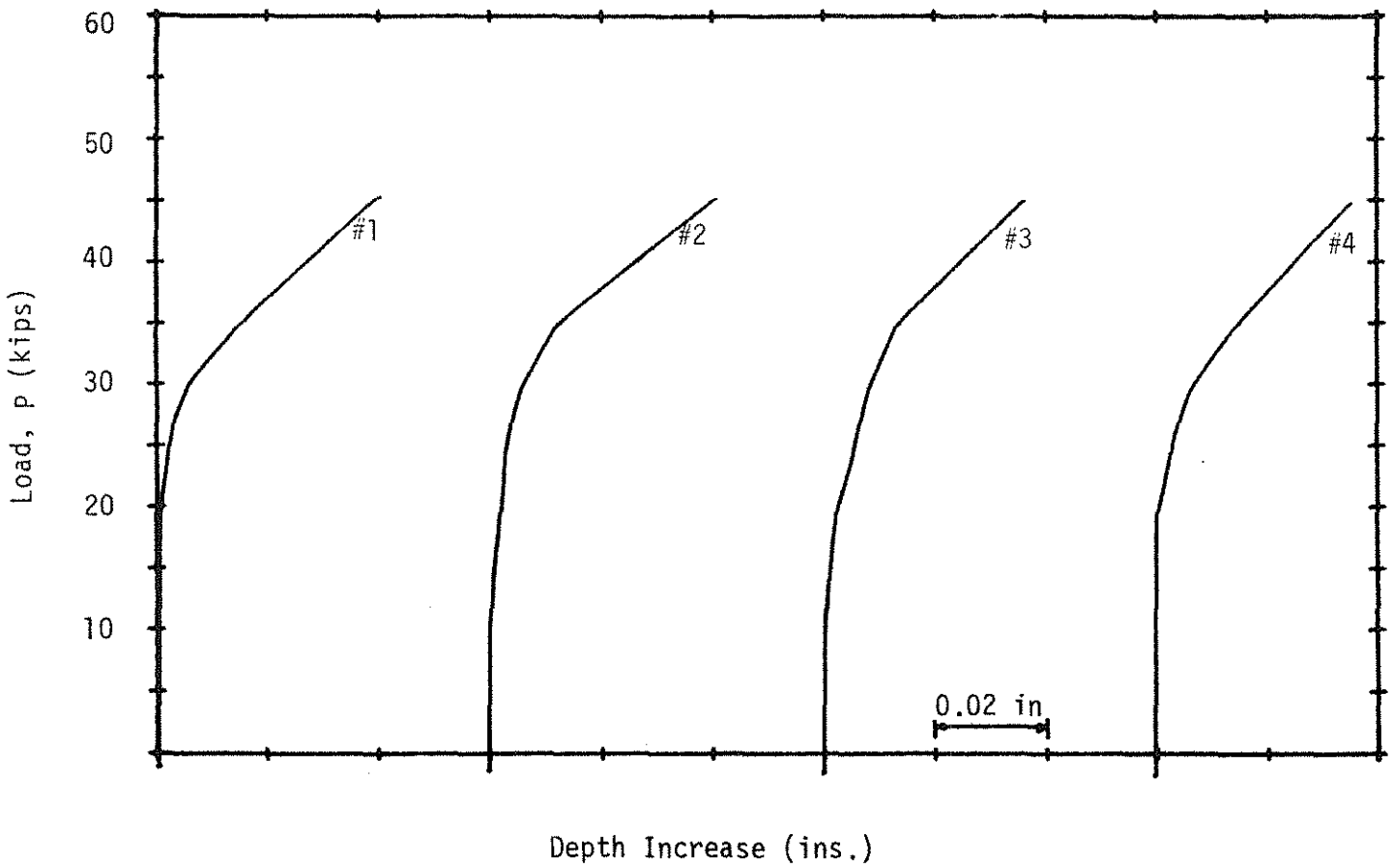

Figure 2.46. Load-Depth Increase Diagrams; Beam C75.

Beam A00

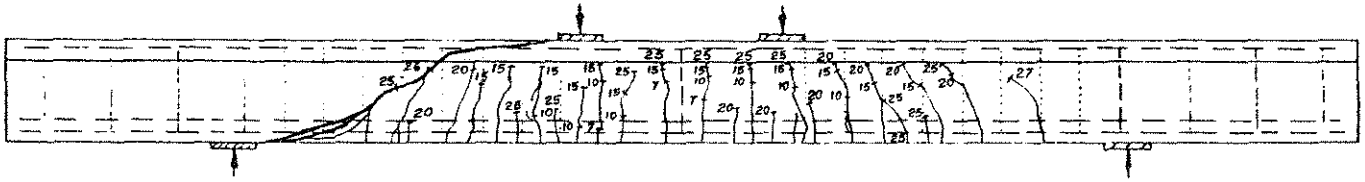

Beam A25

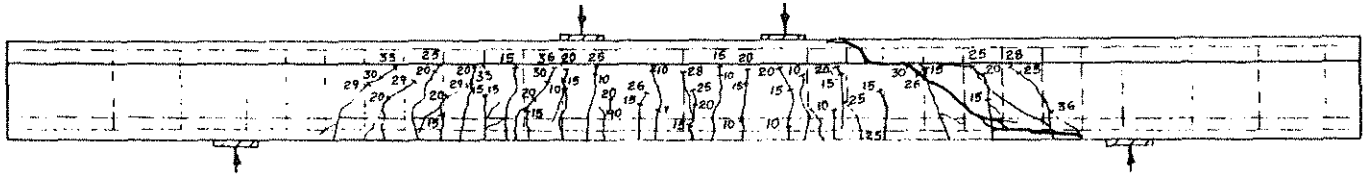

Beam A25a

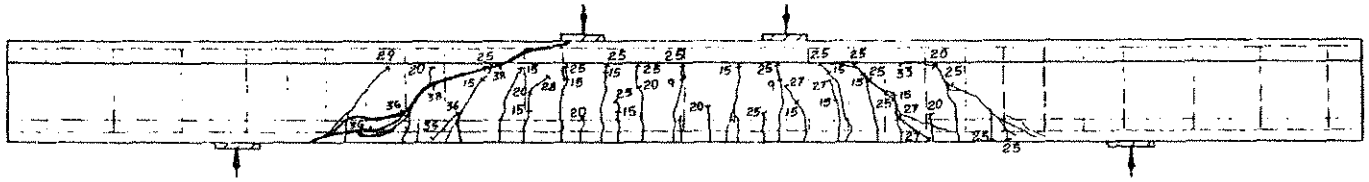

Figure 2.47. Cracking Patterns

Beam A50

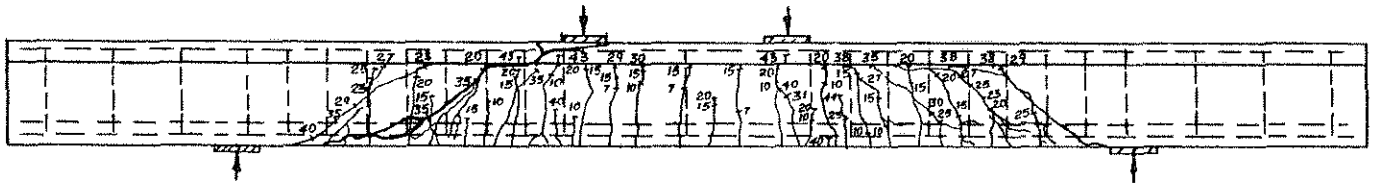

Beam A50a

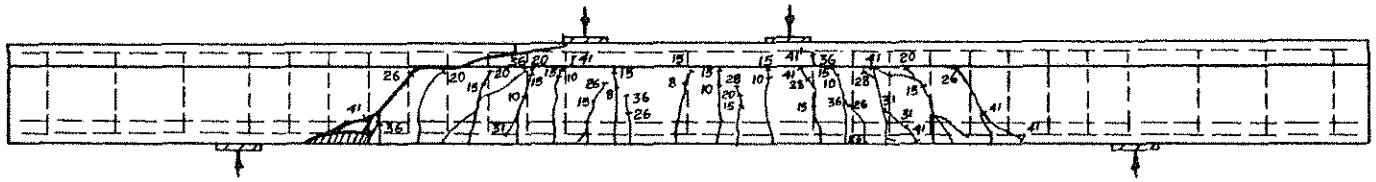

Beam A75

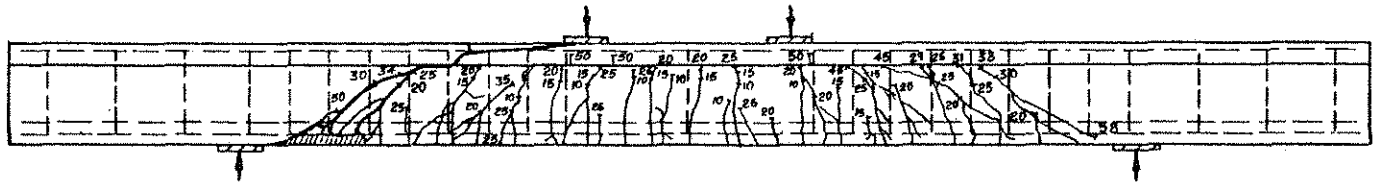

Figure 2.48. Cracking Patterns

Beam B00

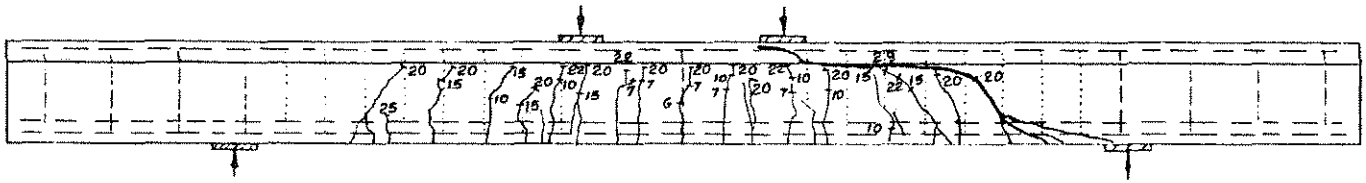

Beam B25

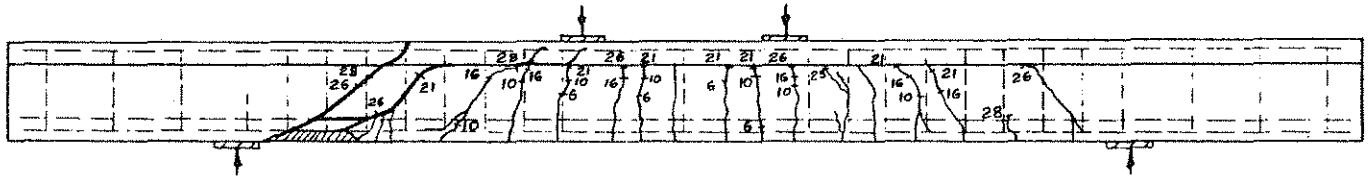

Beam B50

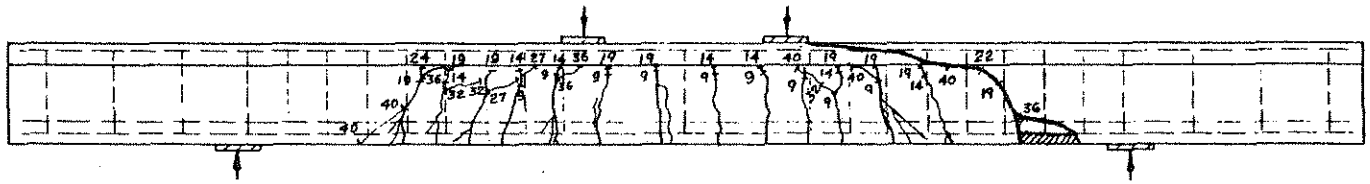

Figure 2.49. Cracking Patterns

Beam C00

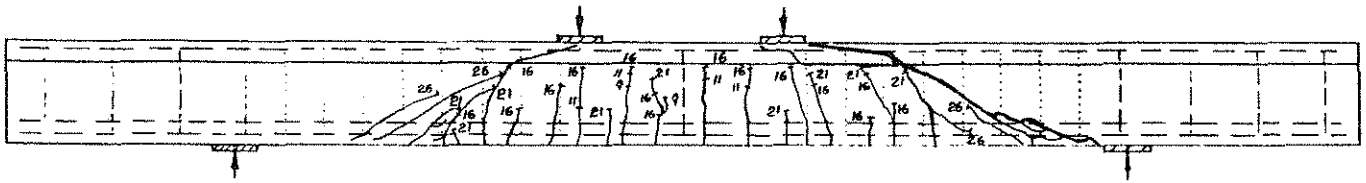

Beam C25

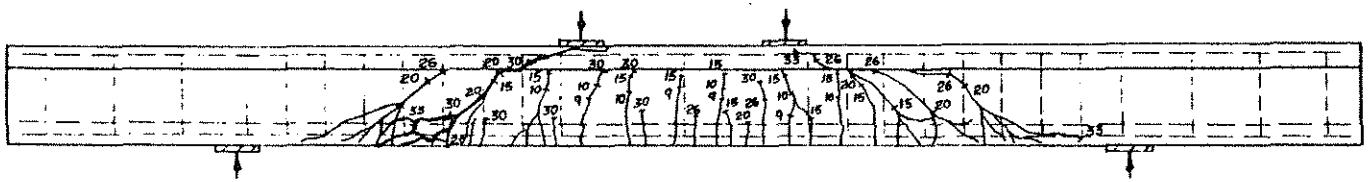

Beam C50

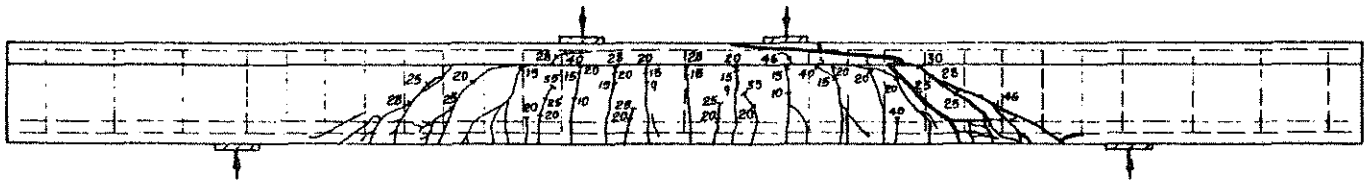

Figure 2.50. Cracking Patterns

Beam C75

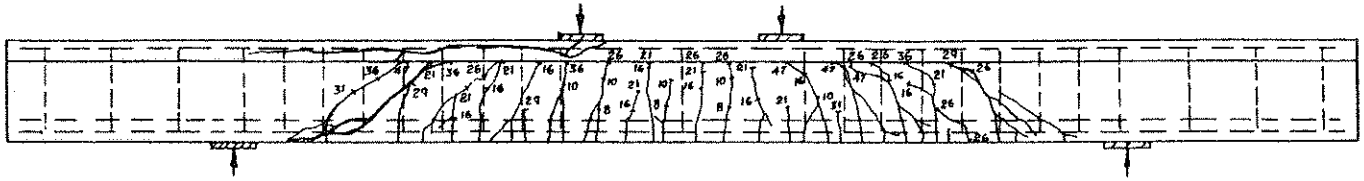

Figure 2.51. Cracking Patterns

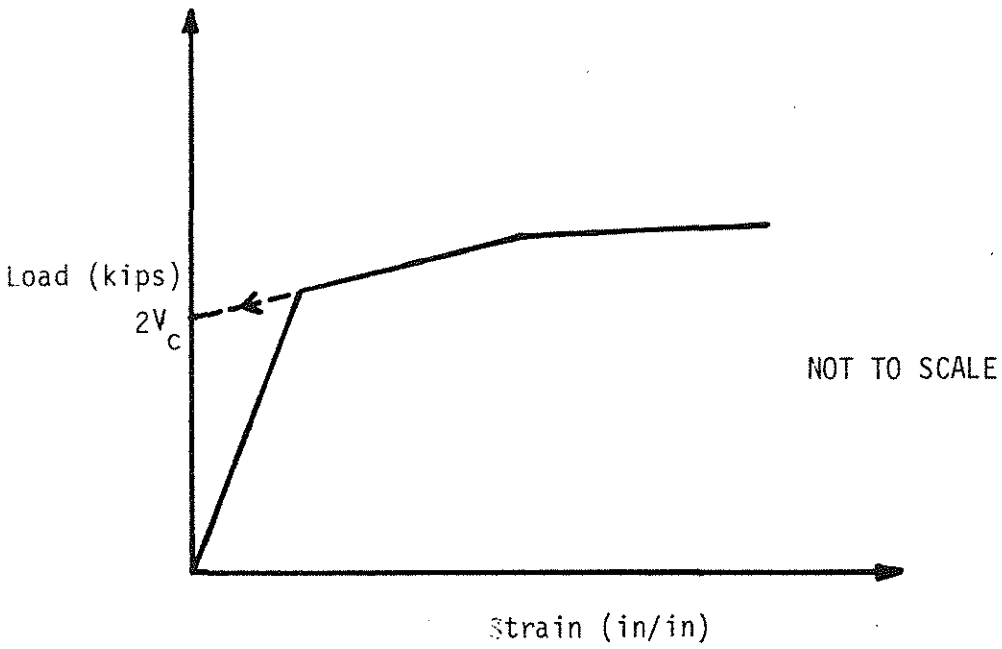

Figure 3.1. Method of Determining Shear Cracking Load from Stirrup Strain and Depth Increase Data.

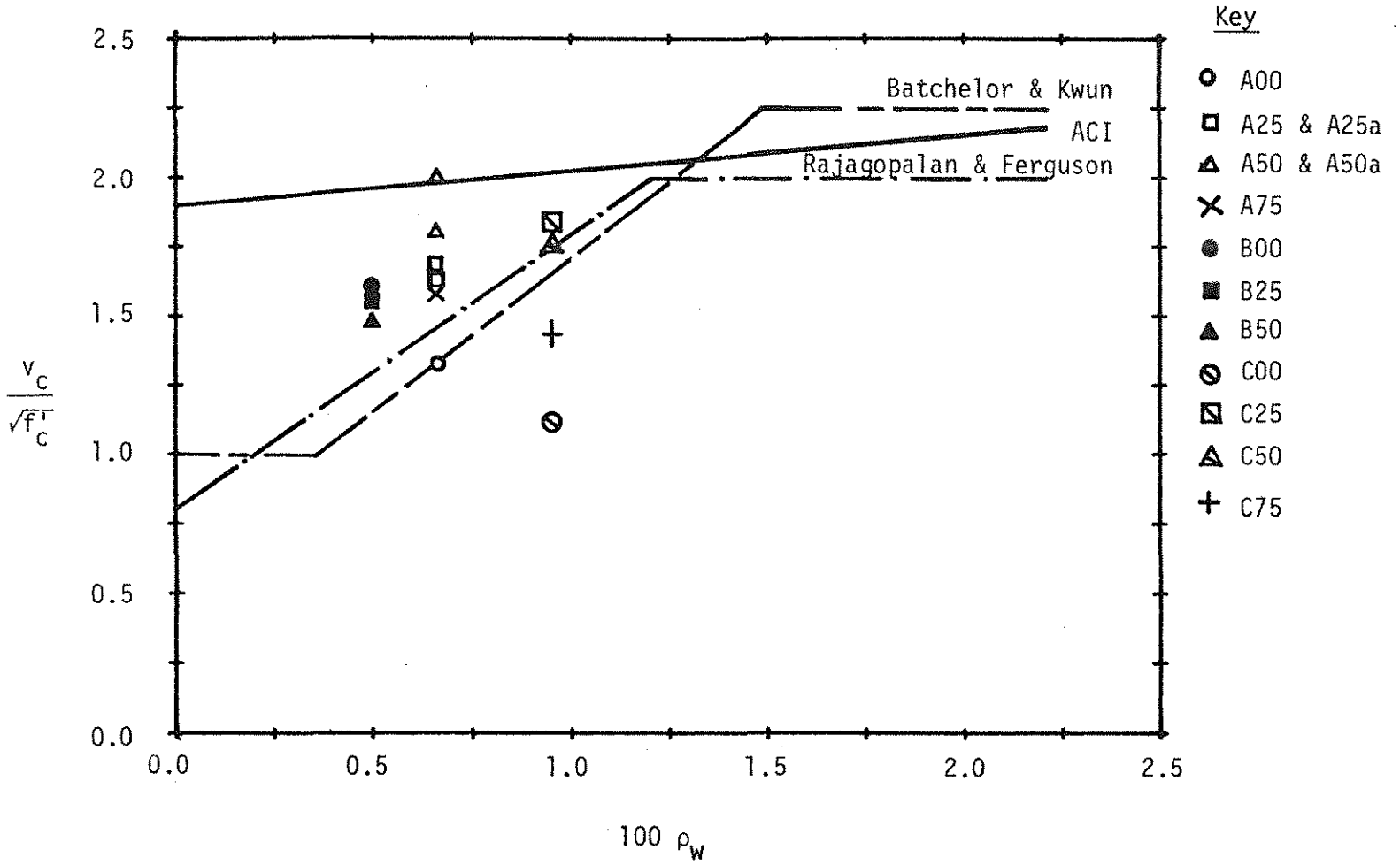

Figure 3.2(a). Stress at Diagonal Tension Cracking, v_c, from Crack Patterns.

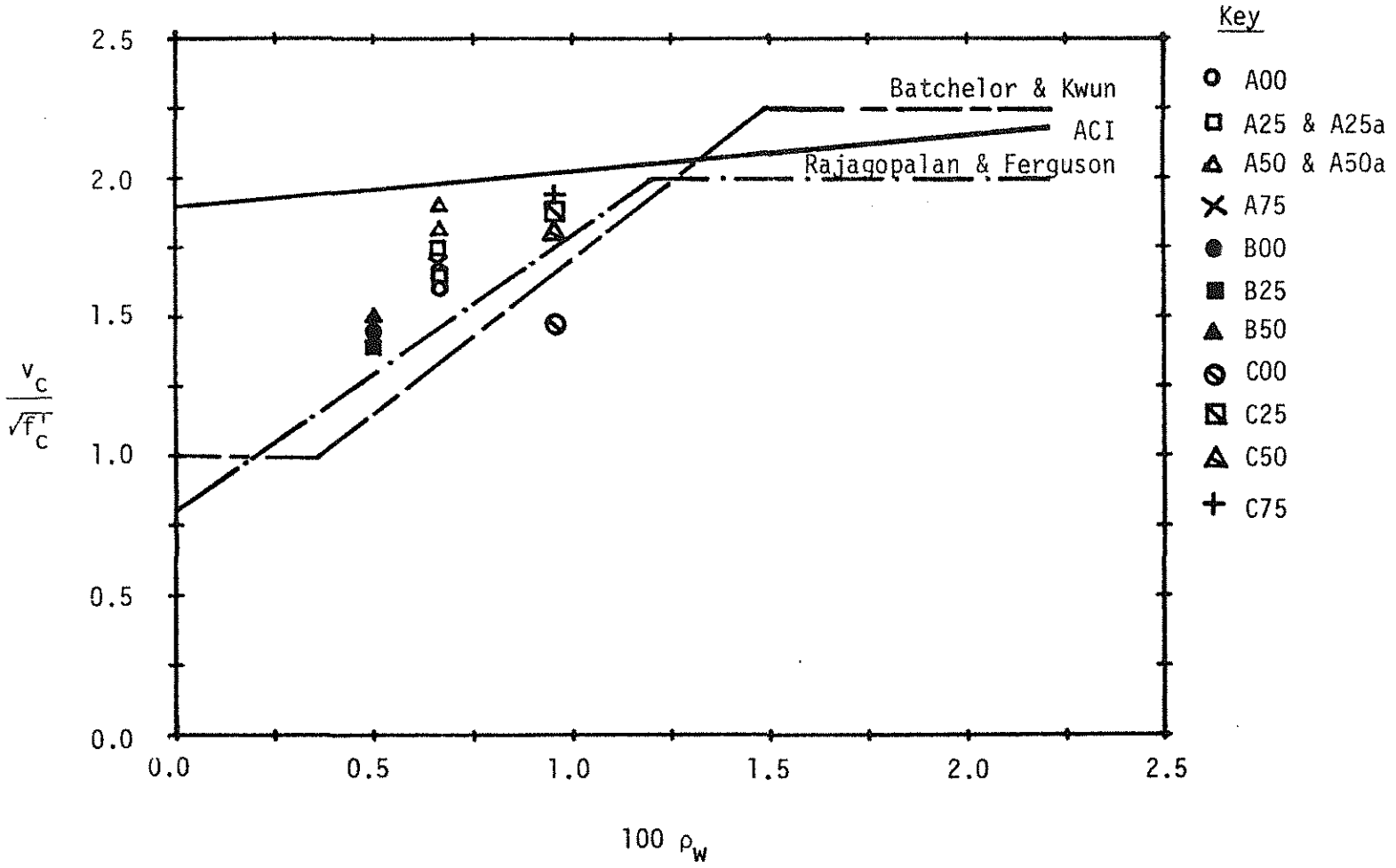

Figure 3.2(b). Stress at Diagonal Tension Cracking, v_c, from Concrete Strain.

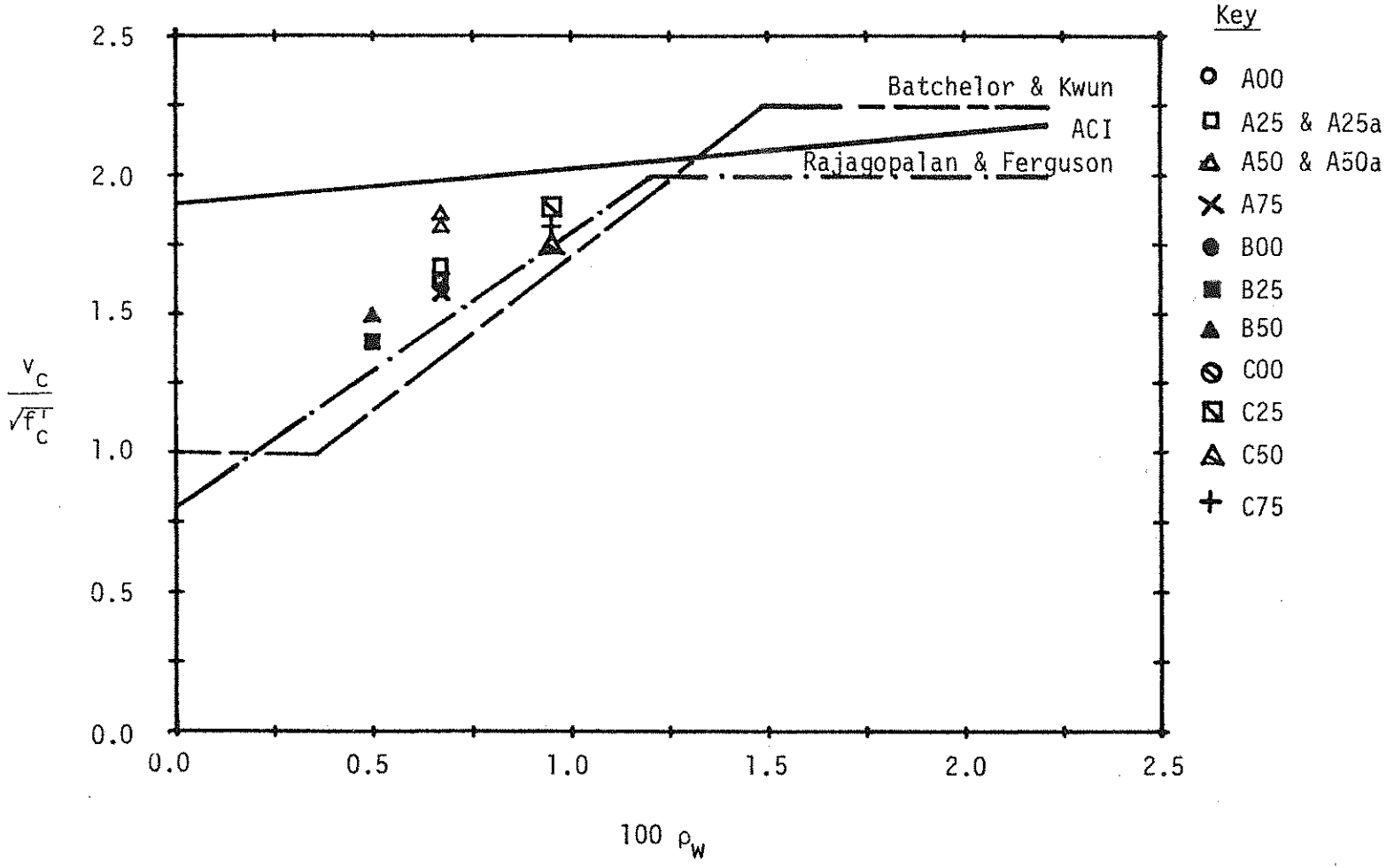

Figure 3.2(c). Stress at Diagonal Tension Cracking, v_c, from Stirrup Strain.

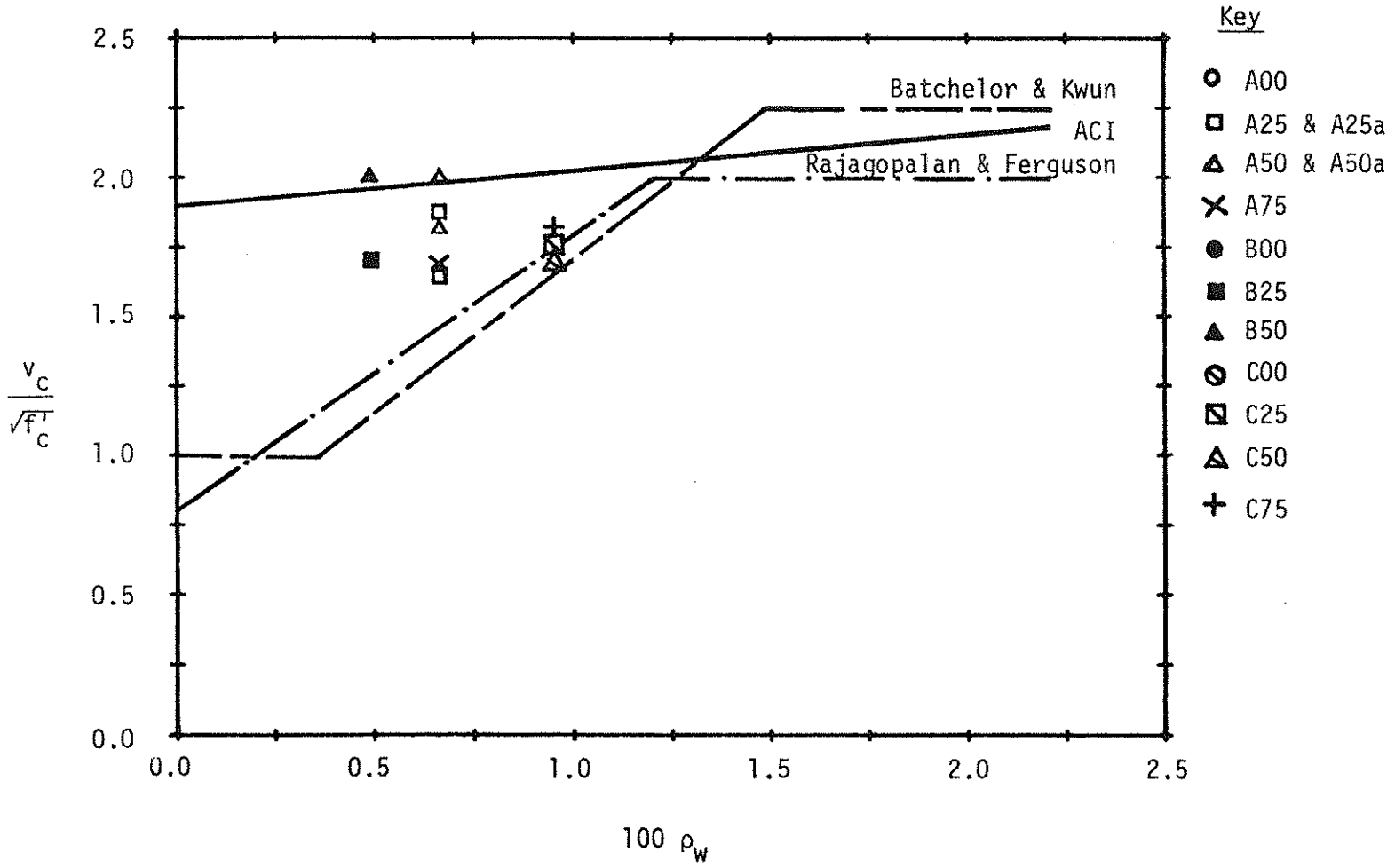

Figure 3.2(d). Stress at Diagonal Tension Cracking, v_c, from Depth Increase.

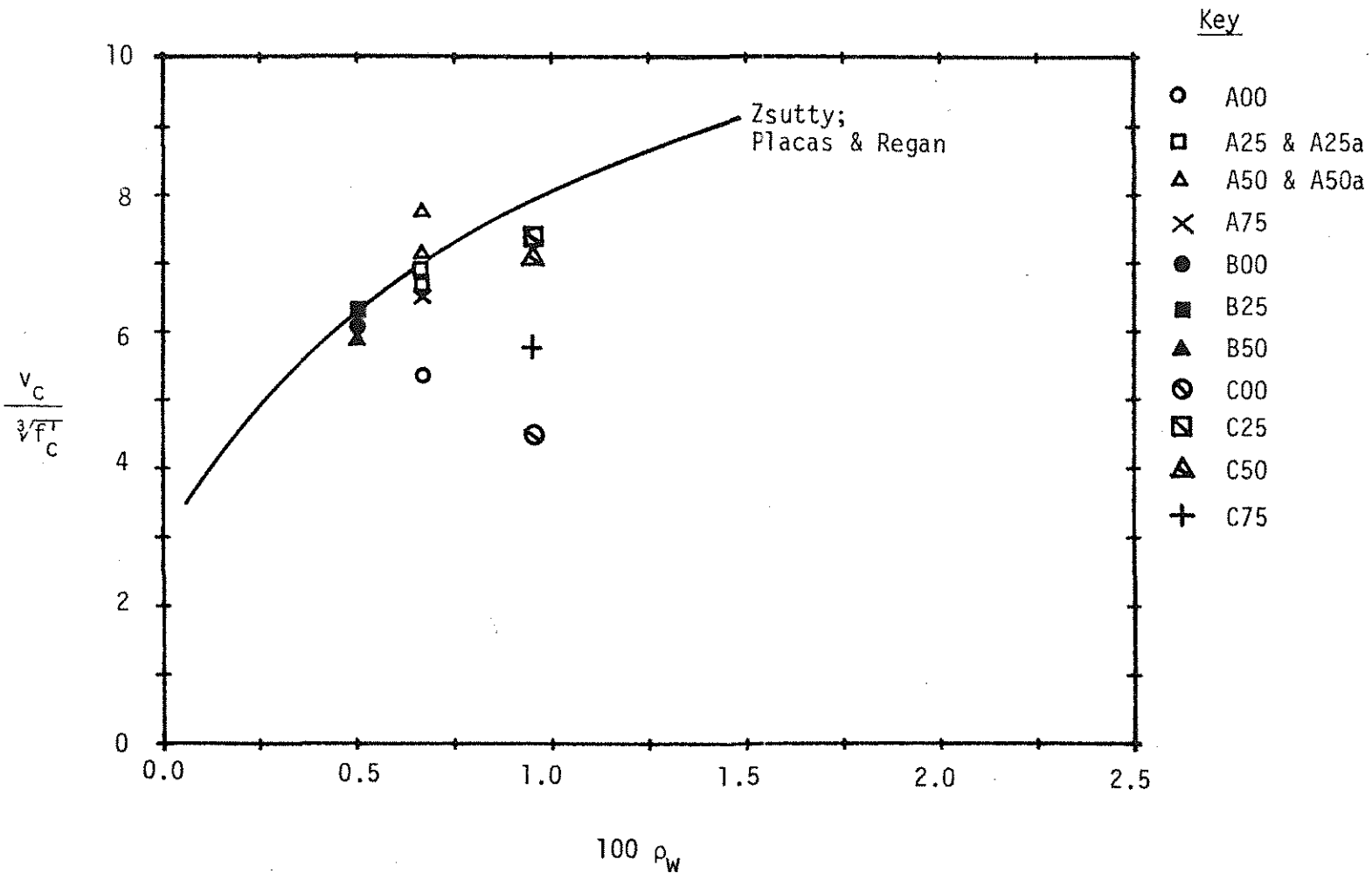

Figure 3.3(a). Stress at Diagonal Tension Cracking, v_c, from Crack Patterns.

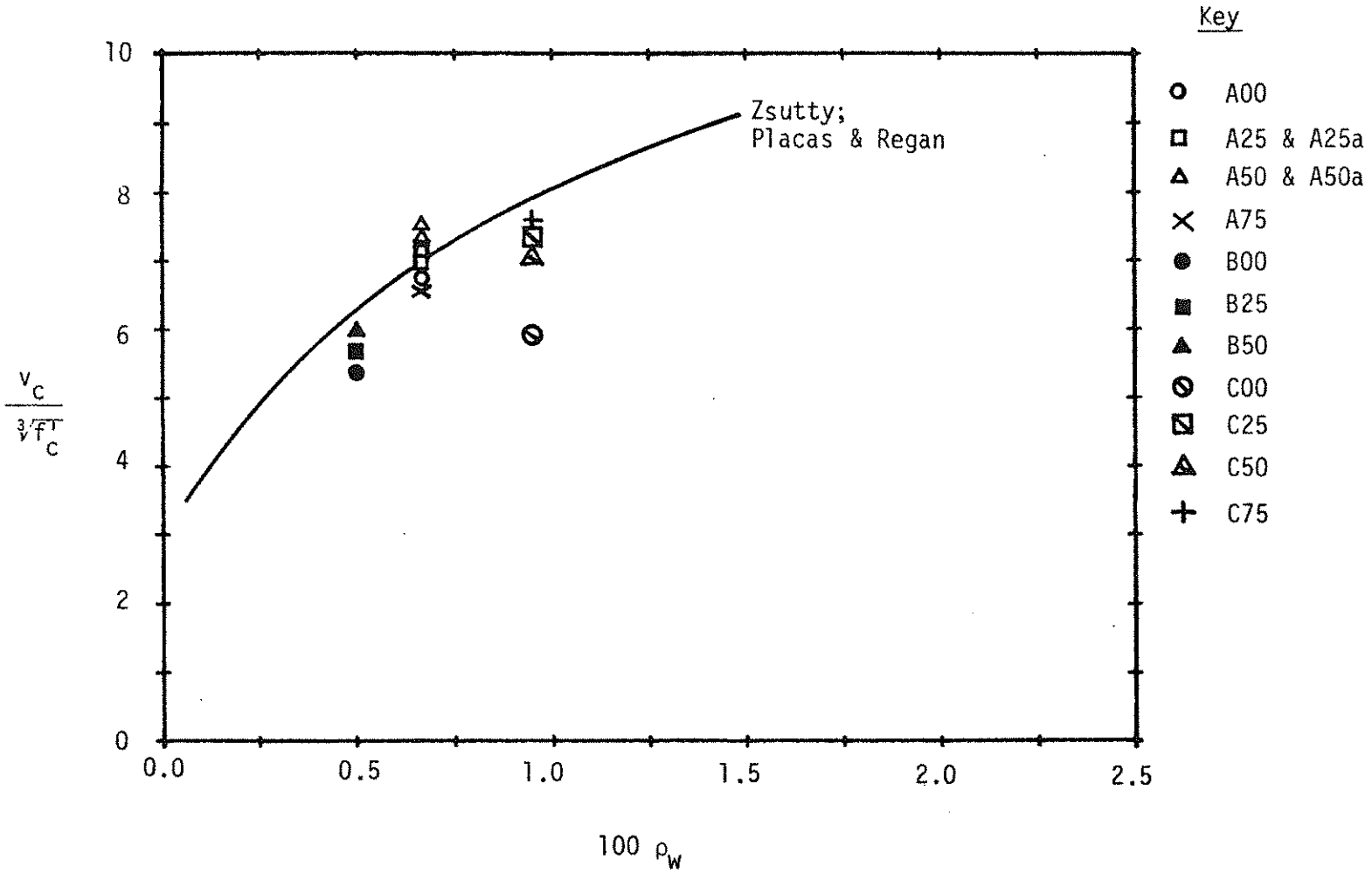

Figure 3.3(b). Stress at Diagonal Tension Cracking, v_c, from Concrete Strain.

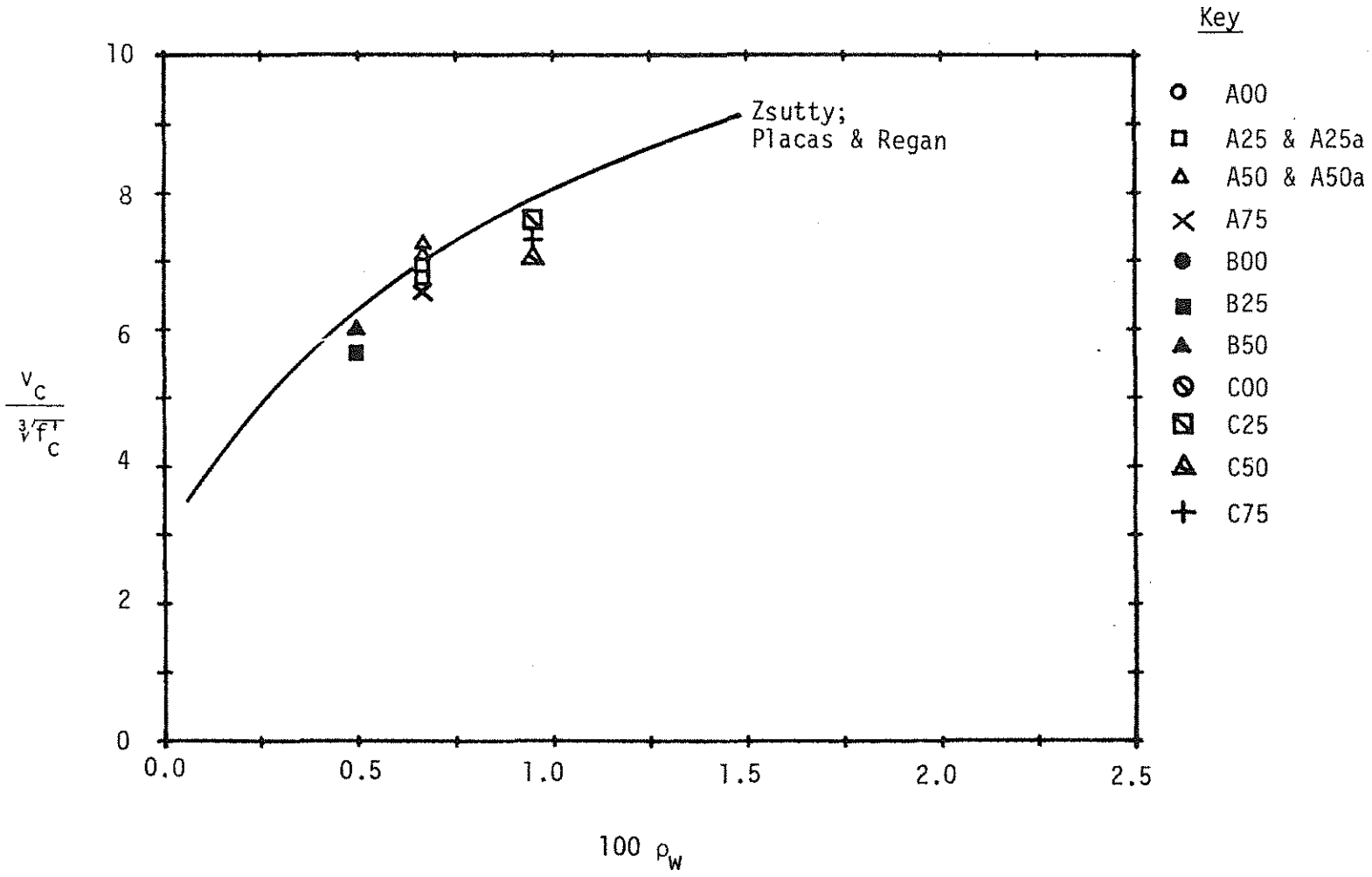

Figure 3.3(c). Stress at Diagonal Tension Cracking, v_c, from Stirrup Strain.

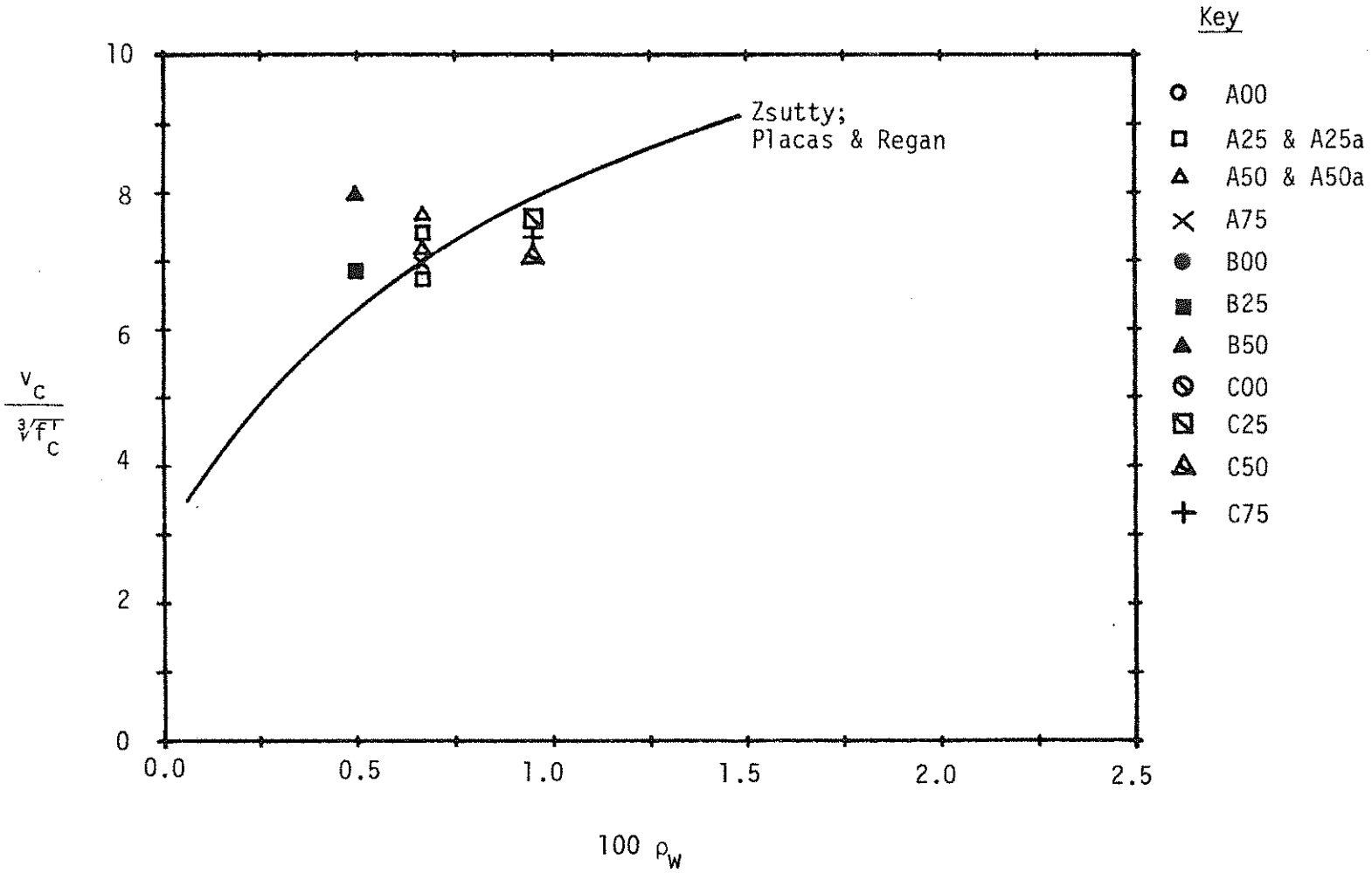

Figure 3.3(d). Stress at Diagonal Tension Cracking, v_c, from Depth Increase.

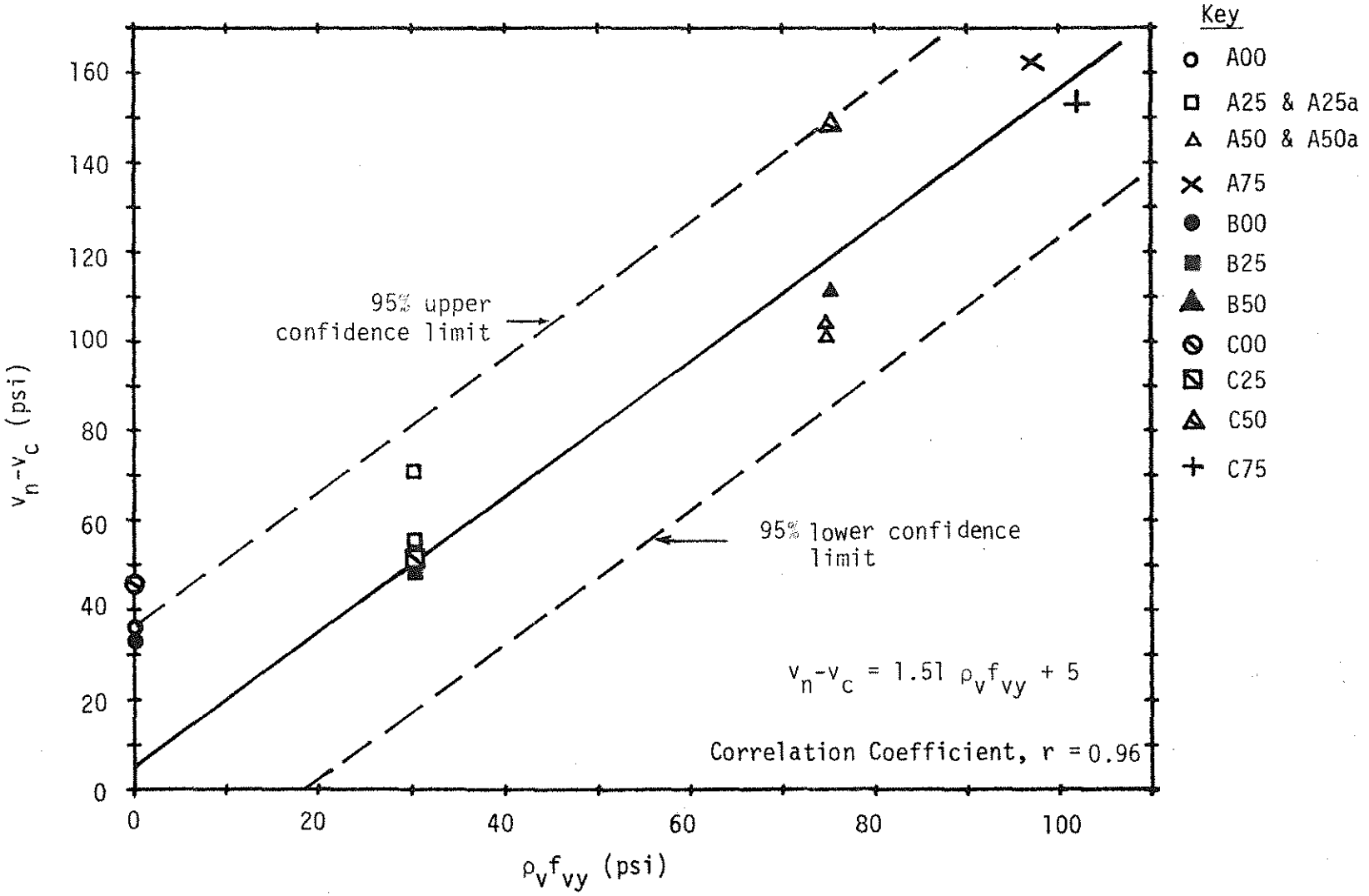

Figure 3.4(a). Effectiveness of Web Reinforcement, $v_n - v_c$, from Crack Patterns.

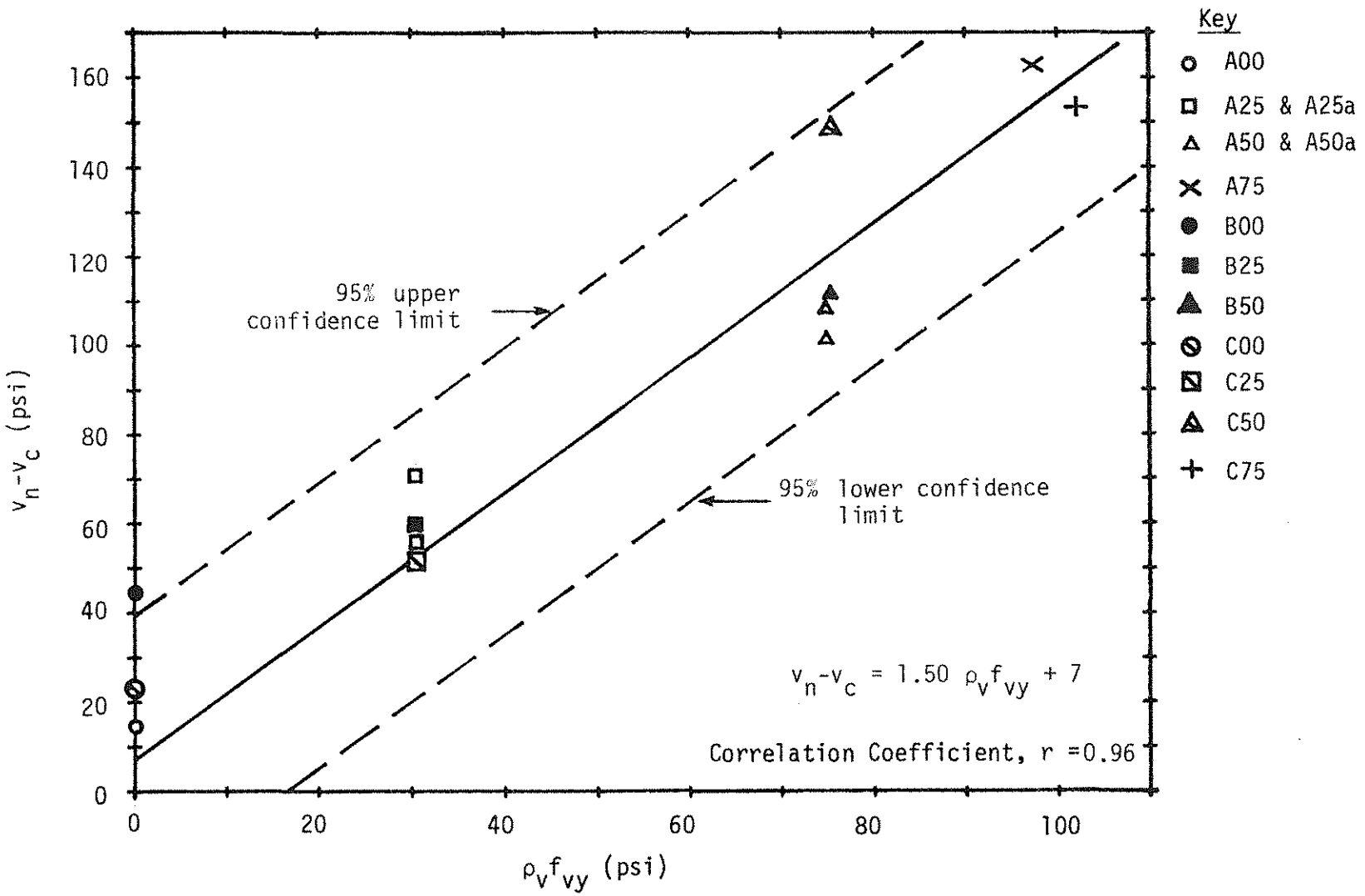

Figure 3.4(b). Effectiveness of Web Reinforcement, $v_n - v_c$, from Concrete Strain.

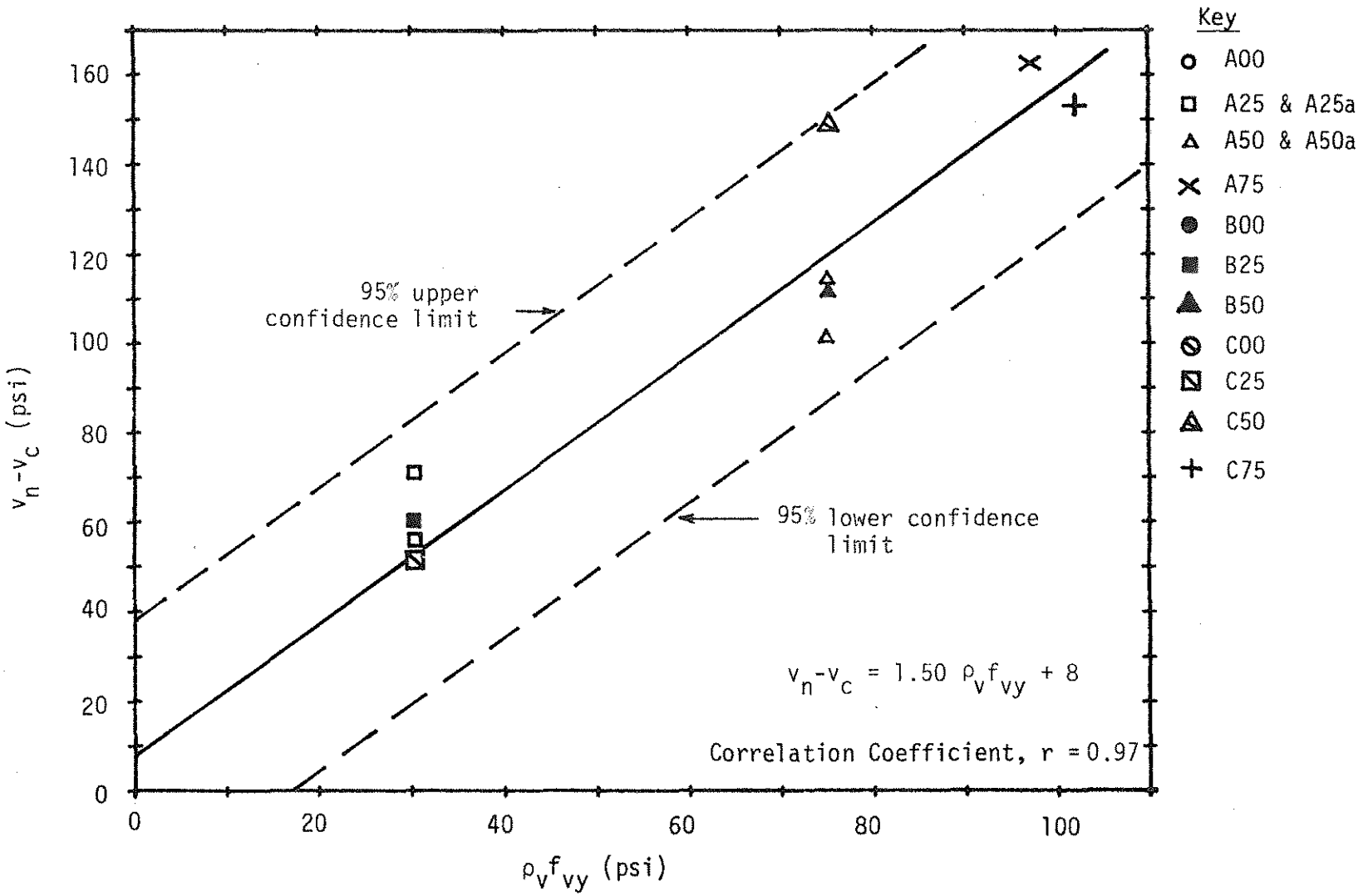

Figure 3.4(c) Effectiveness of Web Reinforcement, $v_n - v_c$, from Stirrup Strain.

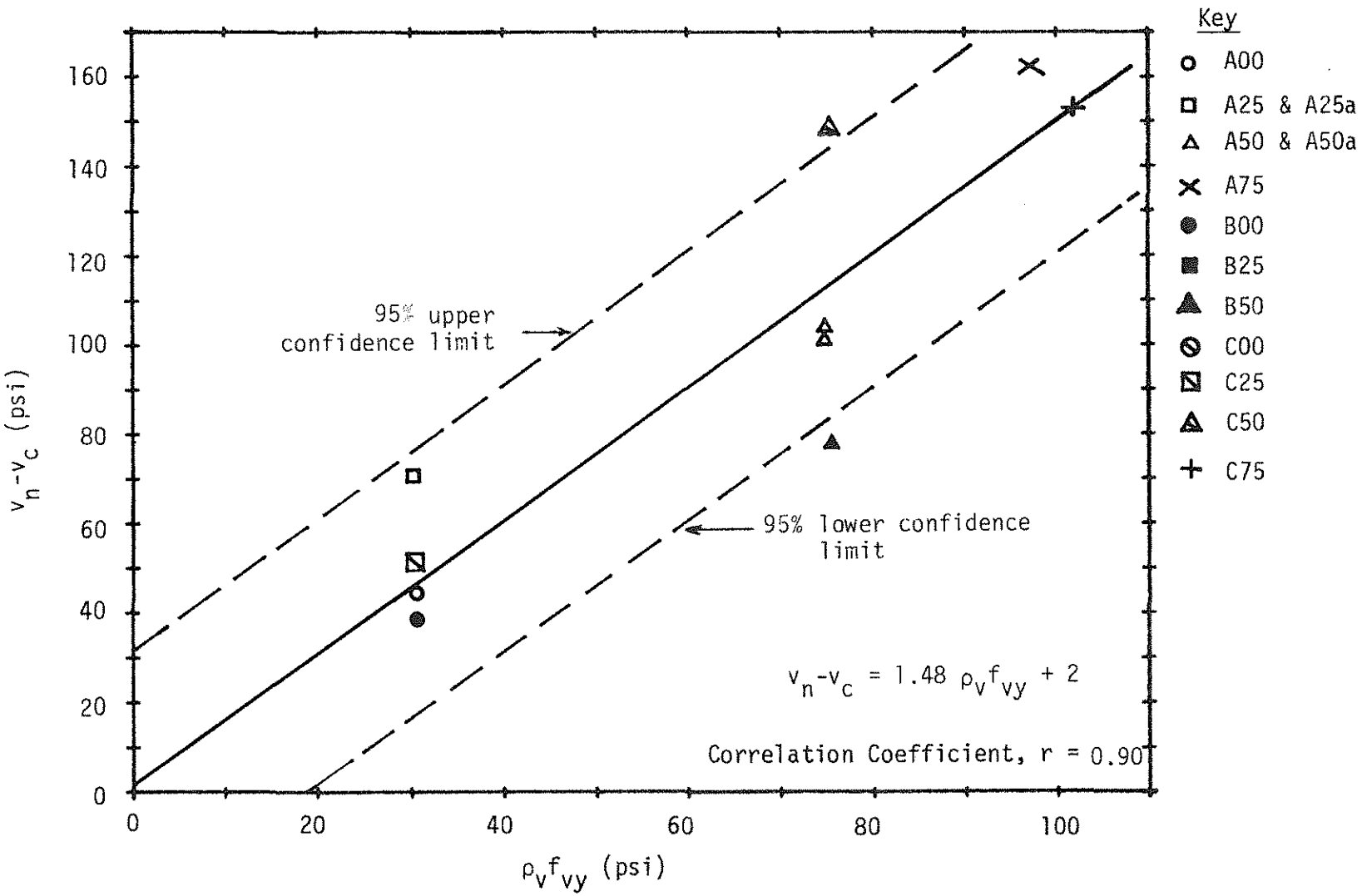

Figure 3.4(d) Effectiveness of Web Reinforcement, v_n-v_c, from Depth Increase.

APPENDIX A

NOTATION

Symbols used in the text are defined where they first appear. A summary of the symbols is presented below.

a = shear span

A_s = area of flexural reinforcement

A_v = area of web reinforcement

b_w = web width of T-beam

C = constant in equation for effectiveness of stirrups

d = distance from extreme compression fiber to centroid of flexural reinforcement

f'_c = compressive strength of concrete measured on 6 x 12 inch cylinders

f_r = modulus of rupture from 6 x 6 x 21 inch flexural specimens

f_{vy} = yield strength of web reinforcement

f_y = yield strength of flexural reinforcement

M_u = factored bending moment at section

r = coefficient of correlation

s = spacing of stirrups in a direction parallel to the longitudinal reinforcement

v_b = basic shear stress, also shear stress carried by concrete

v_c = nominal shear stress carried by concrete, also, shear stress at diagonal tension cracking = $V_c/b_w d$

v_n = nominal shear stress = $V_n/b_w d$

v_u = factored shear stress at section = $V_u/b_w d$

V_c = nominal shear force carried by concrete, also, shear force at diagonal tension cracking.

V_e = coefficient of variation

V_n = nominal shear force (Ultimate strength)

V_u = factored shear force at section

ρ_v = ratio of shear reinforcement = $A_v/b_w s$

ρ_w = ratio of flexural reinforcement = $A_s/b_w d$

σ = standard deviation

ϕ = strength reduction factor

APPENDIX B

LOAD-DEFLECTION CURVES

Figure No.	Beam
B1	A00
B2	A25
B3	A25a
B4	A50
B5	A50a
B6	A75
B7	B00
B8	B25
B9	B50
B10	C00
B11	C25
B12	C50
B13	C75

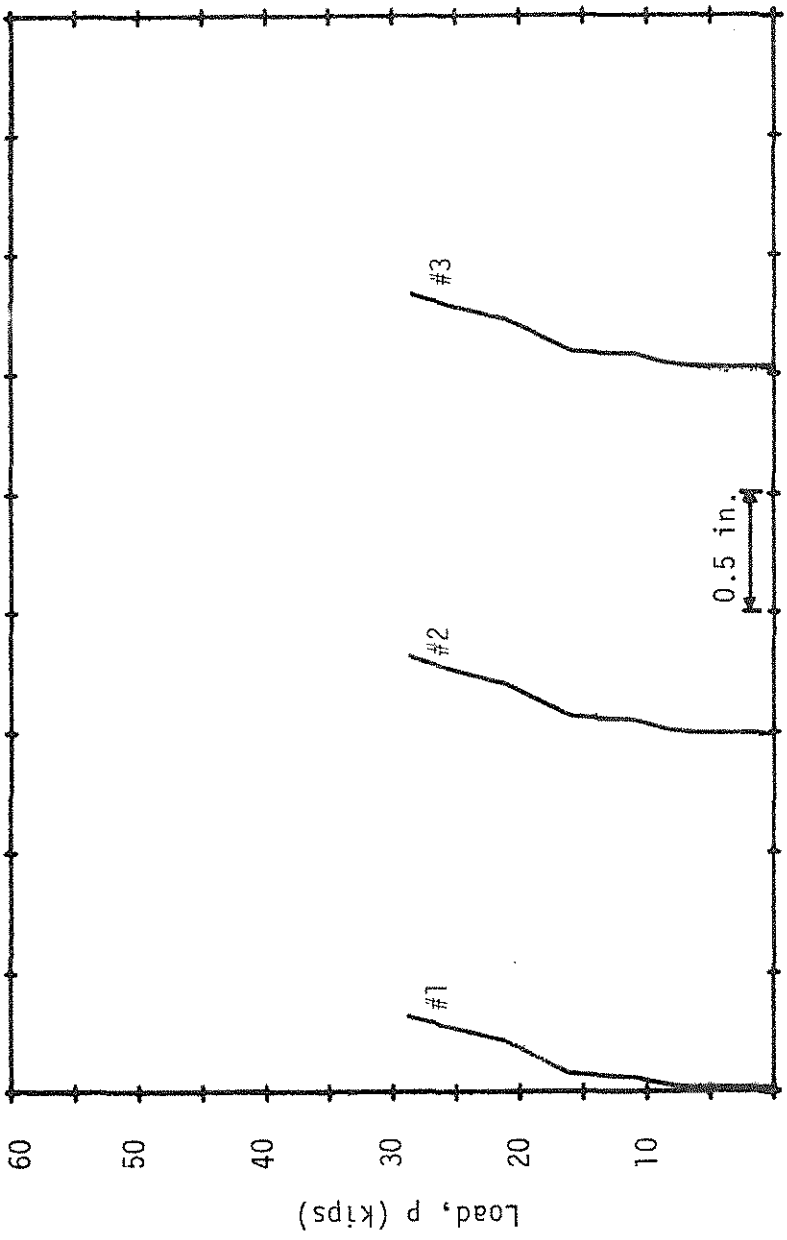

Figure B1. Load-Deflection Curves; Beam A00.

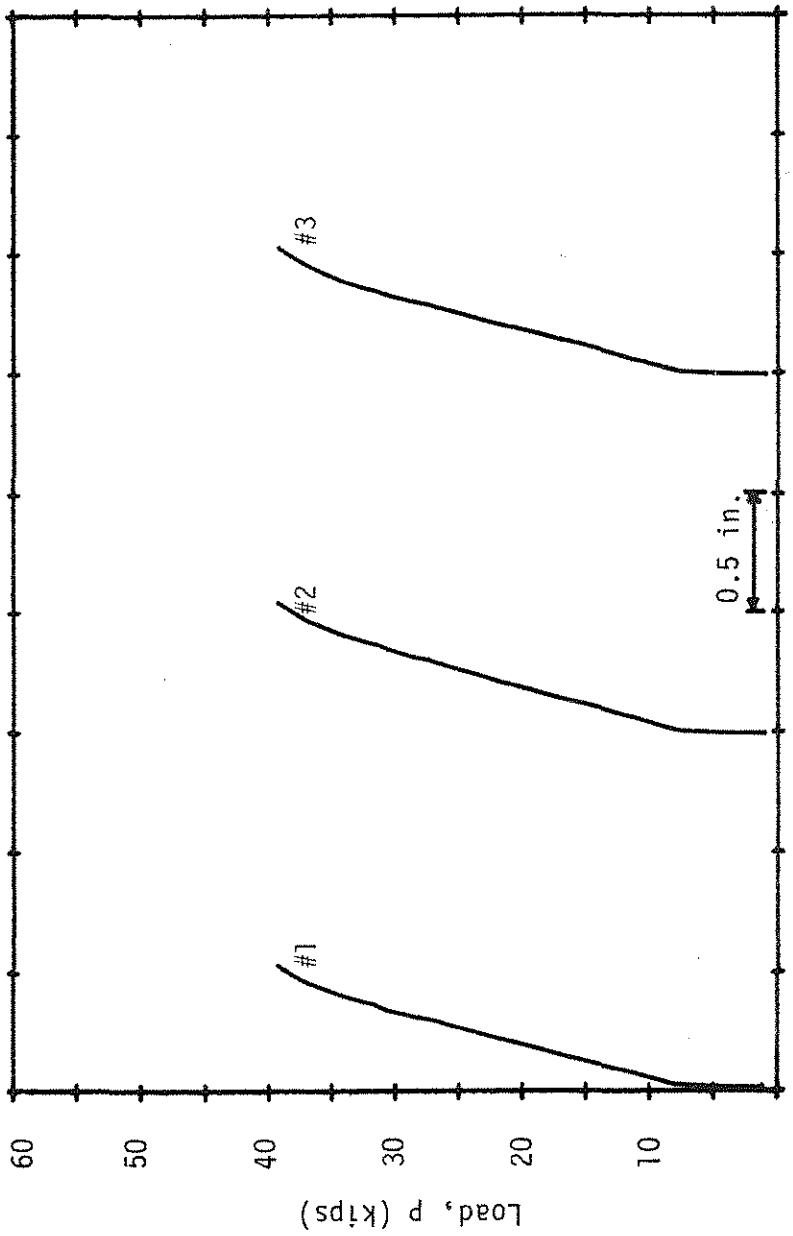

Figure B2. Load-Deflection Curves; Beam A25.

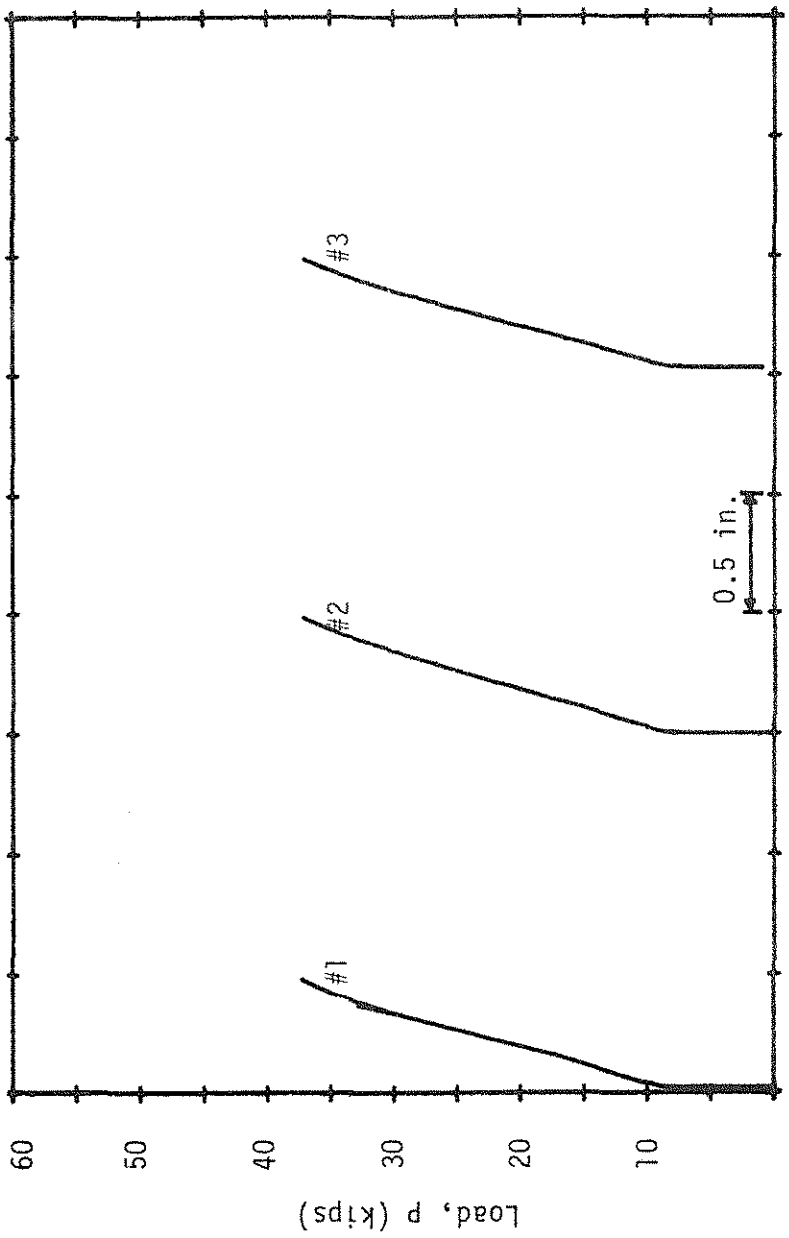

Figure B3. Load-Deflection Curves; Beam A25a.

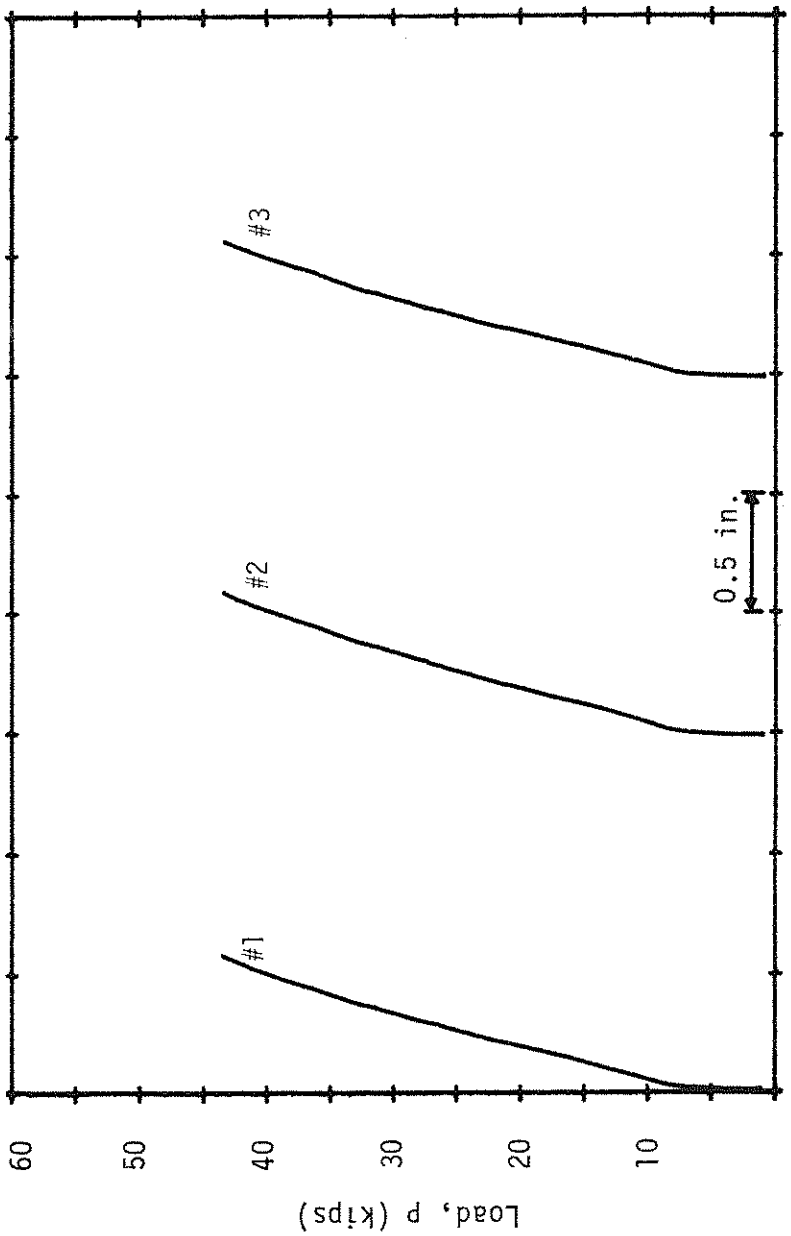

Figure B4. Load-Deflection Curves; Beam A50.

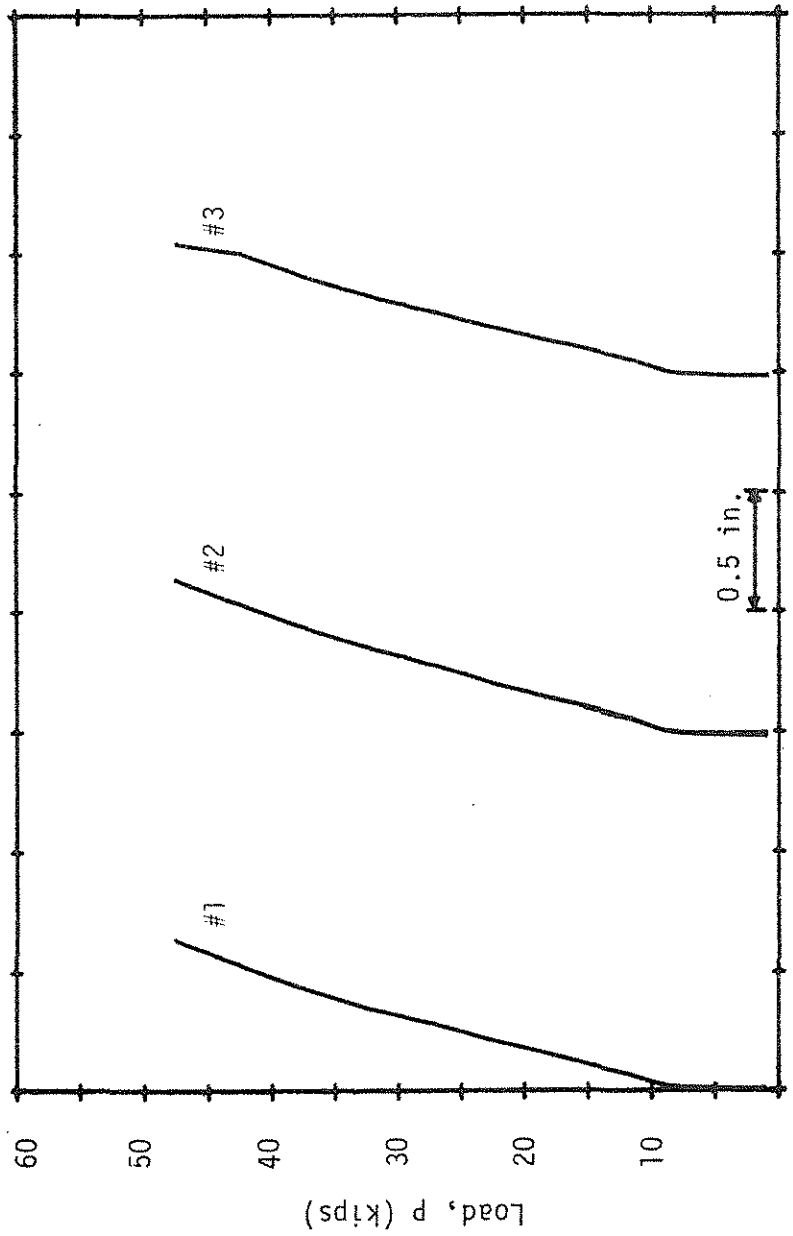

Figure B5. Load-Deflection Curves; Beam A50a.

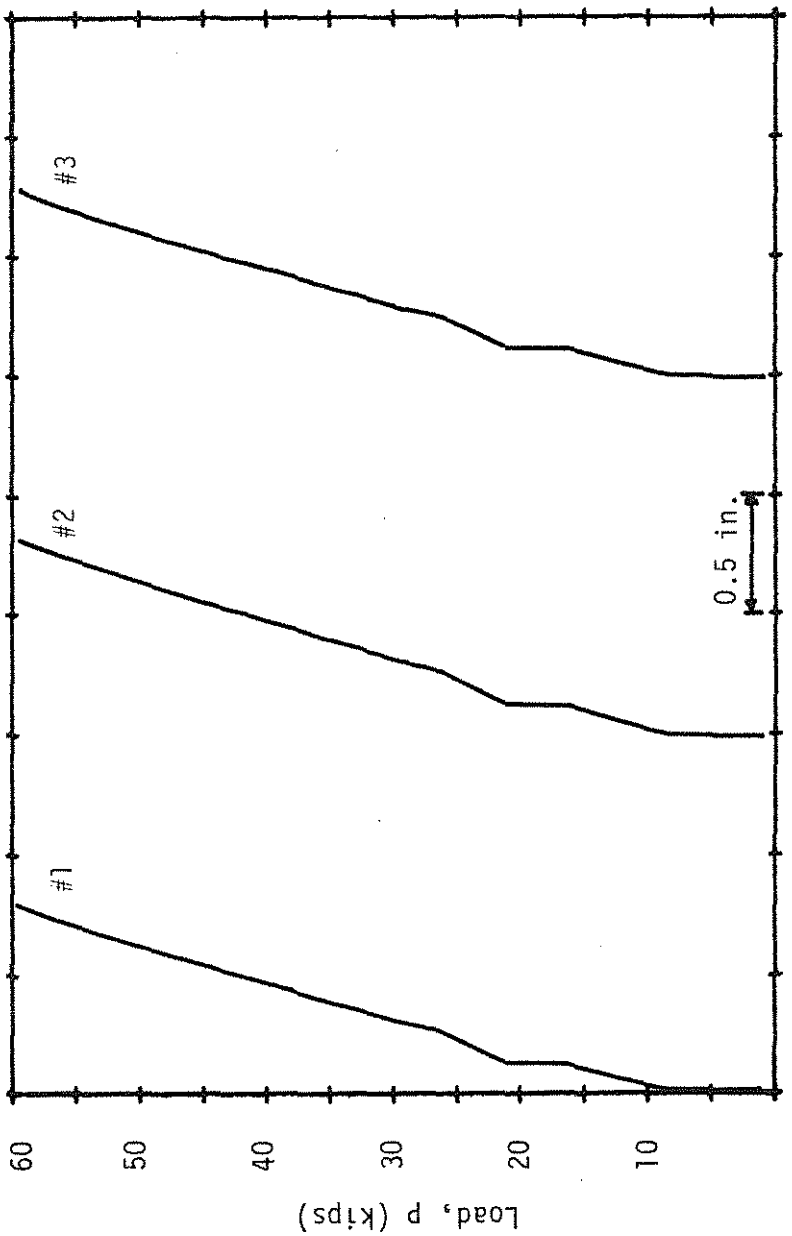

Figure B6. Load-Deflection Curves; Beam A75.

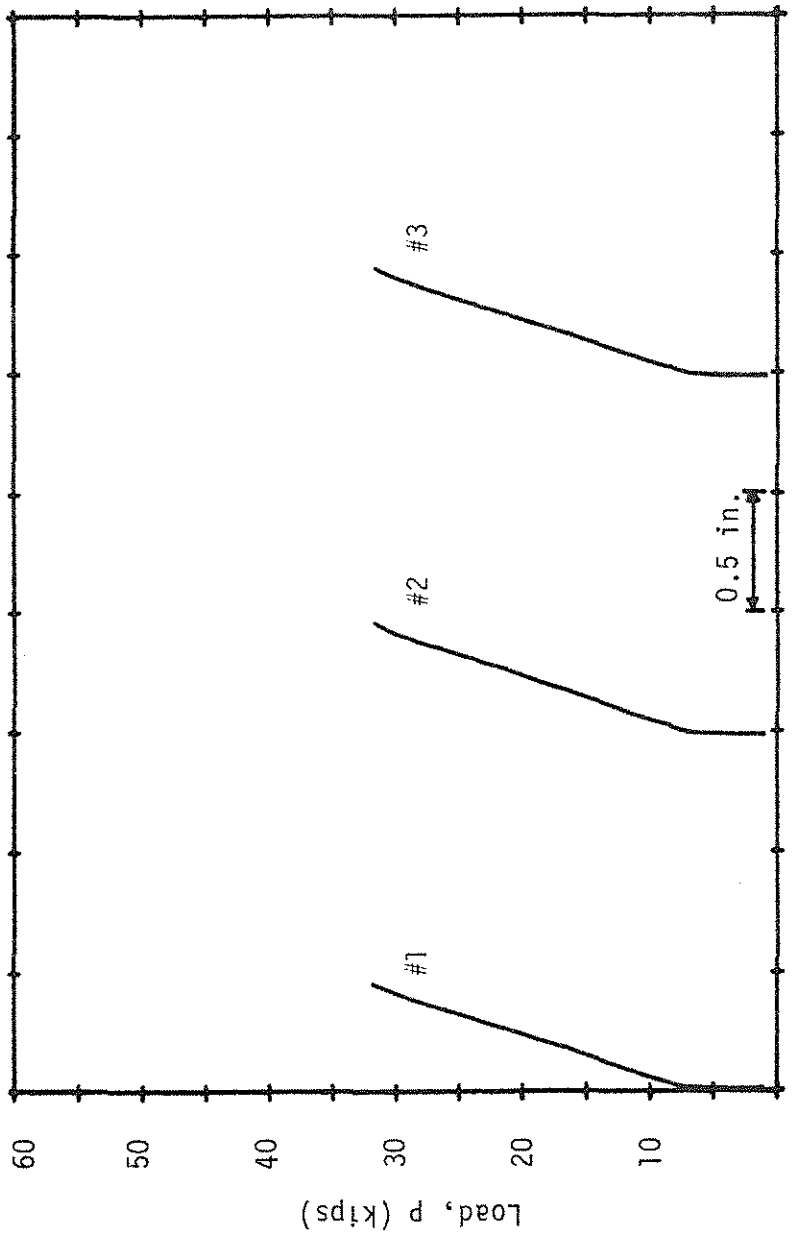

Figure B7. Load-Deflection Curves; Beam B00.

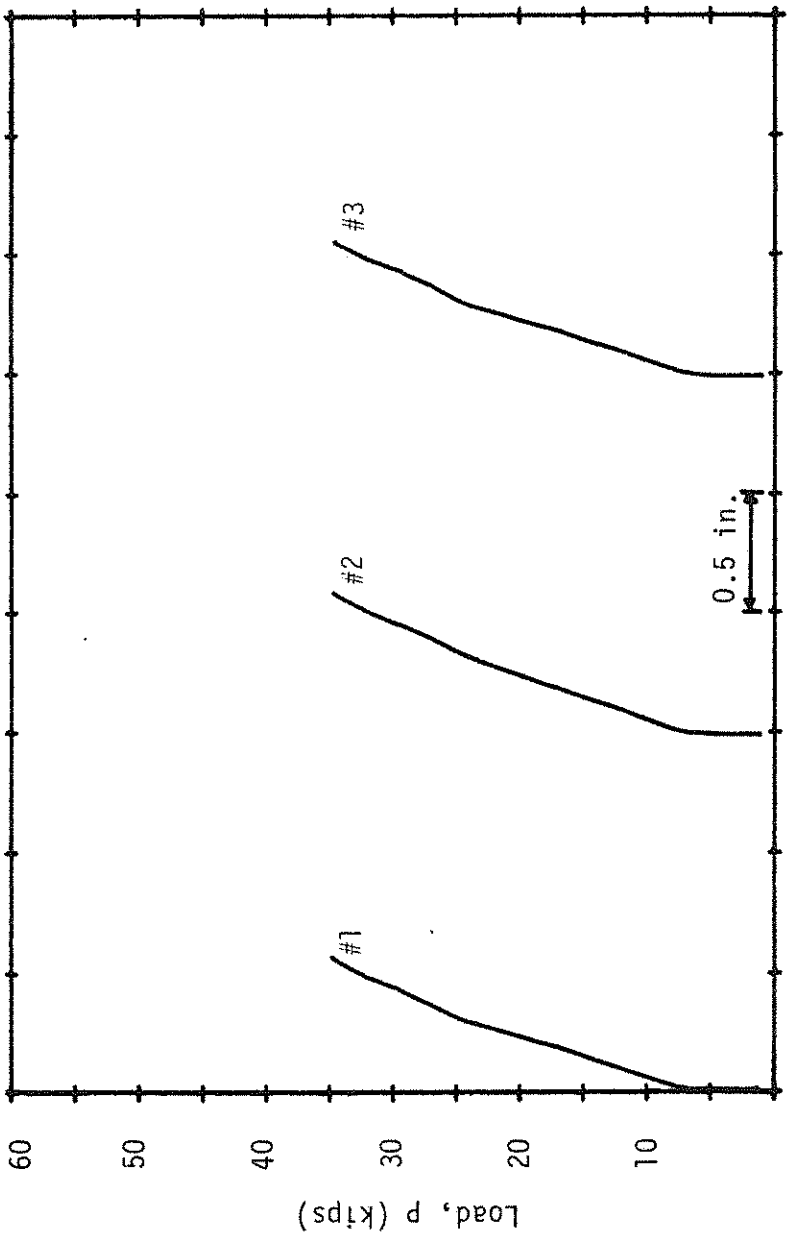

Figure B8. Load-Deflection Curves; Beam B25.

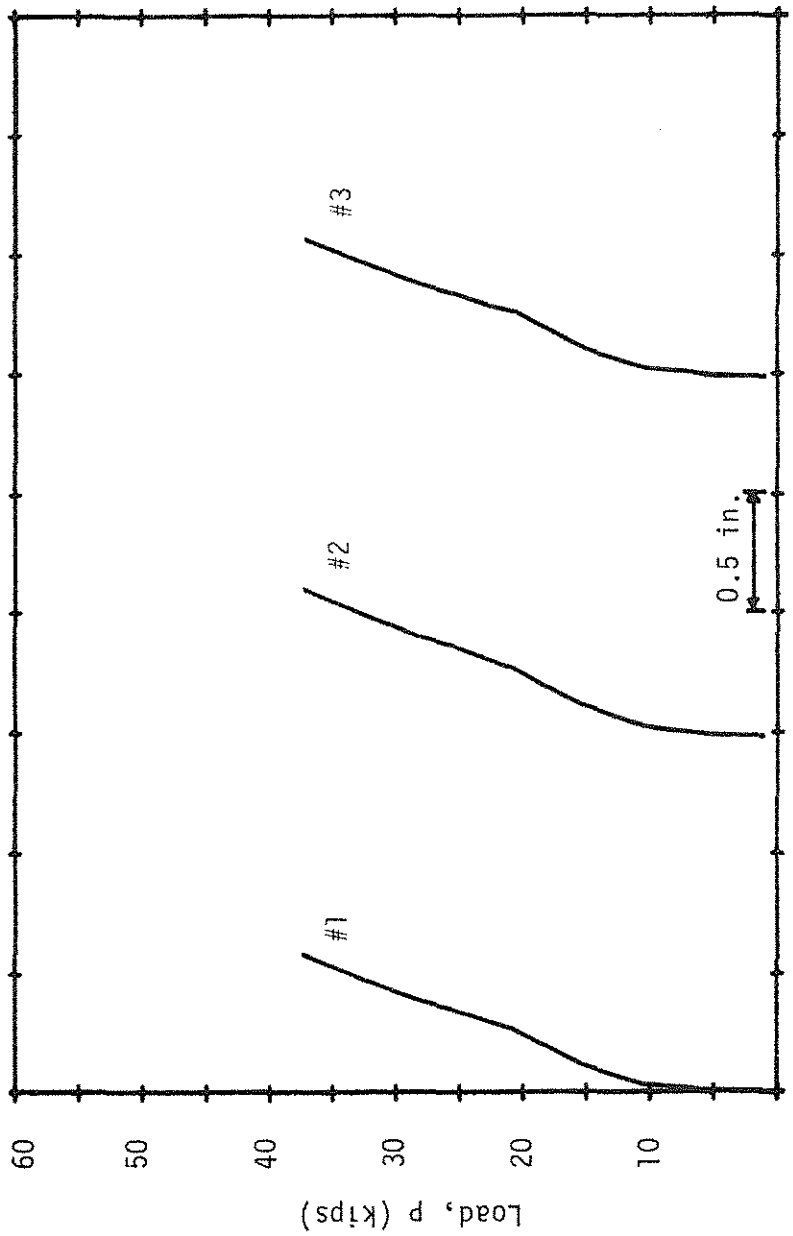

Figure B9. Load-Deflection Curves; Beam B50.

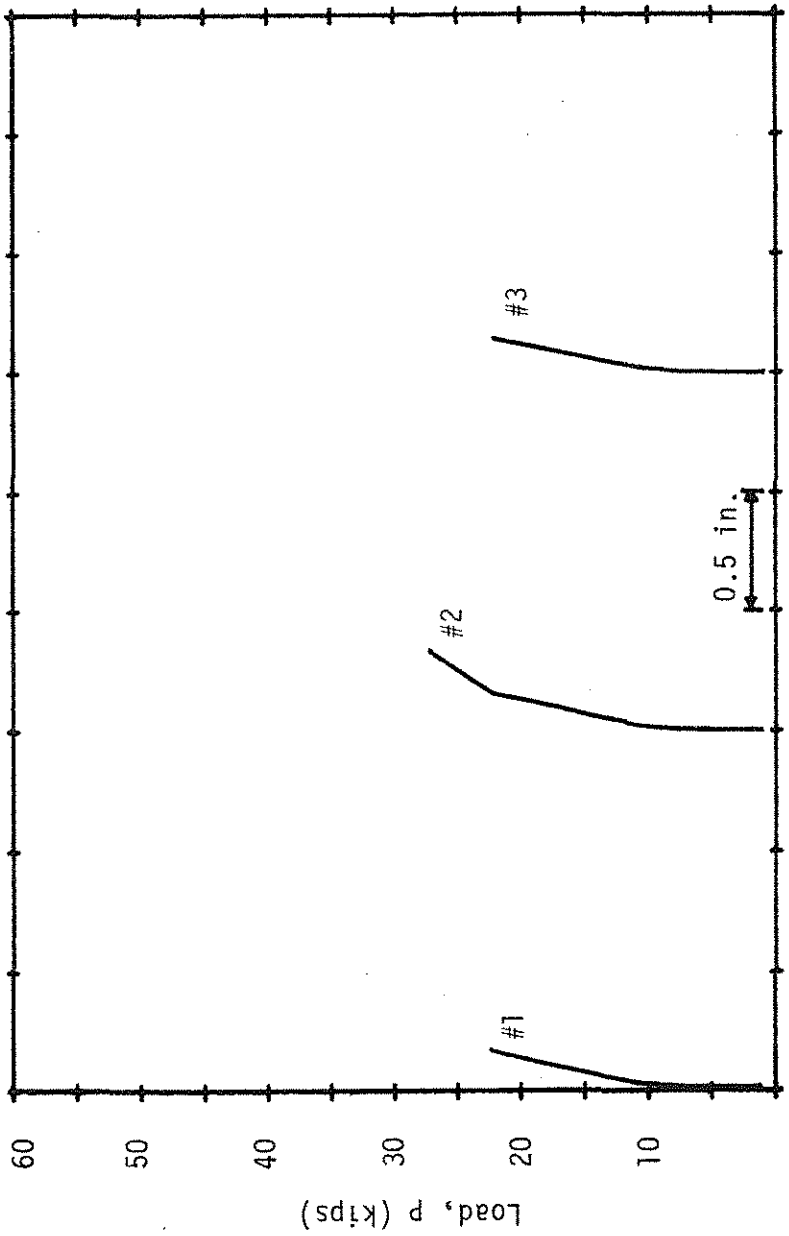

Figure B10. Load-Deflection Curves; Beam C00.

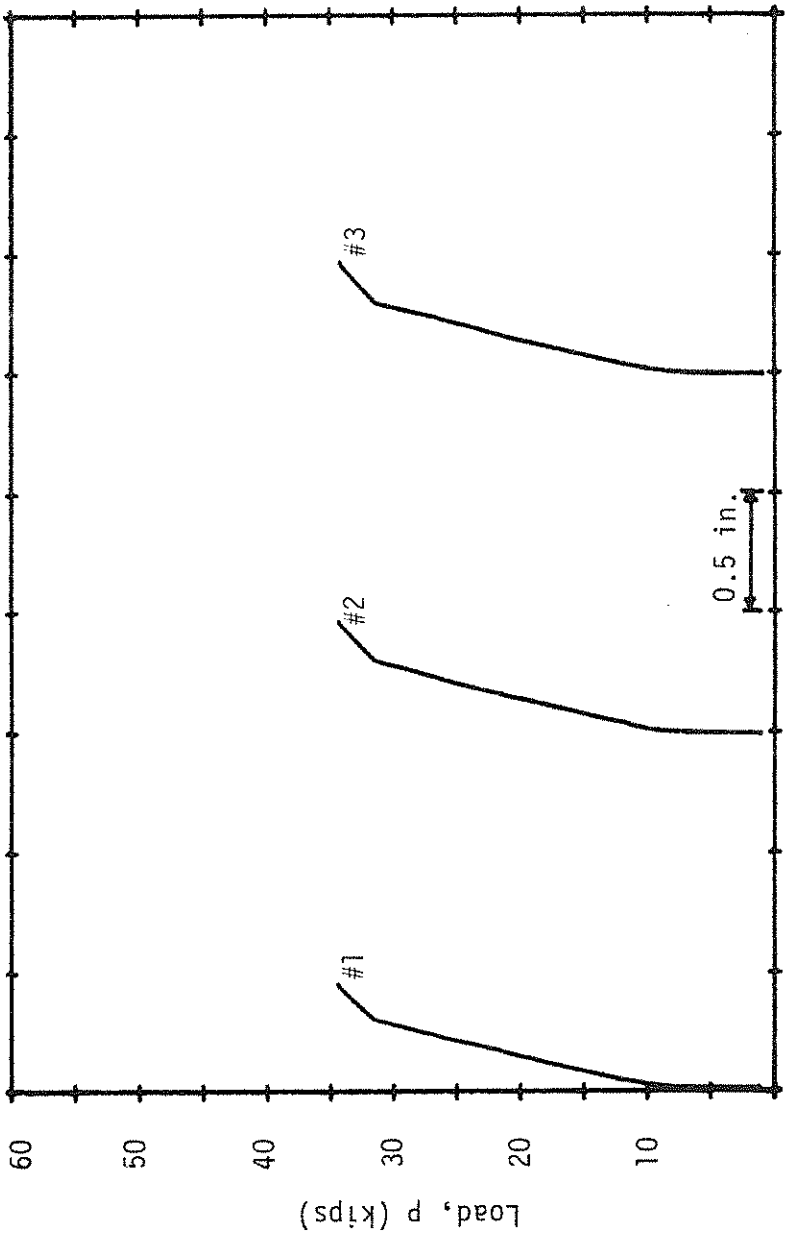

Figure B11. Load-Deflection Curves; Beam C25.

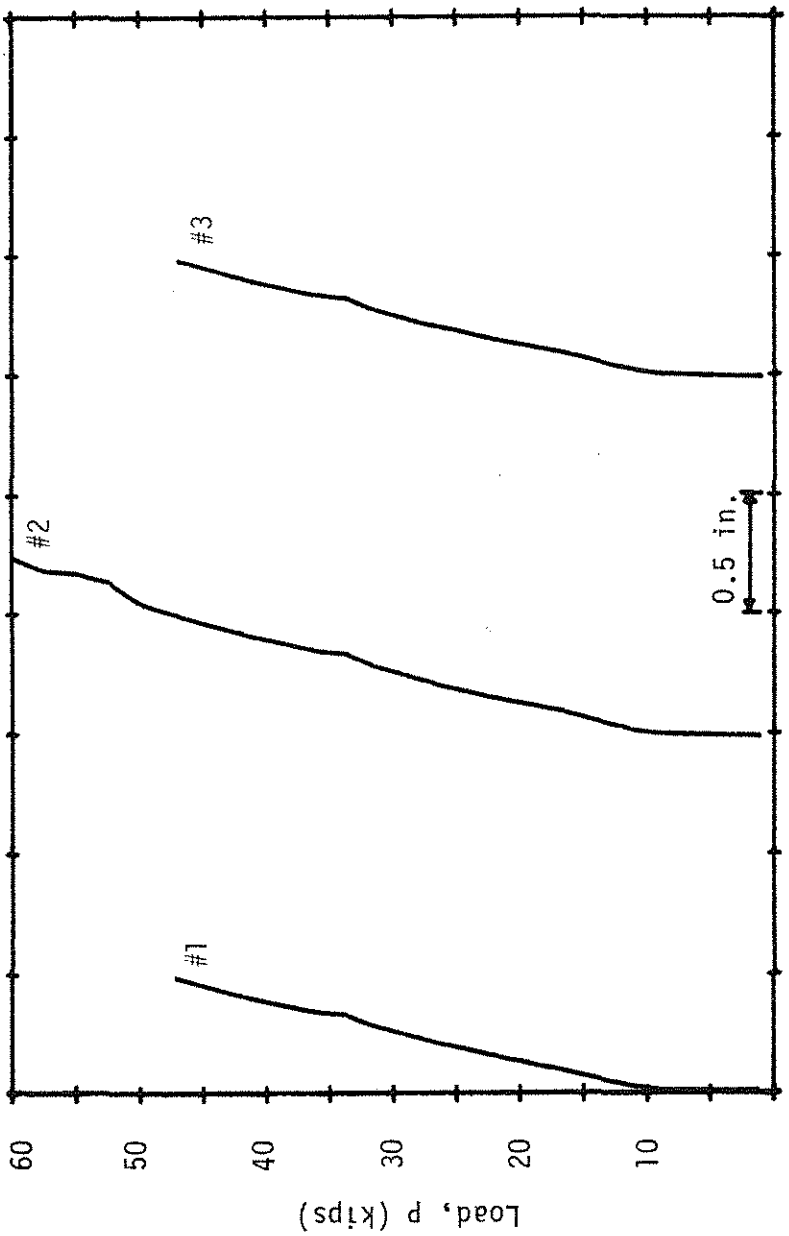

Figure B12. Load-Deflection Curves; Beam C50.

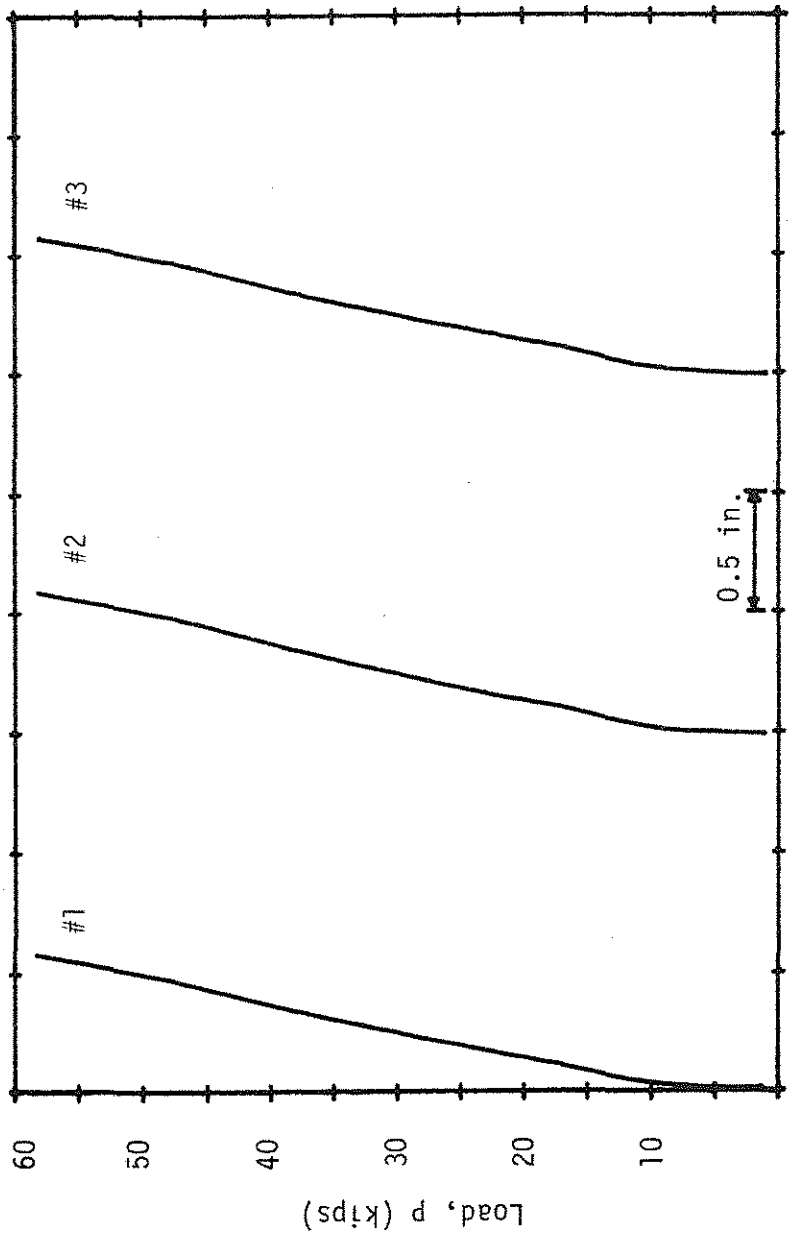

Figure B13. Load-Deflection Curves; Beam C75.

APPENDIX C

LOAD-STRAIN DIAGRAMS FOR FLEXURAL REINFORCEMENT

Figure No.	Beam
C1	A00
C2	A25
C3	A50
C4	A50a
C5	A75
C6	B00
C7	B25
C8	B50
C9	C00
C10	C25
C11	C50
C12	C75

NOTE: Bad gages for Beam A25a

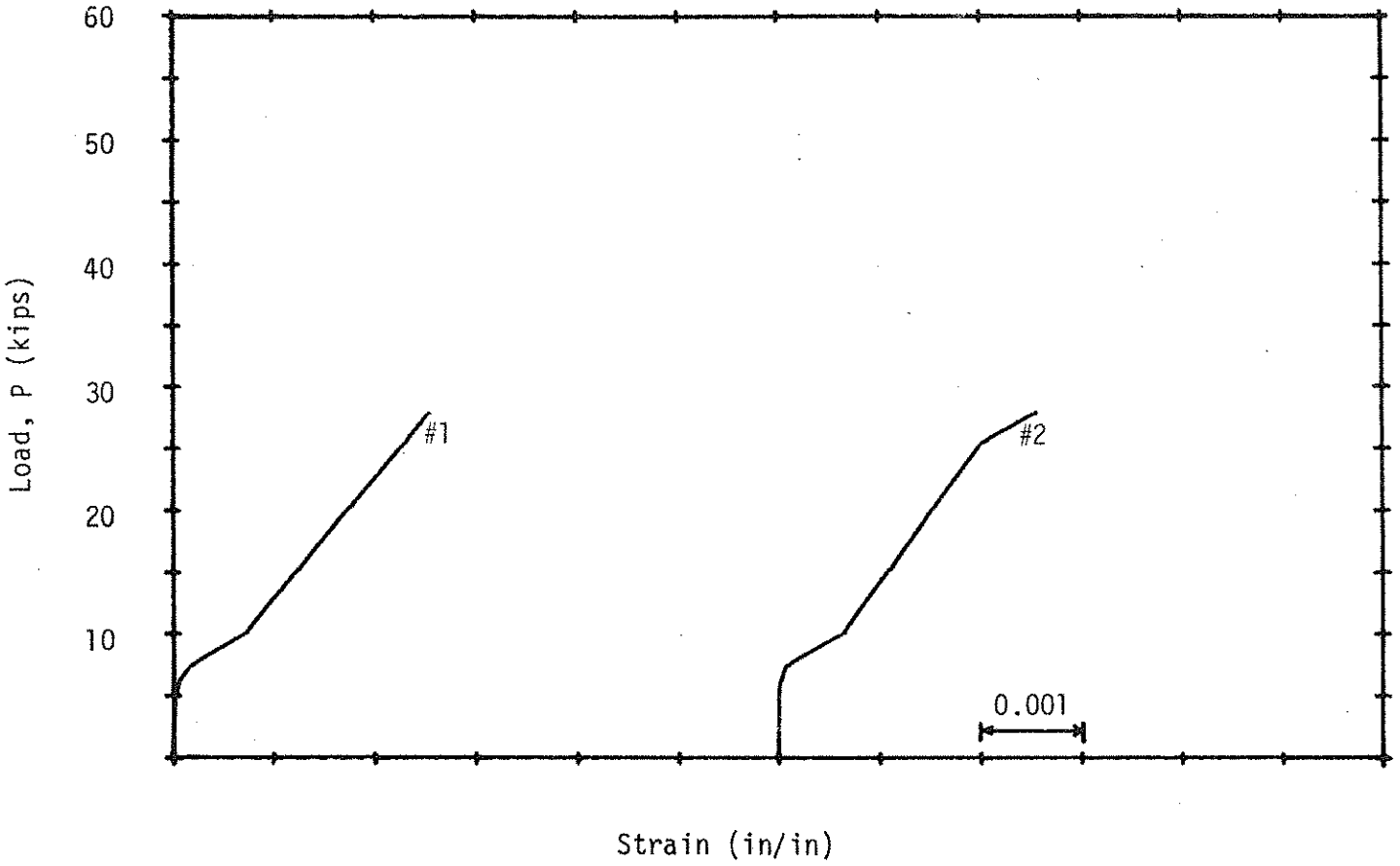

Figure C1. Load-Flexural Reinforcement Strain Diagrams; Beam A00.

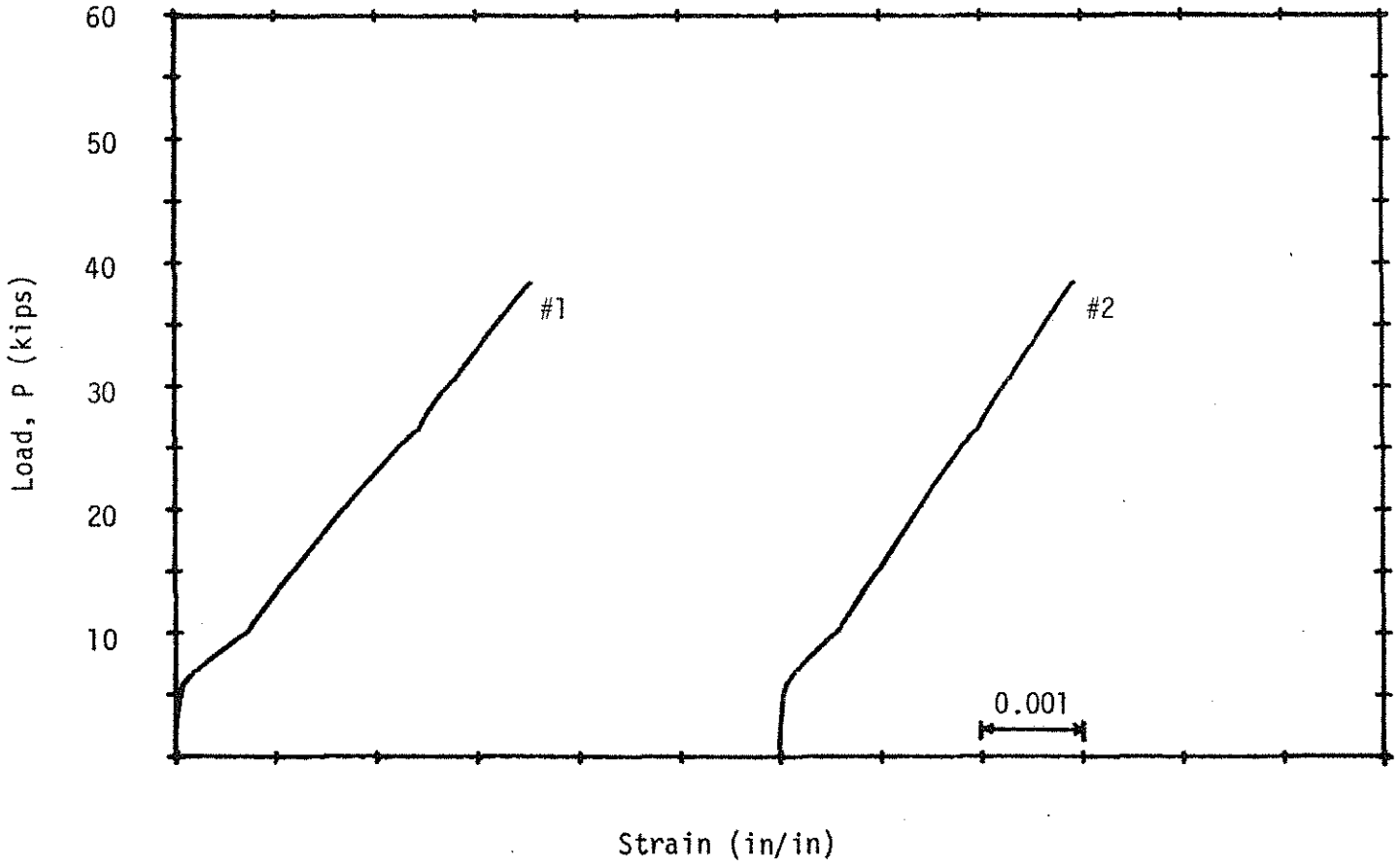

Figure C2. Load-Flexural Reinforcement Strain Diagrams; Beam A25.

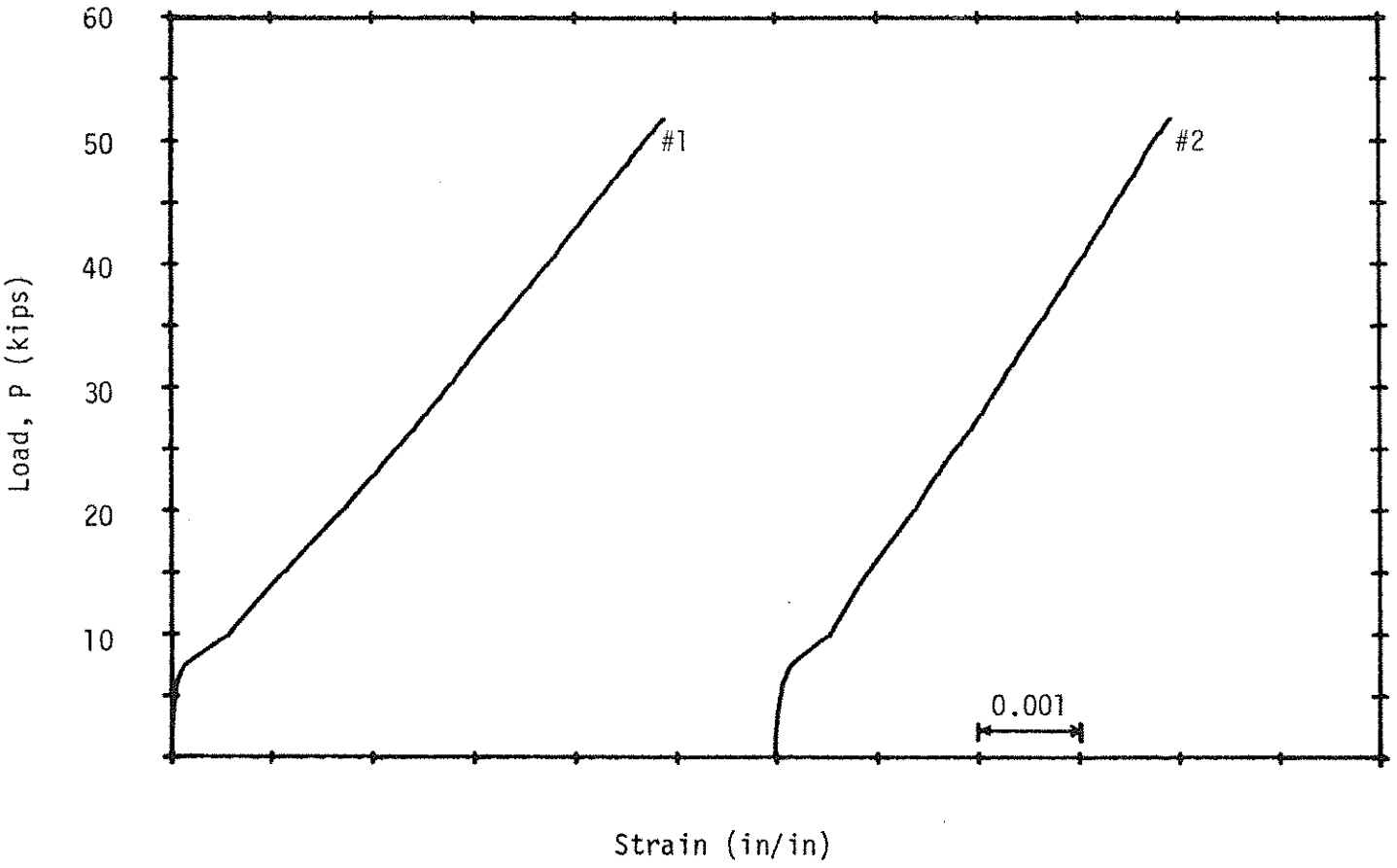

Figure C3. Load-Flexural Reinforcement Strain Diagrams; Beam A50.

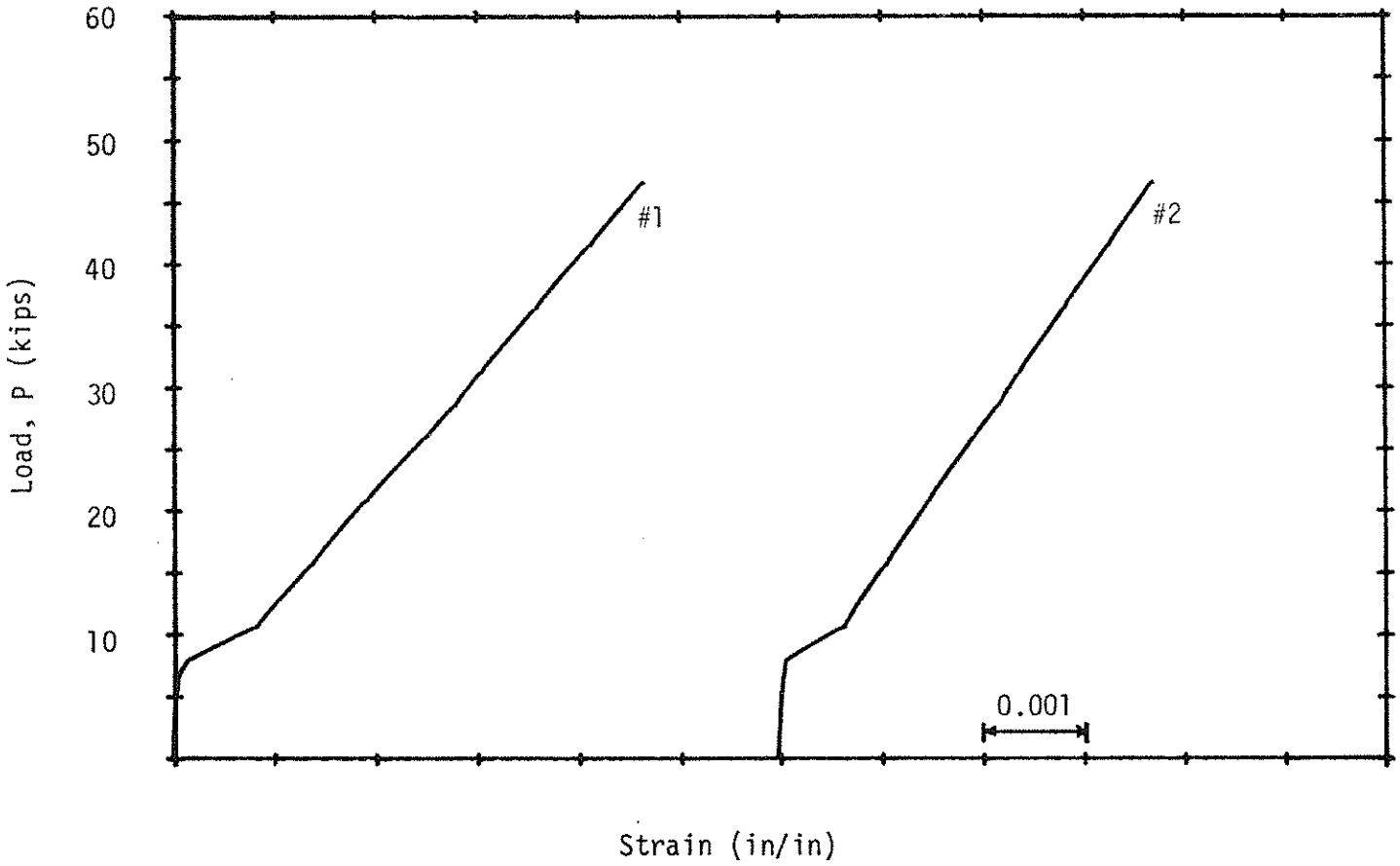

Figure C4. Load-Flexural Reinforcement Strain Diagrams; Beam A50a.

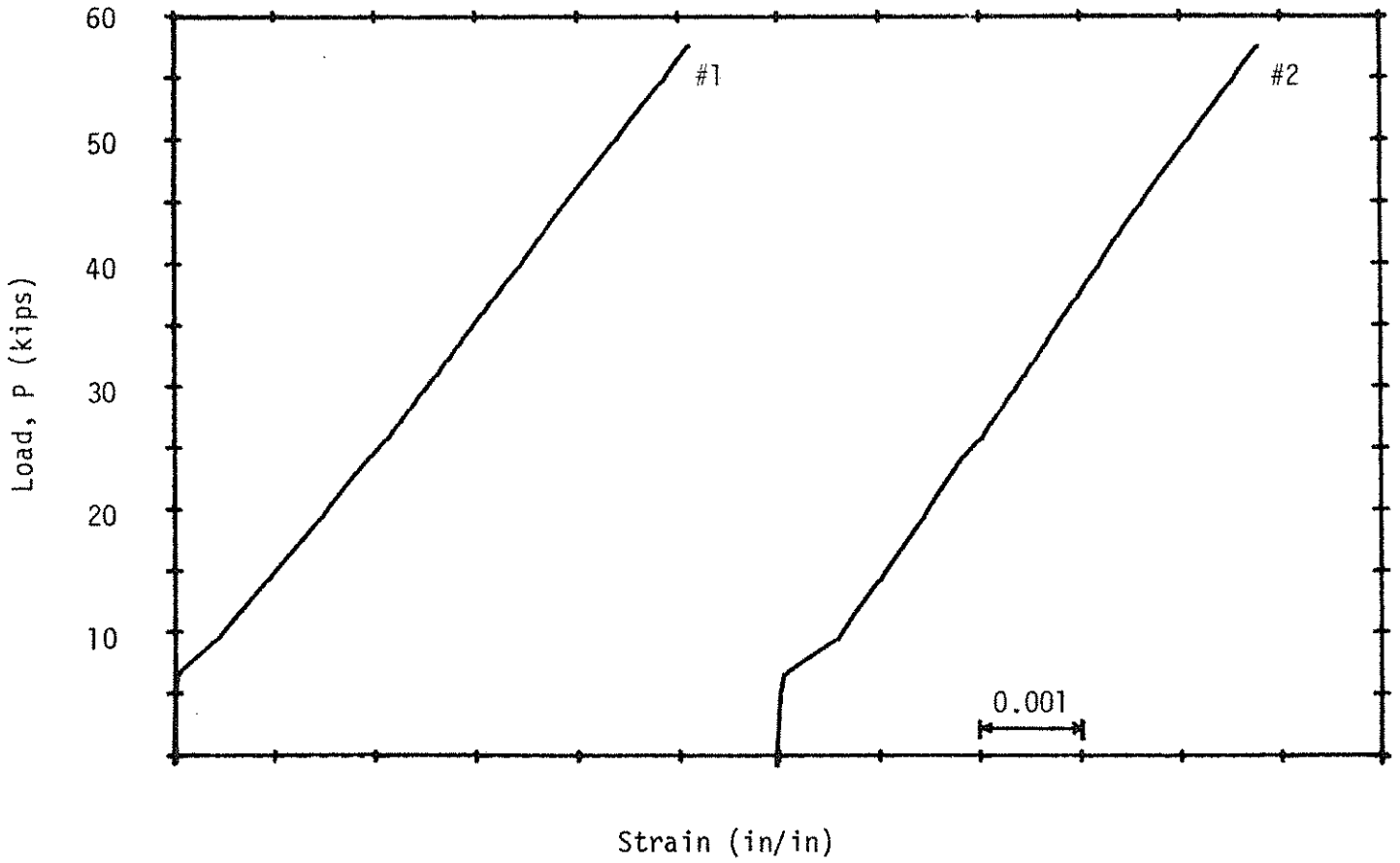

Figure C5. Load-Flexural Reinforcement Strain Diagrams; Beam A75.

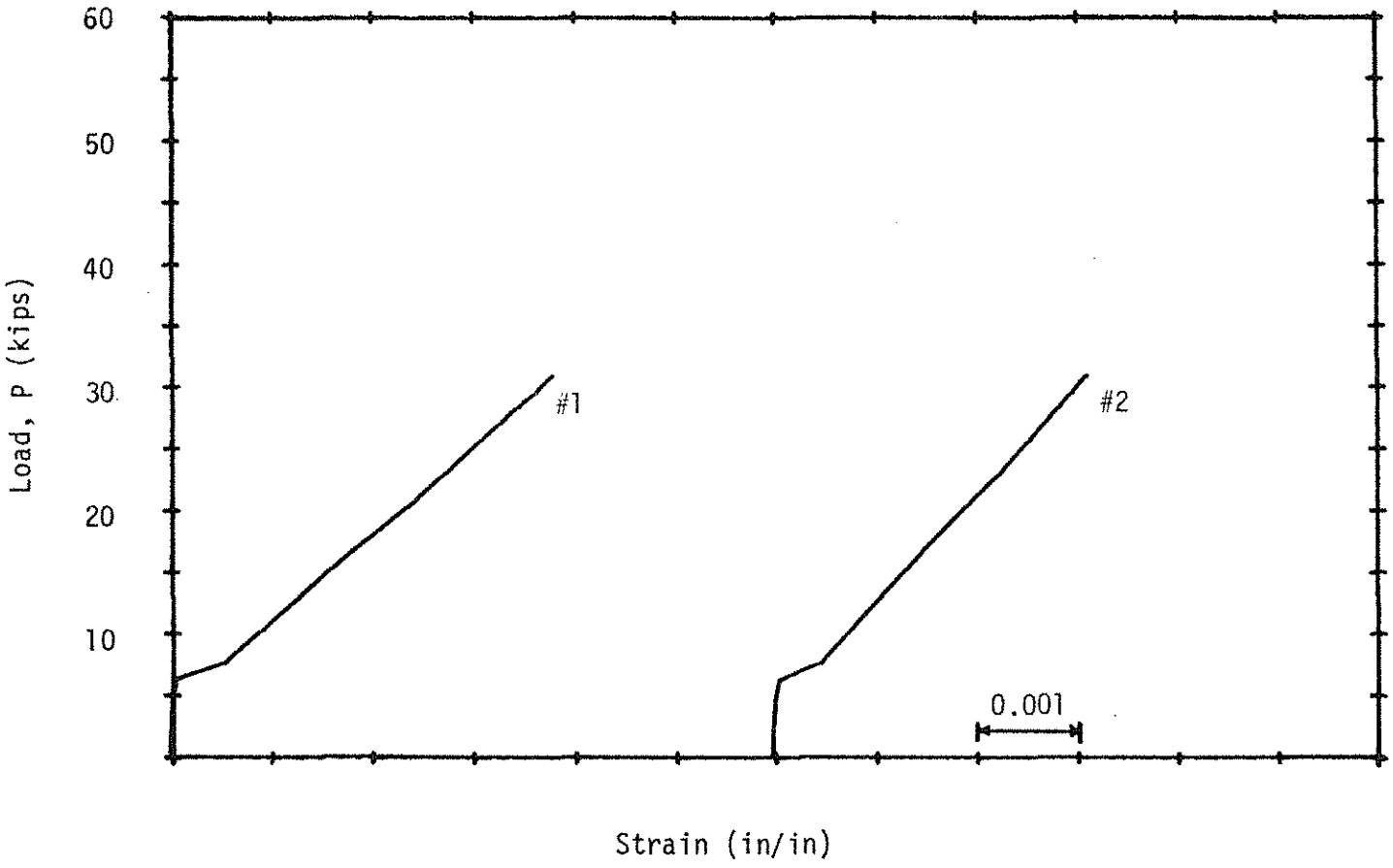

Figure C6. Load-Flexural Reinforcement Strain Diagrams; Beam B00.

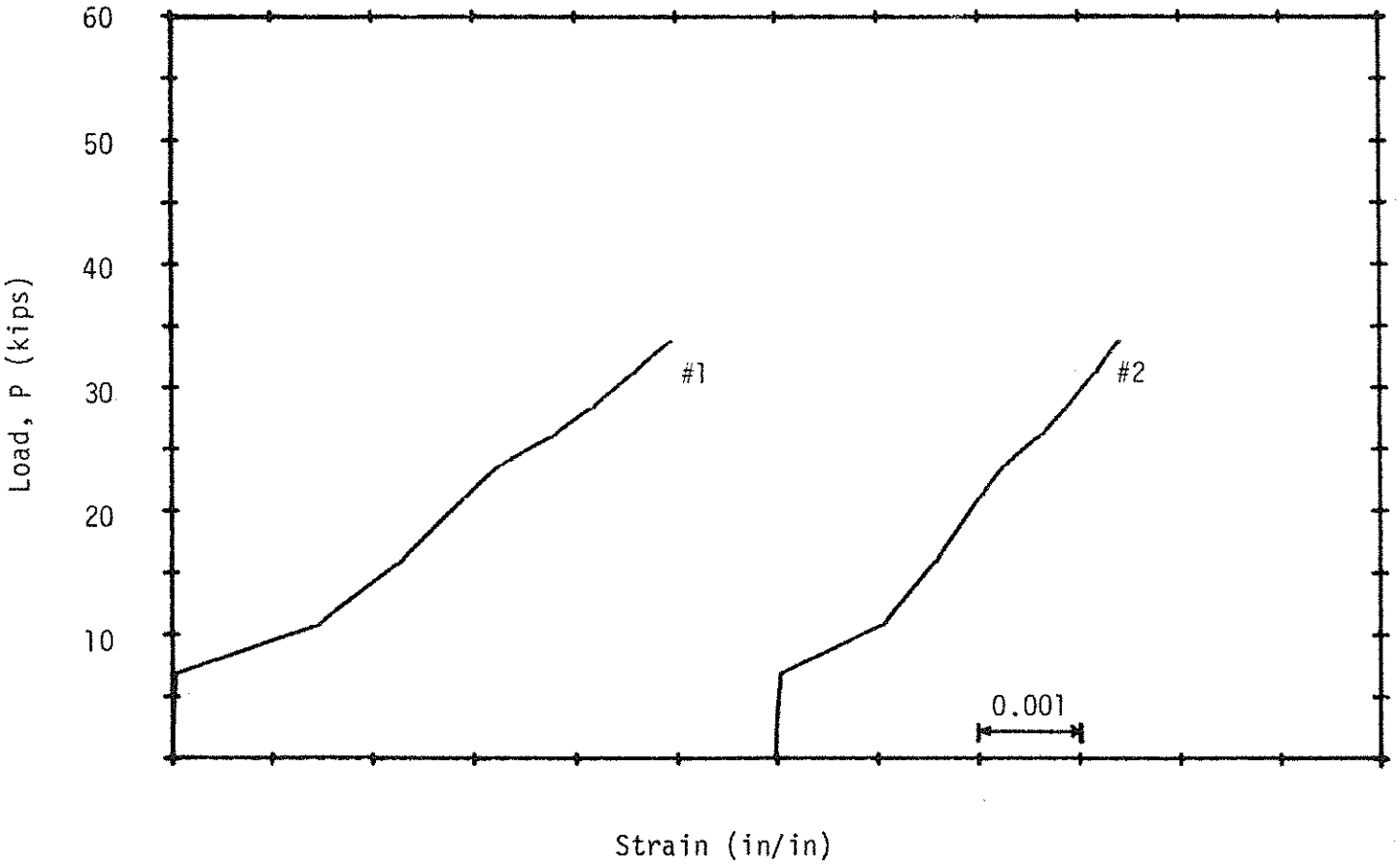

Figure C7. Load-Flexural Reinforcement Strain Diagrams; Beam B25.

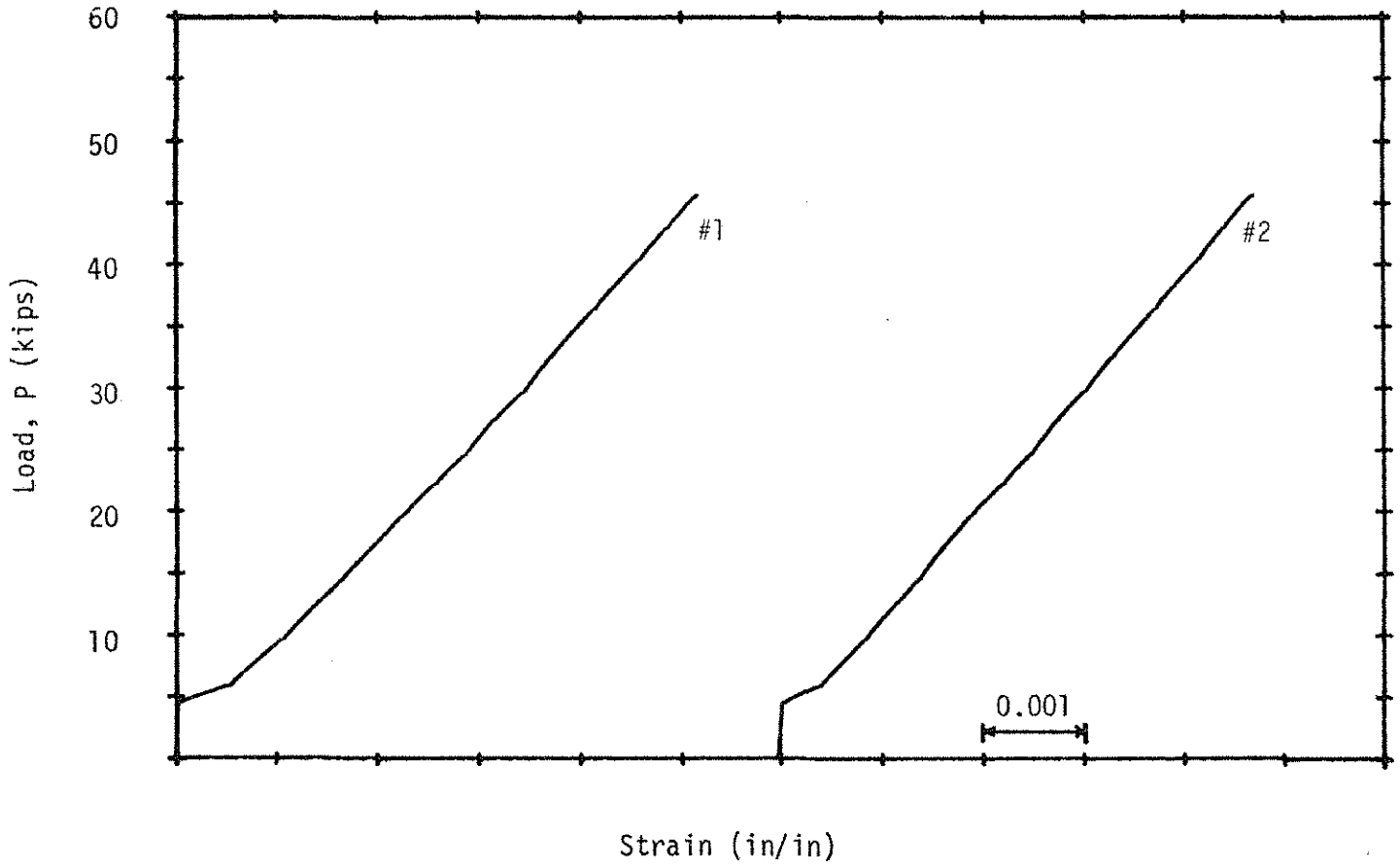

Figure C8. Load-Flexural Reinforcement Strain Diagrams; Beam B50.

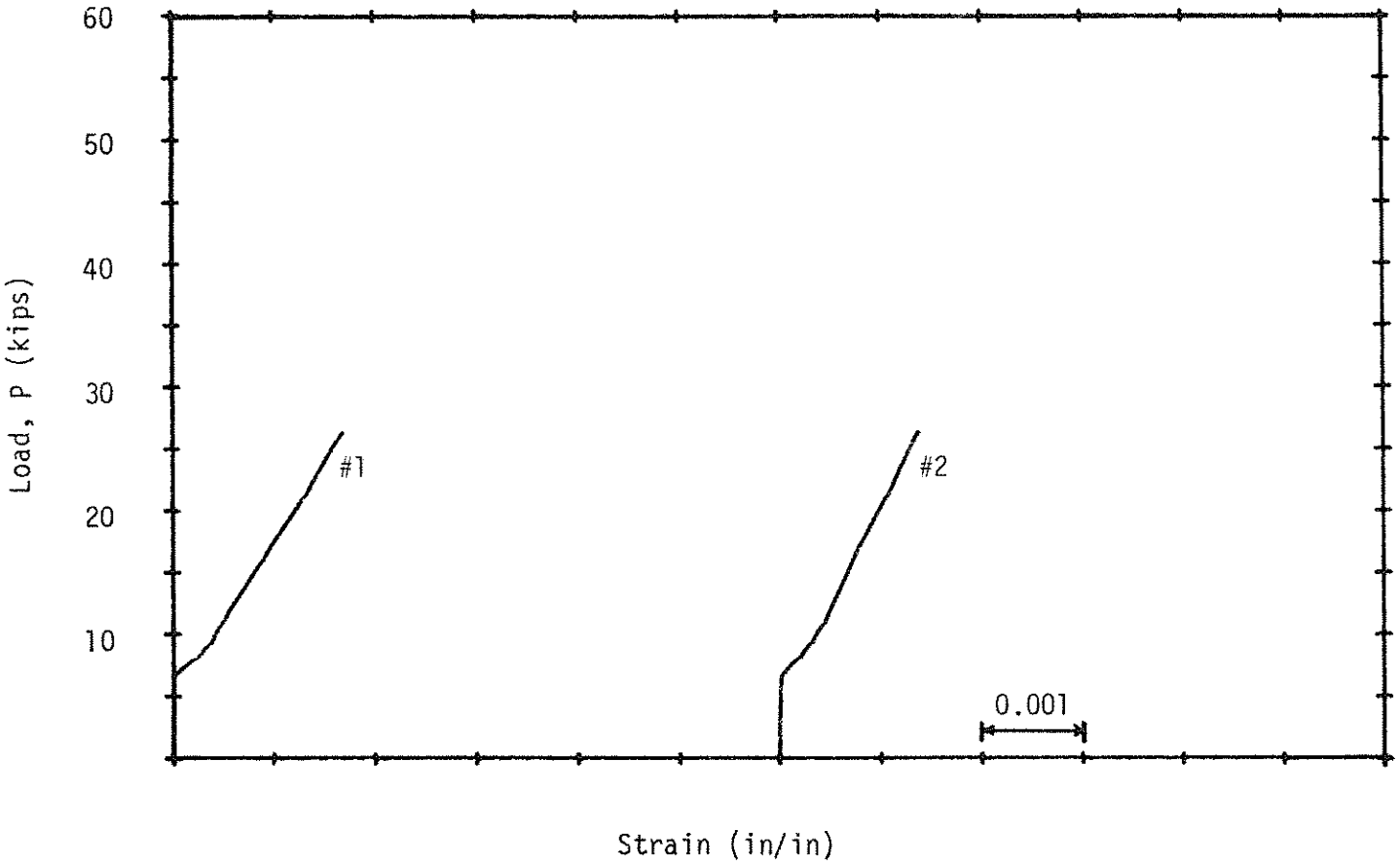

Figure C9. Load-Flexural Reinforcement Strain Diagrams; Beam C00.

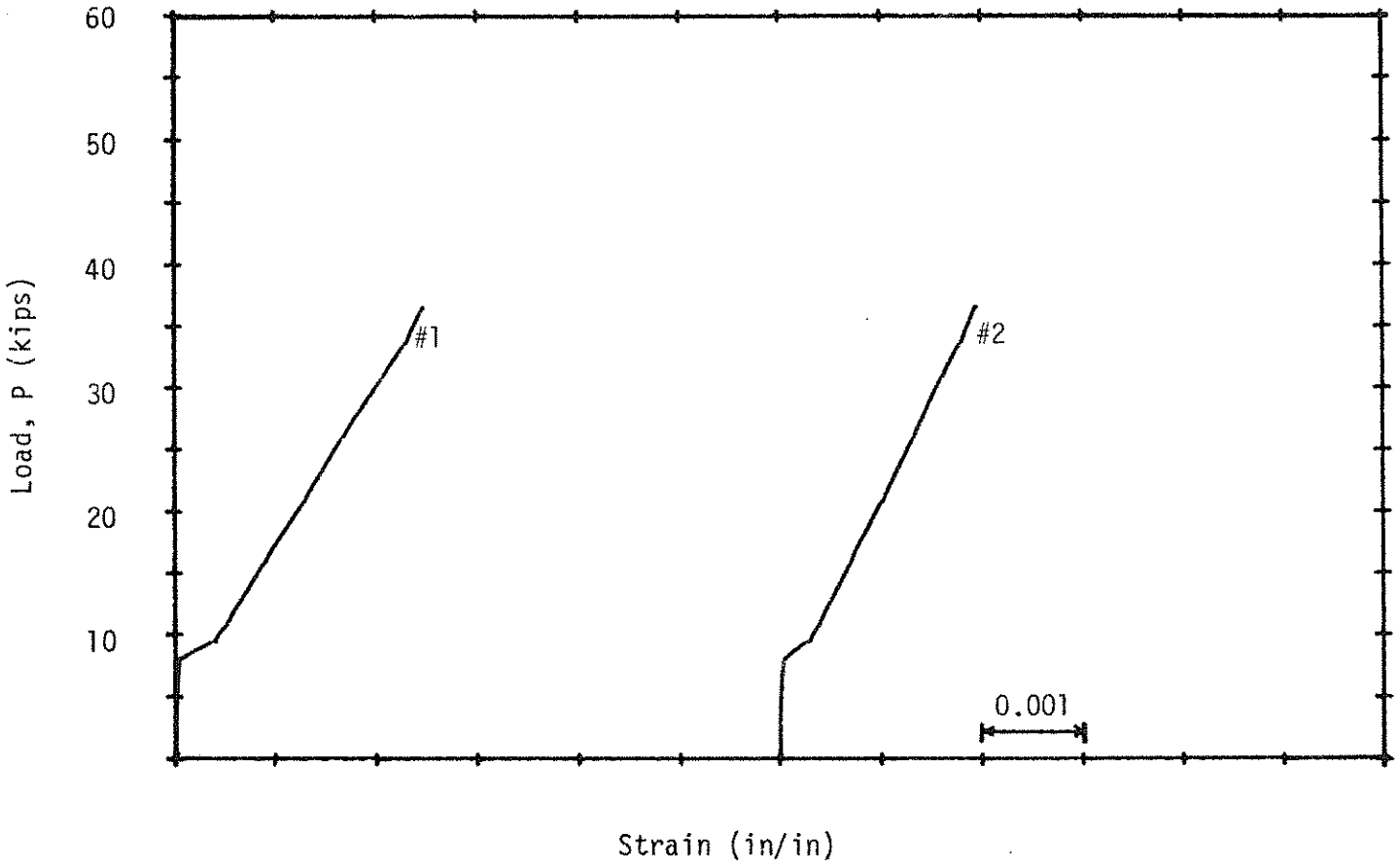

Figure C10. Load-Flexural Reinforcement Strain Diagrams; Beam C25.

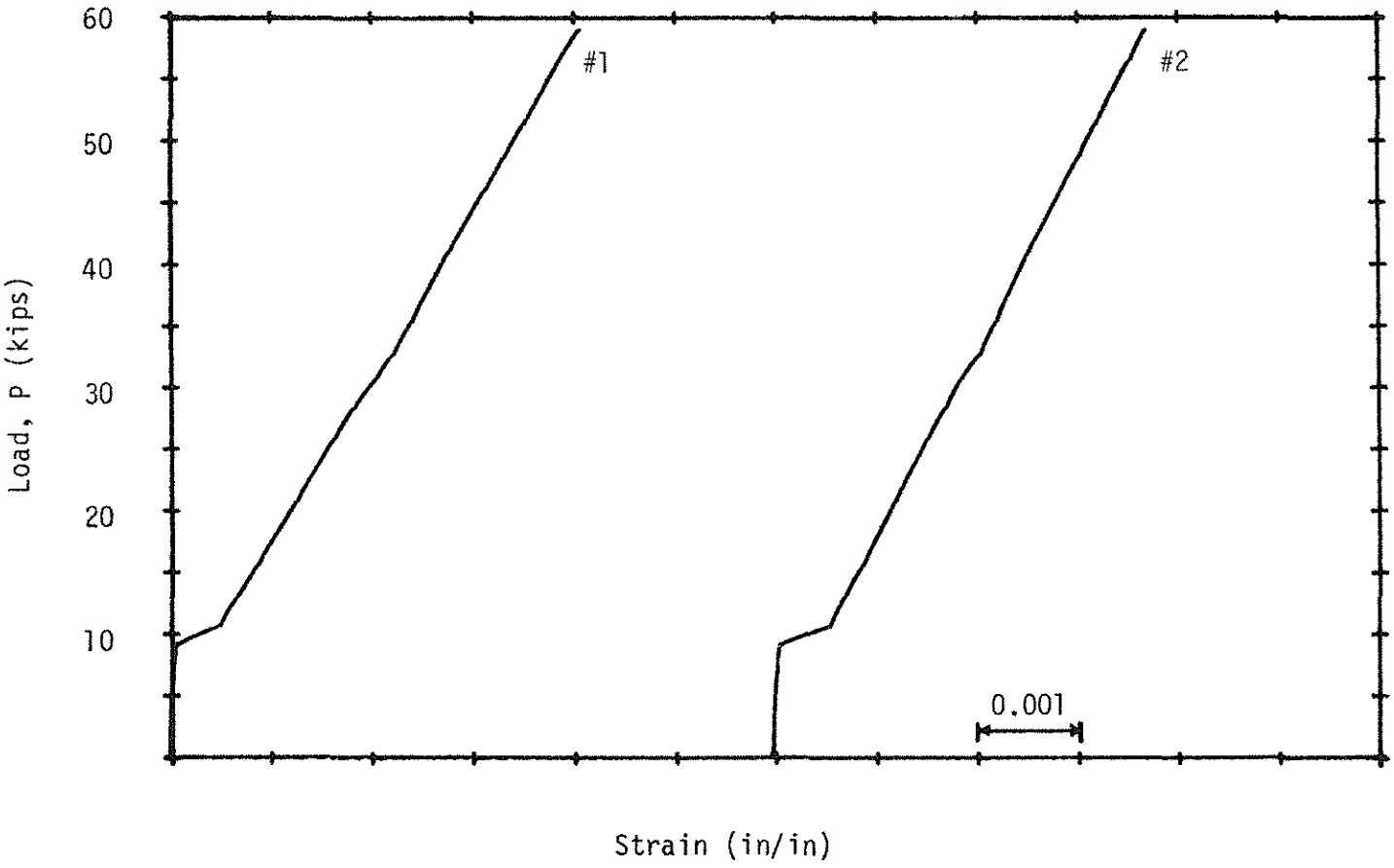

Figure C11. Load-Flexural Reinforcement Strain Diagrams; Beam C50.

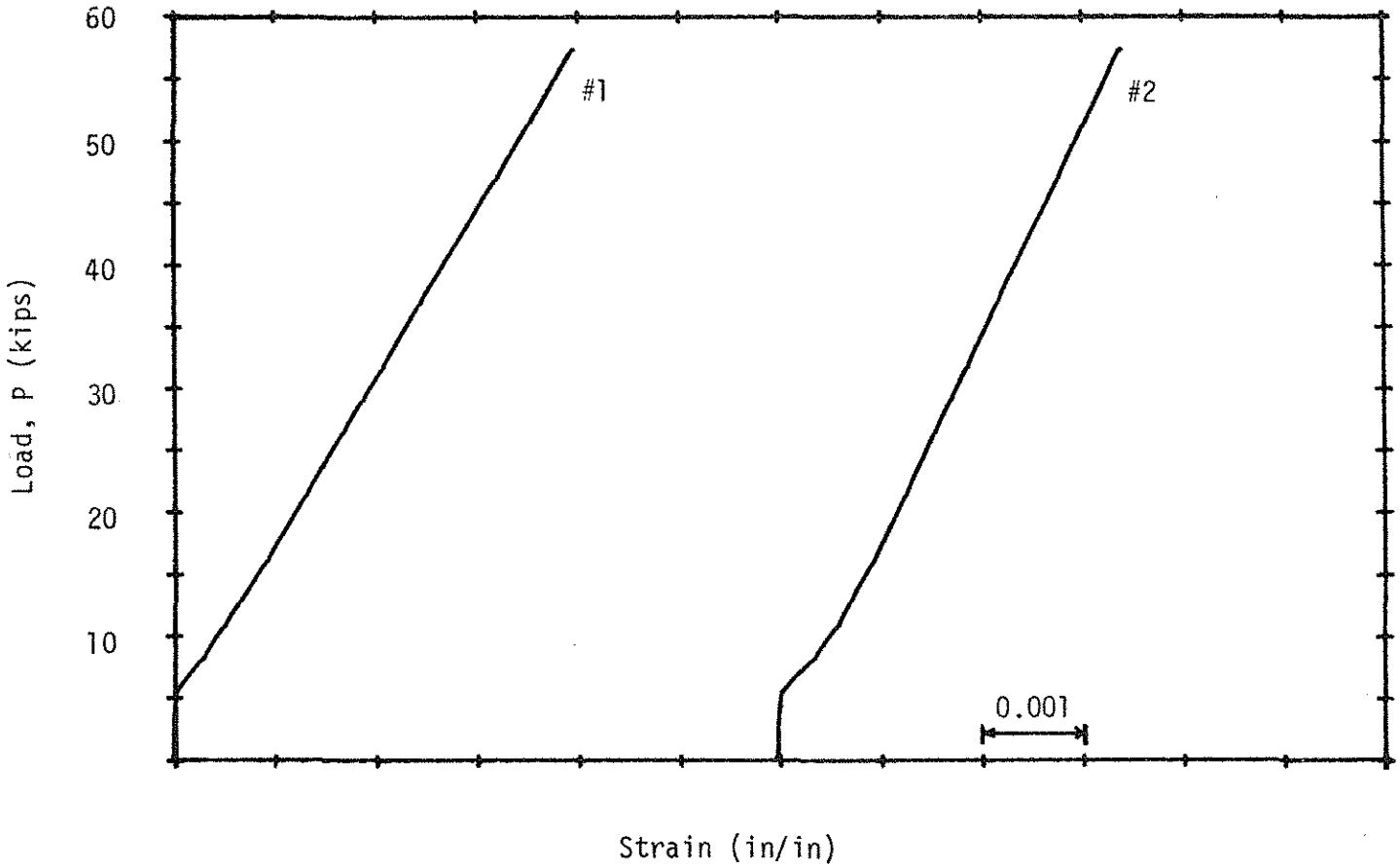

Figure C12. Load-Flexural Reinforcement Strain Diagrams; Beam C75.